MANIPULATION OF EXCITON DYNAMICS IN MACROCYCLE MOLECULES AND INORGANIC SEMICONDUCTOR NANOCRYSTALS

by

Su Liu

A dissertation submitted to the faculty of
The University of Utah
in partial fulfillment of the requirements for the degree of

Doctor of Philosophy

in

Physics

Department of Physics and Astronomy

The University of Utah

August 2012

The University of Utah Graduate School

STATEMENT OF DISSERTATION APPROVAL

The following faculty members served as the supervisory committee chair and members for the dissertation of Su Liu.

Dates at right indicate the members' approval of the dissertation.

John M. Lupton, Chair	05/09/2012 Date Approved
Adam Bolton, Member	05/09/2012 Date Approved
Andrey Rogachev, Member	05/09/2012 Date Approved
Yong-Shi Wu, Member	05/09/2012 Date Approved
Michal Morse, Member	05/09/2012 Date Approved

The dissertation has also been approved by David Kieda

Chair of the Department/School/College of Physics and Astronomy

and by Charles A. Wight, Dean of The Graduate School.

ABSTRACT

The temporal dynamics of excitons and the evolution of excited states of a material system reflect both the excitation conditions and the final destination of the excitation energy. Precise control of material structure through modern nanofabrication provides nanostructures with well-defined relaxation paths of excitons, which can be manipulated and probed using external stimulation. In particular, electrostatic manipulation of exciton dynamics with external electric fields can be used to study electronic properties of novel material systems such as semiconductor nanocrystals and pi-conjugated molecules, which may be well suited for future applications in optoelectronic devices.

In this work, electric field induced quenching of photoluminescence through generation of indirect excitons is performed on colloidal tetrapod heterostructure nanocrystals and a multichromophoric model molecular system. The dependence of quenching on optical excitation density, which shows opposite trends in these two material systems, reflects the specific origin of quenching in each system. The large reduction in decay lifetime of indirect excitons in the tetrapods also enables storage of optical information with external electric field, which can be observed using time-resolved spectroscopy. As a model light-harvesting system with efficient energy funneling from the arm to the core, the tetrapod is an ideal system to study impact of electric field on multiexcitons in the core and the "hot" excitons in the arm, thus providing insight on the effects of an electric field on intrapartical energy transfer. While

energy transfer in the heterostructure tetrapods is through direct charge carrier thermalization, it is the coherent and incoherent energy transfer that couple chromophores in the multichromophoric molecules which mimic the intermolecular interactions in organic electronics. Both single molecule spectroscopy and time-resolved spectroscopy were employed to probe the structural dependent coherent and incoherent energy transfer.

Briefly, this work consists of four main results. (1) Quenching in tetrapods is due to the localization of indirect excitons at trap sites which causes saturation of quenching at high excitation density. (2) Multiexcitons and arm excitons with fast decay lifetimes are not affected by an external electric field since electrostatic manipulation is not instantaneous. (3) Coherent coupling between chromophores causes changes in spectrum and decay lifetime, while the incoherent coupling leaves a dimer as a single quantum emitter and causes structural dependent emission depolarization. (4) Field induced quenching increases with the increase of excitation density and number of chromophores in multichorphoric molecules.

CONTENTS

LIST OF FIGURES

ACKNOWLEDGEMENTS

A Ph.D. thesis is not a single person task. I would not have completed mine without the guidance, help and support from various people and sources. Here are the people who make this work possible.

- **Prof. John M. Lupton**, who was my supervisor since 2007. The past five years' learning and research experience with John has been a pure joy. He is always there when guidance is needed through the weekly group meetings or occasional one-to-one meetings. The broad knowledge John has makes it easy to stay on the right track of graduate study and research. The two things I like mostly about John's mentoring is his firm optimistic attitude toward research problems and sincere interest in science. He has the magic of turning the most disappointing lab results into the most promising ones, which creates a motivating environment for me and the whole group to do our best throughout the Ph.D. study. I also enjoyed and benefited from his high level of professionalism in maintaining a high scientific standard for both the publications and experimental infrastructures. In this respect, I am thankful to the hard work he put in writing grant proposals to keep my research projects funded and the lab updated, which also allowed me to go to conferences to let my work be known and meet people. I appreciate the opportunity he gave to me to join his wonderful group to learn to be a scientist and to experience a professional and encouraging research environment.

- **Prof. Adam Bolton, Prof. Andrey Rogachev, Prof. Yong-Shi, Wu and Prof. Michael Morse** for serving on my thesis supervisory committee, their guidance in full completion of my graduate studies, and time spent on my behalf.
- **Dr. Nick J. Borys,** who was a graduate student and then a postdoc in the group. He was the one who taught me mostly of lab conduct and experimental techniques. His willingness to help and enthusiasm for solving problems made my start in the group so much easier. I am in debt to Nick for his continuous efforts in keeping the labs as a well organized, functional and upgraded research place to work. I cannot thank Nick enough for writing the two papers together with me, during which he put no less than the effort I devoted and offered help when needed. He also proofread my thesis, which significantly improved the language and structure of it. Besides the scientific help he provided, Nick was also dedicated to keeping the group so integrated and hospitable that I enjoyed staying.
- **Kipp J. van Schooten** for setting up the time-resolved spectroscopy lab together with me and purchasing the glovebox system used for device fabrication.
- And all other members in the nanoscale optoelectronics group, **Dr. Sebastian Bange, Dr.Debangshu Chaudhuri, Dr.Dongbo Li, Dr. Eyal Shafran, Douglas Baird** and **Alex Thiessen** for creating a creative, supportive and amiable group.
- **Matt DeLong, Ed Munford, Randy Polson** and **Wayne Wingert** for technical support.
- **Kathy Blair, Heidi Frank, Sara Gardner, Jackie Hadley, Vicki Nielsen**, and **Kathrine Skollingsberg** for help with all the administrative matters.

- **Dr. Golda Hukic** and **Dr. Maria Navas** for doing this together with me and their friendship.

For this thesis, close collaborations with the chemistry groups provided us the unique materials to work with. Special thanks are given to

- **Prof. Sigurd Höger** and **Daniela Schmitz** for chemical synthesis of the macrocycle molecules used in this study and their work on self-assembly using STM.
- **Prof. Dimitri Talapin** and **Dr. Jing Huang** for providing the CdSe/CdS tetrapod heterostructures used in this thesis.

I would also like to thank my beloved parents, **Hongli Pang** and **Yongmin Liu,** for supporting me through this different journey and always believing in me.

CHAPTER 1

INTRODUCTION

In 1959, Dr. Feynman gave a visionary talk on phenomena at small length scales prior to in-depth investigation into this field. Feynman foresaw the "weird" effects that might happen at scales of just a few to a few thousand atoms. Today, 50 years later, scientists are driven by both the curiosity of understanding new science at this scale as well as the rapid decrease in size of semiconductor electronics to a regime when novel effects are already starting to be observed. One unique advantage of the nanoscale is the engineering of properties through the control of physical shape, size and surface properties.[1] Through the collective work of chemists, engineers, physicists and even artists, the fabrication of nanostructures of controllable shape and properties is rapidly progressing. Nanofabrications through both bottom-up and top-down approaches have achieved single atomic layer precision in nanocrystals (NCs)[2,3] and synthesis of molecules with designed structures.[4,5] The precise control of structures enables the engineering of properties to realize desirable functions in a single nanostructure or an assembly of various functional nanostructures.[2,6] Semiconductor NCs, often referred to as quantum dots, show significantly modified properties compared to the bulk counterparts that form the basis of all modern electronics. This modification resultes from spatial confinement of electron and hole wavefunctions in the nanoscale, which increases the band gap of NCs with decreasing size.[7] Consequently, the absorption and emission spectra shift to shorter

wavelengths in smaller NCs.[8] Additional structural properties, such as shape and surface morphology, have been shown to change the polarization, luminescence quantum yield and exciton dynamics of NCs.[3,9-12] Synthesis of heterostructure NCs, which consist of multiple semiconductor materials, opens another route to engineer electronic structure, and consequently, properties.[8] The difference between NCs and the bulk counterparts is even more drastic at the single particle level. The emission of a single NC undergoes both fluorescence intermittency and spectral diffusion due to charging and local electrical field fluctuation, respectively.[13,14] Inspired by the latter effect, an external electric field has been applied and shown to change both emission intensity and energy of a single NC or an ensemble of NCs.[15,16] The colloidal synthesis of NCs through wet-chemical processes is by far the simplest and most successful method, in terms of quality of NCs and precision in control over structure and composition.[17] The simple and precise fabrication, large absorption cross section and photostability compared to organic dyes, in turn motivate application of NCs in various areas such as gain medium in lasers,[18] biolabeling,[2] photovoltaic devices,[19,20] and data storage.[16,21,22]

Unlike inorganic colloidal semiconductor NCs, of which the properties are mainly engineered through control over size during synthesis, organic pi-conjugated molecules show properties that correspond to the chemical structures. They are a class of materials that demonstrate interesting optical and electronic properties that are similar to that of the inorganic semiconductors. In the meantime they also have advantages over the inorganic counterparts originating from their plastic nature. These advantages include easy processing, low cost, mechanical flexibility, and tunability of properties through chemical synthesis. Therefore, a new class of plastic electronics such as flexible large area

displays,[23] organic solar cells,[24] lasers,[25] organic spintronicss,[26] and organic field-effect transistors[27] can be developed using cheap solution processing techniques. The nanotechnology comes into play in this field as a tool to study the complex processes of generation, transport, recombination and dissociation of charge carriers in organic films or crystals which are the active regions of organic electronics.[28-30]

Despite the successful application of both colloidal NCs and organic materials in (opto)electronic devices, there is a large amount of knowledge and plenty of mysteries of optical and electrical properties of these two material systems under practical conditions in devices and a great need for more study. For example, the exact process of separation and dissociation of excitons in NCs and organic molecules in an external electric field is still a mystery. Additionally, answers that address how properties of organic molecules are modified due to the presence of surrounding molecules are needed for optimization of devices. In this work, a systematic study of the interplay between photophysical properties and interchromophoric interaction (Chapter 3) and manipulation of excitons using an external electric field (Chapter 3 and 4) are performed, with the goal of revealing the dynamics of excitons in organic and inorganic semiconductors for practical applications.

The scope of this thesis is as follows:

Chapter 1 gives an introduction to the relevant properties of organic pi-conjugated molecules and inorganic colloidal semiconductor NCs. Both material systems exhibit optical and electrical properties that can be engineered through control of structural properties such as size, shape, or surface morphology. Studies of the dynamics of the excited states in these two materials systems provide insight into how excitons form,

relax, transfer, recombine and separate in the nanoscale systems. Manipulation of excitons with an external electric field through the Stark effect is shown to provide an additional channel to control separation and storage of charge carriers.

To study optoelectronic and dynamical properties of NCs and pi-conjugated molecules, two gated spectroscopic setups are used in this work. Chapter 2 first gives a detailed introduction to the operation principle of gated spectroscopy and its applications in the study of dynamics. Then, an introduction to the two material systems–colloidal heterostructure NCs and a model molecular system, as well as the fabrication techniques of samples, are given. At the end, the operation of the two setups is described.

Chapters 3 and 4 present detailed discussions of experimental results. Chapter 3 starts with a systematic investigation of interchromophoric intramolecular interactions and electric field induced intensity quenching using a model molecular system. Then, in Chapter 4, intensive study of exciton separation, storage and detrapping with an external electric field is performed on colloidal NCs.

Chapter 5 summarizes the main results and the scientific contributions, which are followed by an overview of future work.

1.1 Colloidal Semiconductor Nanocrystals

Among several methods to fabricate nanostructures, the wet-chemical process for the synthesis of colloidal NCs stands out as the most versatile one due to its simplicity and high controllability over the size and shape of as-synthesized II-VI semiconductor NCs.[2,17,20] Thus II-VI colloidal semiconductor NCs are the most frequently studied systems, among which CdSe has become the model system which is frequently studied to reveal the optical and electrical properties of NCs. CdSe is also the core material of the

heterostructure NCs under investigation in Chapter 4. In addition, colloidal synthesis of III-V semiconductor NCs, such as InP,[31] and nonepitaxial growth of metal-semiconductor hybrid NCs,[6] have also been developed to exploit rich phenomena in these systems. Through careful selection of experimental conditions, such as temperature, reagent concentration, surfactant, etc., NCs of spherical, rod and branched shape can be synthesized with nearly atomic precision of the size of a few to tens of nanometers. [17]

The nanometer spatial extent of NCs applies an extra boundary condition that confines the electron wavefunction in a region that is smaller or comparable to the exciton radius. This confinement causes NCs to differ from their bulk counterparts through the so called *quantum confinement*. As a direct consequence, size tunability of optical and electrical properties of NCs enables applications in the full visible-IR spectral range. For example, quantum dot based lasers of tunable wavelengths can be designed simply by exciting particles of different size.[18] Another unique effect in NCs is fluorescence intermittency and spectral diffusion, which is due to trapping of charges on localized trap sites in NCs and the sensitivity of NCs to the fluctuations of local electric field, respectively.[32] These temporal fluctuations in emission have long been an obstacle in the application of NCs in biolabeling, which has now been lifted by the successful synthesis of non-blinking quantum dots through various surface passivation methods,[10,33,34] which remove surface defects that are the main sources of trap sites. Proper surface passivation can significantly reduce the number of surface defects and increase the fluorescence quantum yield of NCs. The remaining defects can still influence properties and the interaction with external stimuli such as an electric field.

In this section, the basic structural, optical and electrical properties of semiconductor NCs will be introduced, with emphasis on carrier delocalization and the generation of multiexcitons in heterostructure NCs.

1.1.1 Structure Properties

Depending on whether the conduction band is empty, nearly full, or partially full (10-90%),[35] solid state materials can be characterized into insulator, semiconductor and metal, respectively, based on their conductivity. Although categorizing materials is largely determined by the elements they consist of, the relative electrical and optical properties of each type of material are solely shown in the bulk solid state, not in the atomic level. Therefore, how each atom is periodically arranged to form bulk materials of certain crystal structure, also plays an important role in determining the collective properties of all the building blocks. A typical example arises from carbon based materials, where diamond and graphite have exactly the same chemical composition, but are characterized as insulator and semimetal respectively. As shown in more detail in Section 1.2, pi-conjugated molecules consisting of the same atoms can also have distinctive conducting properties due to differences in chemical structures. Similar structure-property relations also exist in semiconductor NCs due to spatial confinement where quantum phenomena are present. However, the quantum confinement applies in different ways in inorganic semiconductor NCs compared with organic pi-conjugated molecules. The wavefunction is confined by the size and the shape in the former system but is confined in broken conjugation segments in the latter case. Nanostructures of various sizes and shapes can be fabricated using modern nanofabrication techniques with atomic precision.

There are two approaches to fabricate nanostructures: the *top-down* and the *bottom-up*. The *top-down* methods for nanofabrication involve patterning and refining materials in the macroscopic scale into small subunits in the nanoscale. Lithography, masking and etching are three typical *top-down* techniques that are heavily used in traditional semiconductor industry. With the most state-of-the-art e-beam lithography,[36] sub-10 nm spatial resolution has been achieved. In the opposite way, the bottom-up approach assembles building blocks, such as atoms, molecules and nanoparticles, into functional superstructures by chemical synthesis, layer-by-layer epitaxial growth, self-assembly, scanning probing microscope lithography etc.[5,8,20,37-41] The latter approach goes beyond the achievements of the top-down methods, with capability of fabricating nanostructures with predictable, designable and controllable properties through control of size, shape, composition and morphology. This approach may potentially lift the limitation on fabrication of traditional electronics.

Two of the well-established bottom-up techniques for fabrication of crystalline nanostructures or NCs are epitaxial growth and colloidal synthesis. The term epitaxial refers to growth of thin films on top of crystalline substrates, where the grown film is atomically arranged in the way accepted by the crystallographic structure of the substrate. Developed from the fabrication of quantum wells, strain driven formation of semiconductor NCs can be realized by depositing a layer of highly lattice mismatched film (e.g., InAs) on top of a substrate (e.g., GaAs). The uniform size and shape distribution is permitted by a controlled ripening process under selected deposition conditions.[42] Thus-formed NCs have well-defined boundaries and are much more stable than the colloidal ones. They have been used for the study of nanoscale optical and

electrical properties,[38,43] quantum coupling,[44] spintronics,[45,46] lasers,[47] and data storage.[21,22]

Colloidal NCs are synthesized from hot solutions in simple glasswares, and can be ready to use in solution or freely dispersed into other media. This simplicity is a great advantage over the epitaxial growth of NCs bonded to substrates which also require sophisticated apparatus. The colloidal synthesis has been proven to be the most successful method also in terms of quality and monodispersity of synthesized NCs. This approach expands the scope of the parameter space that can be exploited in terms of shape, surface morphology and composition. With this great flexibility, a collection of NCs, ranging from homogeneous spherical particles[48] to more complicated heterostructure nanotetrapods[49] and core/shell/shell/shell nanoparticles,[50] have been synthesized and studied. And the composition in a single NC has gone beyond pure semiconductor material, to hybrid organic-inorganic or semiconductor-metal.[6,10,51] Colloidal NCs that are equipped with functional groups for either biocompatibility or targeting are successfully used in biolabeling and biosensing.[2,51,52] More importantly, the easy realization of colloidal heterostructure NCs consisting of two and three semiconductor materials opens an additional channel to manipulate charge carrier thermalization. Figure 1.1 demonstrates a few examples of the structure of colloidal NCs.

Generally, the colloidal synthesis is temporally separated into two steps: relatively rapid nucleation and the following slow growth, for narrow size distribution.[48] Nucleation is initiated by quick injection of the precursor into the hot coordination solvent, resulting in decomposition of precursor regents and supersaturation of monomer that is relieved by the generation of nuclei. Then the growth of particles is followed by adding monomers to

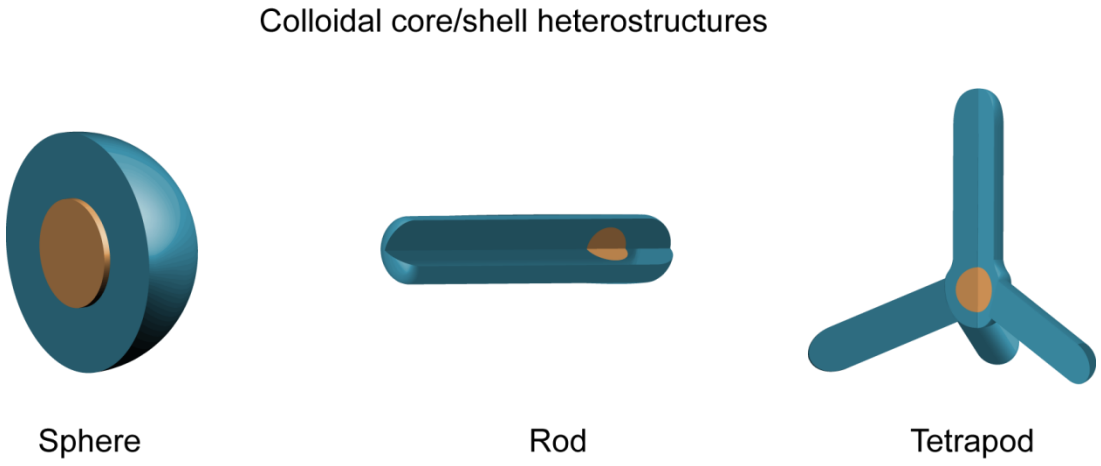

Figure 1.1 Structures of three colloidal heterostructure nanocrystals.[12]

the existing nuclei, which grow into large particles at lower temperature. Size is controlled by reaction temperature, precursor concentration, concentration of coordinating ligands and so on;[17,53] shape can be controlled through selective adhesion of ligands to prevent growth in certain direction,[53] suitable monomer concentration,[54] or growth from seeds of specific crystal structure.[49] Due to the high surface to volume ratio of NCs, surface defect emission can dominate the photoluminescence (PL) spectrum and significantly reduce PL quantum yield.[55,56] Therefore, surface passivation using either organic ligands or an outer inorganic shell of large band gap has become a standard practice.[1,3,10] Blinking and spectral diffusion are more delicate phenomena that are directly linked to surface states.[32] Suppression of blinking can principally be achieved in large particles,[46,57] or through various surface passivation techniques, such as alloy types of interface,[34] thick epitaxially grown shell,[33] or good organic capping ligands.[10] The effect of defects, commonly termed “traps”, on optical and electronic properties will be further discussed in Section 1.4.1.

1.1.2 Electronic Properties

The most important parameter of a semiconductor material is the energy gap between the conduction band and the valence band. In bulk materials, atoms are arranged periodically according to the crystalline lattice to approximately infinity, where electrons move in the periodical potential of the lattice. To explain the existence of electronic bands and the band gap, a simple picture of just two atoms, each of which contributing one conduction electron, is a good place to start. Depending on whether the wavefunctions of the two electrons overlap (bonding) or repel (antibonding) each other, two energy levels form: the bonding state of lower energy and the antibonding state of higher energy, which are similar to the highest occupied molecule orbital (HOMO) and lowest unoccupied molecular orbital (LUMO) levels in the molecular orbital theory (see Section 1.2.2). Without external stimuli, both electrons occupy the bonding state, which is the ground state. In the bulk semiconductor, 2N electrons fill up the lower energy bonding states of negligible spacing compared to the thermal energy, and thus form the filled valence band; in the meantime, the antibonding states of higher energy form the empty conduction band.[35,58] In the language of the Bloch theorem, the two standing waves forming at the boundaries of the Brillouin zone, respectively, represent the anti-bonding state where electron density concentrates around atoms and the bonding state where electron density concentrates between atoms.[35] An energy gap forms between the conduction band and the valence band where no energy state is allowed. The size of the band gap of a bulk semiconductor is a material constant that does not change with physical dimensions. However, in semiconductor NCs of finite spatial extent, an additional standing wave condition is imposed by the confinement boundaries in one

dimension or multiple dimensions and allows only a few transitions out of the continuous band in the bulk.[7] Therefore NCs form discrete energy states of spacing larger than the thermal energy, similar to that of molecular compounds, as shown in Figure 1.2, rather than the continuous energy distribution as in the bulk.

The energy gaps of NCs increases inversely with size *R* roughly following a function $1/R^2$ due to the increase of kinetic energy in smaller NCs, which is the reason of the size-dependent shift of absorption and emission spectra as shown in Figure 1.3.[59-61] This effect in low dimensional semiconductor systems is referred to as *Quantum confinement* and was first investigated by Efros and Brus.[7,62] Due to band filling or weak interaction, the quantum confinement effect sets in at a relatively larger size in semiconductors compared to metal, insulator or molecular crystals.[1] The energy diagram of NCs shown in Figure 1.2 is very simplified based on the particle-in-a-sphere model for spherical particles. Each hole energy level is eightfold degenerate,[61] which is lifted when taking into account the shape asymmetry, crystal field and the exchange interaction. Consequently, each

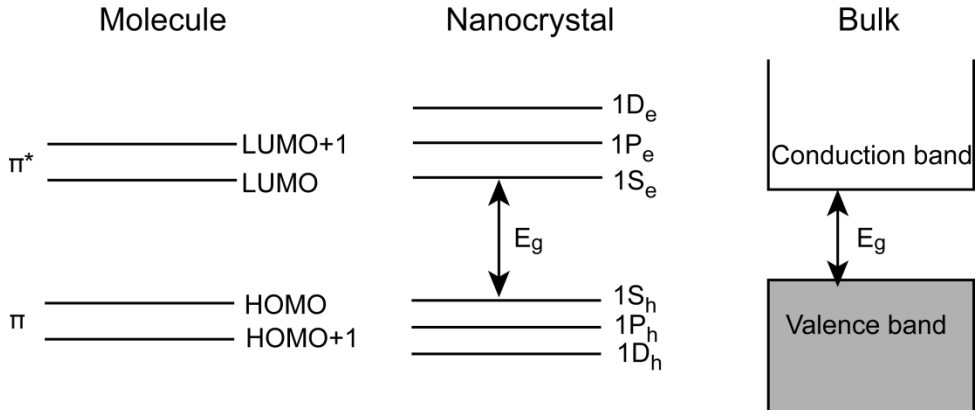

Figure 1.2 Band diagrams of the molecule, nanocrystal and bulk semiconductor. Compared to continuous conduction and valence band that are separated by an energetic gap E_g in bulk, each molecular orbital is a discrete energy level in the molecules. Nanocrystals show features that bridge the gap of both extremes.

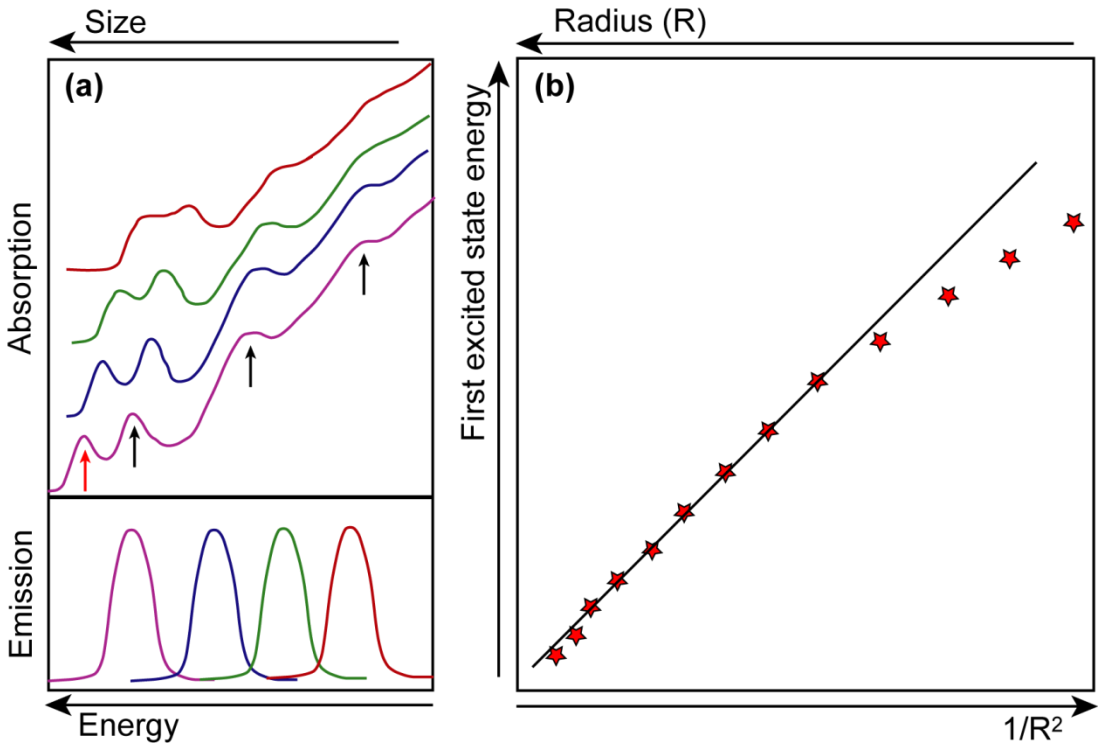

Figure 1.3 Size dependence of absorption and emission spectra. (a) The absorption and emission spectra shift to a higher energy as size of nanocrystals decreases. Several peaks (indicated with arrows) can be observed in the absorption spectrum due to the splitting of the band edge state.[63] (b) The energy of the first excited state (indicated by the red arrow in (a) is plotted as a function of $1/R^2$.[61] Black line is a guide to the eye.

degenerate level can split into a set of sublevels, which explains the fine structure observed in the absorption spectrum and the existence of the "dark exciton."[64,65] As a NC is optically or electrically excited, an electron is promoted from the $1S_h$ state to the $1S_e$ or higher states, leaving a hole behind and forming a bound exciton with the hole. The exciton binding energy in the bulk semiconductor depends on the exciton Bohr radius r and can be defined as

$$E_b = \frac{e^2}{8\pi\varepsilon\varepsilon_0 r^2} \tag{1.1}$$

where e, ε_0 and ε are the charge of a electron, vacuum permittivity, and the relative dielectric constant of the semiconductor, respectively. The exciton Bohr radius in bulk CdSe is 5.4 nm, corresponding to a binding energy of 16 meV.[66] This small binding energy characterizes these weakly bound excitons as the Mott-Wannier type of excitons. Due to quantum confinement, the exciton binding energy in NCs increases with the decrease in size as the coulombic interaction between charge carriers gets stronger.[66] For example, as the size of a CdSe nanoparticle decreases to 2.5 nm, the exciton binding energy increases to about 400 meV.[67] The above binding argument works best in the region where the size of NCs is smaller or approaching the Bohr radius, where the coulombic interaction is the main force.[66,68] In the strong quantum confinement regime, where size is smaller than the Bohr radius (the diameter of the CdSe cores of NCs in this study is 4 nm), the treatment of the electron and hole as a bound pair becomes difficult. Instead, it is more appropriate to treat them separately.[60] But the size tunability of properties is still valid.[66]

An important effect arising from strong quantum confinement in NCs is the increased interaction between excitons due to the forced wavefunction overlap and the reduced dielectric screening.[69] This effect results in formation of multiexcitons[63] and rapid Auger processes at sufficiently high excitation density.[70] The Auger processes can also result in charging of NCs which largely modify the electrical properties of NCs. Due to its importance to this study and the length consideration, a detailed discussion of charging will be given in Section 1.4.1.

The above statements are made based on homogeneous semiconductor NCs, which consist of one semiconductor material. As mentioned in the proceeding text, higher band

gap materials are very often grown as an outer shell on top to passivate the inside core, which eliminates surface states, for example, in the CdSe/ZnS core/shell spherical NCs. In this type-I heterostructure, both electrons and holes are confined in the core of lower band gap as shown in Figure 1.4a.[3] But the conduction band and the valence band of the shell can also be easily tuned to be either aligned, lower or higher than that of the core through size changes or use of different materials.[49,71] Consequently, electron (hole) can localize in either the core or the shell, or delocalize over the entire NC.[8,12,72] When electrons and holes are localized in separate regions within a single heterostructure NC, the type-II band alignment is achieved as shown in Figure 1.4b.[71,73] One important application of type-II heterostructure NCs is in lasers[18,71] due to the internal electric field induced by separated electrons and holes that lifts the degeneracy in the lowest excited state through the Stark effect. Therefore optical gain in the single exciton region can be obtained, which removes the obstacle of necessitating rapid optical gain decay due to nonradiative Auger recombination from the development of quantum dot lasers.[18] Between the type-I and the type-II band alignment there lies an interesting region–the quasi type-II band alignment–where either conduction bands or valence bands of two different materials are aligned; as a consequence, one type of charge carrier is delocalized

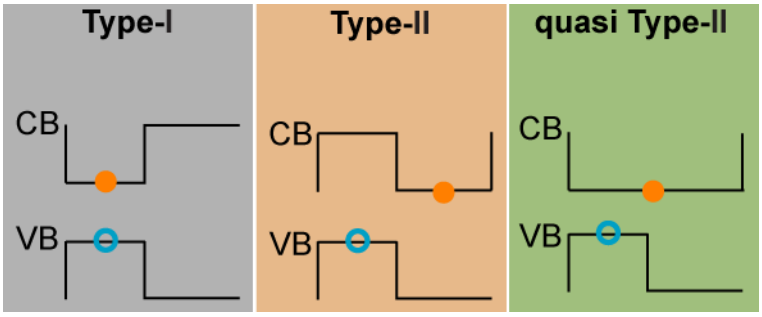

Figure 1.4 Three types of band structures of heterostructure nanocrystals. The electron is indicated as filled orange dot and the hole is indicated as blue open circle.

over the entire heterostructure while the other is localized in a smaller region.[12,16,74] This wavefunction engineering realized in heterostructure NCs offers a new route to manipulate charge carriers through external stimuli such as electric field and charges,[21,75] which are a significant part of this study.

One great advantage of heterostructure NCs is the separation of the light absorbing region from the emitting region, which enormously increases the luminescence quantum efficiency of NCs as a light-harvesting system.[3,49] For example, in CdSe/CdS nanotetrapods of 50 nm long CdS arms, 99% of incident light is absorbed in the arms rendering PL efficiency above 75%.[49] After exciting with incident light of photon energy higher than the band gap, charge carrier pairs are first generated in the absorbing region and then rapidly relax into a suitable region within the heterostructure following the band structure as illustrated in Figure 1.4. In the CdSe/CdS nanorods of quasi type-II band alignment, it takes about 650 fs for the hole to localize in the CdSe core when excited in the CdS arm.[76] However, the delocalization of the electron to the CdS arm is almost instantaneous when excited in the CdSe core.[76] The presence of trap states can also affect the thermalization of charge carriers in heterostructure NCs by localizing the electron or hole at the trap sites instead of relaxing to quantum confined states.[77]

To provide further independence of wavefunction engineering of different functional regions within a single heterostructure NC, a type of core/shell/shell(/shell) spherical NCs was developed. This NC demonstrates dual-color emission from both the core and a shell layer.[50,78] Independent tunabilities of both the core and the shell emitting regions enables control over the direction of energy flow between the core and the shell and the optimization of overall emission color as a white light source.[50,78]

Due to the small dimension of NCs, the shape also has a large impact on properties. For example, the shape asymmetry lifts the degeneracy in the band edge states which then split into a few sublevels. Each of these sublevels forms an peak in the absorption spectrum as shown in Figure 1.3.[63,79,80] In CdSe/CdS heterostructure nanorods, the "bulb" of excess CdS formed around the CdSe-CdS interface has been shown to affect the sign of exciton-exciton binding energy and the transfer of excitons from the CdS arm to the CdSe core.[12,81] In branched NCs like tetrapods, small variations in arm-to-arm diameter can shape the wavefunction to be more or less delocalized towards a certain arm and thus affects the emission anisotropy.[74]

1.1.3 Optical Properties

Similar to the electrical properties, optical properties of NCs also exhibit structural dependence. In the early days, the study of optical properties of colloidal semiconductors was significantly hindered by the low quality of the materials. The large linewidth of emission spectrum due to the broad size distribution[60] and strong defect emission obscured the observation of any structure-property relation.[82] As discussed in Section 1.1.1, high quality NCs can be synthesized through improved synthesis methods, which show narrow size distribution, defect free emission, and high luminescence quantum yield. Size dependent absorption and emission of NCs as predicted by theory can be clearly observed as shown in Figure 1.3. The Stokes shift, defined by the energy difference between the first absorption peak and the emission peak, also decreases with increasing size.[60,83] The PL emission generally originates from the band edge states even when the NCs are excited with photons of energy that are higher than the band gap. Thus generated "hot" electrons quickly relax to the band edge state through quick intraband

relaxation within a few hundred fs.[80,84,85] Emission from a higher excited state is made possible through state filling when excitation density is sufficiently high. The dependence of optical properties on the shape of NCs is highly linked to wavefunction engineering as mentioned briefly in the last section. When the shape of the NCs changes from 0-D sphere to 1-D rods, the emission becomes linearly polarized along the long axis.[86] This effect was later attributed to the large dielectric contrast between the nanorod and the surrounding matrix.[9,87]

The PL decay dynamics of NCs is strongly affected by the optically forbidden band edge state– the "dark" state–which is one of the splitting band edge states due to the exchange interaction. At room temperature, the PL intensity of NCs shows a monoexponential decay with a lifetime of a few to a few tens of ns at short delay time before it evolves into a power-law decay mediated by trap states at long delay time.[59,64,88] The decay lifetime depends strongly on both the size of NCs and the temperature. Several experiments have shown that the lifetime decreases with the increase of size.[59,60] This observation was first ascribed to surface localization of holes which generates two surface states of high and low oscillator strengths respectively.[60] However, later investigations revealed that surface modification of NCs shows no effect on the lifetime, which disagrees with the surface state argument.[83,89] Further experiments performed at liquid helium temperature or under magnetic field,[64,89] established that the size and temperature dependence of the decay lifetime of NCs can be explained through band edge fine structures.

As a simplified model, the band edge transition $1S(e)$-$1S_{3/2}(h)$ split into two transitions due to exchange interaction: the "dark" state ($|D\rangle$) that is optically passive and

the "bright" state (|B>) that is optically allowed as shown in Figure 1.5. The exchange interaction is proportional to the overlap of the electron and hole wavefunction, which can be up to tens of meV in NCs compared to a few meV in the bulk.[83] Therefore, the energy gap $\Delta E_{B\text{-}D}$ between the bright and the dark state is size dependent and larger for smaller NCs,[83] which is the origin of the size dependence of radiative lifetime of NCs.[59] When the thermal energy is lower than $\Delta E_{B\text{-}D}$, the thermalization rate γ_{th} between the "bright" and "dark" states is slow, and it is mostly the dark state that is populated through intersystem crossing γ_0.[64,83] Therefore, a single NC shows biexponential decay. The initial fast decay and the following slow decay are attributed to the bright exciton and the dark exciton, respectively.[64] As temperature increases to a point that the thermal energy is

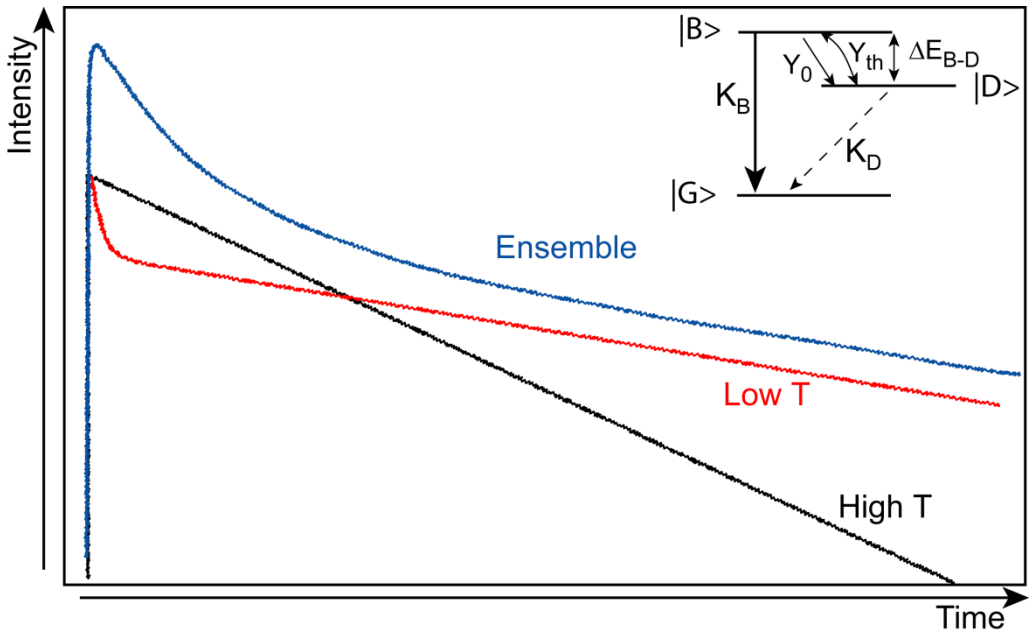

Figure 1.5 Temperature dependent PL decay of single NCs (redrawn from Ref.64). At the low temperature, the single NC shows biexponential decay (red) due to the initial rapid recombination of the "bright" excitons and the following slow recombination of the "dark" excitons, respectively. At the high temperature, the decay curve becomes monoexponential (black) as thermalization between the "bright" and the "dark" states is faster than the recombination rate K_B. For comparison, an ensemble of NCs shows a multiexponential decay (blue) due to different decay rates of NCs of different sizes.

close to or bigger than ΔE_{B-D}, both states are equally populated since γ_{th} is larger than the radiative decay rate K_B of the "bright" state. In this case, the emission mostly stems from the "bright" state and shows a monoexponential decay with a lifetime that is twice the lifetime of the "bright" exciton.[64] Mediated through the size dependence of ΔE_{B-D}, the decrease of the "dark" exciton lifetime with increasing size is possibly due to a stronger mixing between the "bright" and "dark" state at a smaller energy gap.[59]

It has been shown that emission of NCs are extremely sensitive to local environmental fluctuations due to their small size.[14,15,75] A single NC has been shown to randomly jump between an emissive "on" state to an less emissive "off" state in time ranges from milliseconds to minutes.[32] Furthermore, the emission peak position randomly diffuses.[14] But in general, NCs are more stable compared to organic dye molecules, which makes NCs very suitable for applications as biolabels,[2] especially the non-blinking NCs.[33,34] The conventional charging model provides a fairly good explanation to most of the blinking related behavior in single NC.[13] But recent experiments suggest modification to this theory is needed to take into account new-discoveries.[90,91]

1.1.4 Multiexcitons

At low excitation density, the excitation pulse generates one electron-hole pair, which then relaxes to the lowest excited state and forms a single exciton as shown in Figure 1.6a. At higher excitation density, there is a considerable possibility of exciting more than one electron-hole pairs a single NC, which form multiexcitons. The two mechanisms that govern the generation of multiexcitons are *state filling* and *coulombic interaction*. Considering a scenario that involves no more than three electron-hole pairs in a single NC, a simplified four-level system is used here to discuss the generation of a single

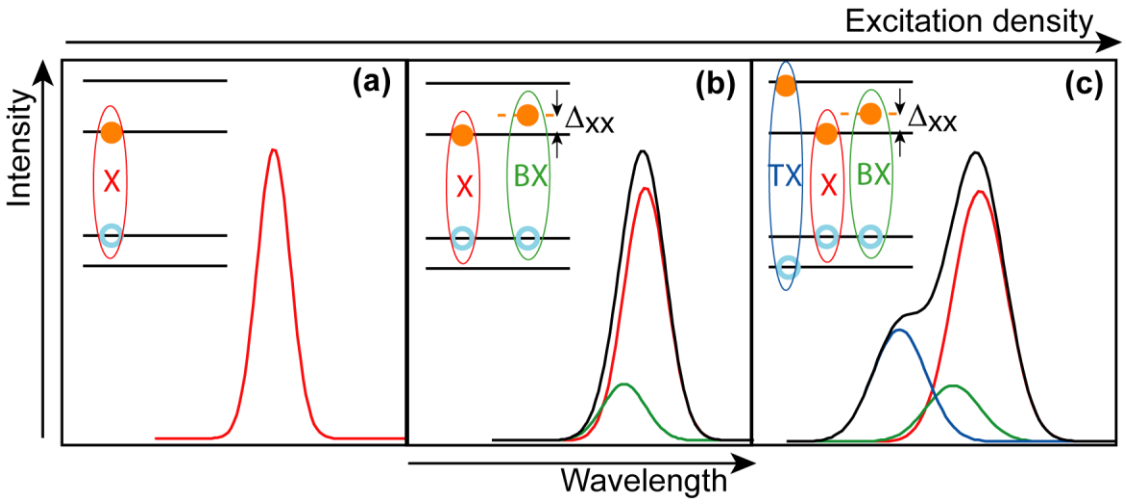

Figure 1.6 Generation of multiexcitons. (a) At the low excitation density, only the single exciton X (red) is formed. (b) As excitation density increases, biexciton BX (green) starts to appear. Coulombic interaction between excitons shifts the energy of the biexciton by Δ_{XX} (positive in this case) with respect to the single exciton. (c) At very high excitation density, the newly generated exciton occupies a higher excited state due to the Pauli exclusion principle, which is the triexciton TX (blue). The PL spectra at different excitation densities consist of emission of the populated exciton species.

exciton, a biexciton and a triexciton. Because of the Stark effect resulting from the coulombic interaction between the pre-existing exciton and the newly generated one, the energy of the latter is shifted by Δ_{xx} from that of the first exciton as shown in Figure 1.6b. Together these two excitons form a biexciton. The binding energy Δ_{xx} can be either positive (when the exciton-exciton interaction is repulsive like in this case) or negative (when the exciton-exciton interaction is attractive) depending on the electronic structure of the NCs. Because the coulombic interaction is inversely proportional to the distance, the binding energy of the biexciton in NCs scales with size and increases as size decreases.[63,92,93] When the excitation density increases to a point where the absorption rate equals the biexciton Auger recombination rate, the biexciton population saturates and higher excited states start to be occupied.[94] Due to the Pauli exclusion principle and state filling, the third exciton is excited to a higher energy as illustrated in Figure 1.6c, which

emits as a triexciton.[95] Note that the triexciton is sometimes defined as a charged biexciton.[63] The number of excitons generated on a single NC is governed by a Poisson distribution

$$P(N) = \frac{\langle N \rangle^N e^{-\langle N \rangle}}{N!} \tag{1.2}$$

where P(N) is the probability of having N excitons, and <N> is the average number of excitations per NC as calculated from the absorption cross section and excitation density.

Although the binding energy is usually negative in bulk semiconductors and large epitaxially grown quantum dots,[96] recent experiments on GaN quantum dots have shown that the binding energy can switch from positive to negative with decreasing exciton emission energy.[68] The underlying mechanism of this controversial trend is similar to the switch of exciton binding energy from negative in type-I heterostructure NCs to positive in (quasi) type-II heterostructure NCs.[81,94,97] Experiments have suggested that this switch is due to two reasons: increased correlation interaction resulting from increased electron-hole separation,[98] and repulsive coulombic interaction in fixed single-particle orbitals.[94] This control mechanism offers another route to design NCs that are especially suitable for applications as gain medium for lasers.[18,81] While separation of the electron and hole wavefunctions might be beneficial for biexciton yields due to suppressed Auger recomnination,[99] it reduces the yields of the triexciton, since the oscillator strength of the triexciton is proportional to the overlap of the electron and hole wavefunctions.[94,97]

Multiexcitons can be identified by additional emission peaks in the PL spectrum appearing with increasing exciton density as shown in Figure 1.6.[18,68,71] Depending on whether the biexciton binding energy is positive or negative, the observed biexciton peak

either shifts to the red or blue with respect to the single exciton peak.[68,81,97] The assignment of the biexciton peak can be confirmed by a quadratic power dependence of emission intensity on excitation density since it is a two-photon process.[63] The triexciton peak is always blue shifted compared to the single exciton peak since it originates from a higher excited state. An example of the evolution of PL spectrum with excitation density is shown in Figure 1.6.

Due to the nonradiative Auger recombination that is intrinsically associated with multiexcitons, they usually decay within a few ten to a few hundred picoseconds in type-I hetero-NCs. Therefore, the PL decay rate of NCs increases with increasing excitation density as shown in Figure 1.7. This decay lifetime scales with the volume of NCs, which has been observed in both CdSe and PbSe systems[18,100] and is consistent with theoretical predictions.[70] Morphology is another route to control the Auger process. Elongated nanorods have been shown to have longer biexciton Auger lifetime[101] and improved optical gain compared to the spherical NCs.[102] In CdSe/CdS core/shell nanorods– where the electrons are delocalized into the CdS shell while holes are localized in the CdSe core, a strong suppression of Auger recombination and long lifetime of the optical gain is observed using the transient absorption measurement.[99] The common feature in systems of extended Auger lifetimes is the separation of the electron and hole. As a consequence of the charge carrier separation, the Auger lifetime no longer scales with volume V, but is modified to scale with $V \cdot \Gamma_{rad}$, since the radiative lifetime Γ_{rad} is greatly affected by this charge separation.[94] As a consequence, the biexciton lifetime can be increased to 2 ns.[94]

To study the rapid decay of multiexcitons, fast spectroscopic tools are required. The two commonly used techniques are the transient absorption and the time-resolved

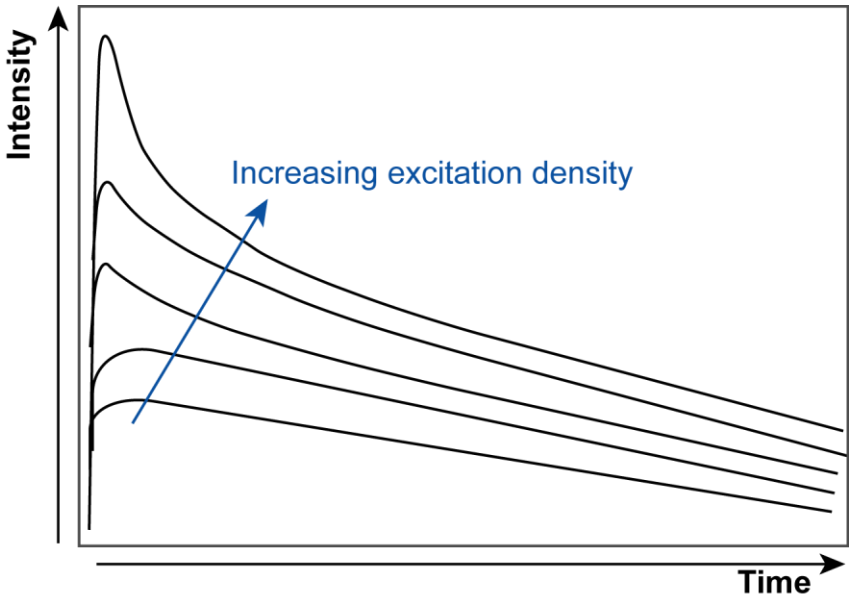

Figure 1.7 Increase of decay rate with increasing excitation density. The rapid increase of the initial decay rate is attributed to the fast nonradiative Auger recombination.

fluorescence spectroscopy. The former method can probe multiexcitons in the excited state in a time range from a few fs up to a few ns, during which formation of multiexcitons either results in additional peaks or a spectral shift of the single exciton bleaching peak.[63] On the other hand, the latter technique records emission from multiexcitons from picoseconds up. This technique offers direct measurement of the energy of the multiexcitons, their decay lifetimes, and any signature of lasing. In this study, time-resolved spectroscopy was performed using two systems: a streak camera with a resolution of a few ps and a gated intensified charge-coupled device (ICCD) with a resolution of a few ns.

Exciton (or carrier) multiplication- which is the generation of multiple excitons through the absorption of a single photon of an energy that is at least three times greater than the band gap– is another effect stemming from the strong coulombic interaction

between carriers in NCs.[100,103,104] However, this effect is still under heavy debate due to controversial experimental results,[100,104] and lack of a solid theory.[103]

1.2 π-Conjugated Molecules

In the last section, inorganic semiconductor NCs were introduced. There it was shown that NCs behaved like an emissive organic molecule of discrete energy levels by reducing the size of the particle to a few nm. Here we will see that organic macromolecules built from a few to thousands of atoms can also behave like semiconductors. Organic semiconductors can be built in two approaches. One approach is by arranging small organic molecules periodically to form crystalline structures, in which molecules are held together by the weak van de Waals force. Properties of this type of material systems largely depend on the collective interaction of the participating molecules.[29,105] Study in this field since the 1960s has yielded the realization of organic field effect transistors, a cheaper alternative compared to the traditional Si based devices.[27] The second approach is through synthesis of conjugated polymers of length scale from a few nm to μm, in which delocalized pi-electrons over the conjugated backbone set the basis of the electrical properties of these macromolecules. Since the pioneering work of A. J. Heeger, A.G. MacDiarmid and H. Shirakawa in 1978 on doped polyacetylene of metal-like conductivity, research on organic semiconductors has gone beyond scientific interests into commercial products. For example, conjugated polymer based organic lighting emitting diodes (OELDs) have been successfully used in color displays on cell phones, televisions and various other appliances;[23] and organic solar cells are approaching the required efficiency to compete with amorphous silicon counterparts.[24] At the same time, chemists are also working on designing and synthesizing materials of novel chemical

structure to give desirable electrical and optical properties, based on empirical data or quantum chemical calculations.

In this section, the intrinsic optical and electrical properties of pi-conjugated molecules will be introduced starting from molecular building blocks-atoms, to functional moieties, then to a chromophore and an exciton forming on the chromophore. The chromophore serves as the fundamental unit of optoelectronic materials.

1.2.1 *Pi*-conjugation

The term pi-conjugation is given to organic molecules with alternating single-double bond or single-triple bond, in which unhybridized p orbitals of adjacent sites overlap with each other and form larger delocalized pi-orbitals or pi-bonds as shown in Figure 1.8. Despite the term "organic semiconductors" that is associated with pi-conjugated organic materials, the optical and electronic properties of these materials is better described using molecular orbital model than the early band models such as the SSH model.[106]

π-orbitals form through sp^2 or sp hybridization. By mixing the 2s and three 2p orbitals of a fully hydrogen saturated carbon atom, a set of four equivalent orbitals are created, referred to as sp^3 hybridization. When two carbon atoms are linked by a single bond, the sp^3 orbitals of an atom overlap with that of the other and form one sigma bond of cylindrical symmetry as shown in Figure 1.8. It is also possible for the 2s and 2p orbitals to form sp^2 (sp) hybridization when only two (one) of the three p orbitals are mixed with the s orbital, while the remaining one (two) orbital remains unmixed as in the case of double (triple) carbon bond. Consequently, the pure p orbitals of neighboring carbon atoms can overlap with each other and form the pi-orbitals or pi-bonds in addition to the sigma-orbitals. Figure 1.8 illustrates sp hybridization using acetylene as an example,

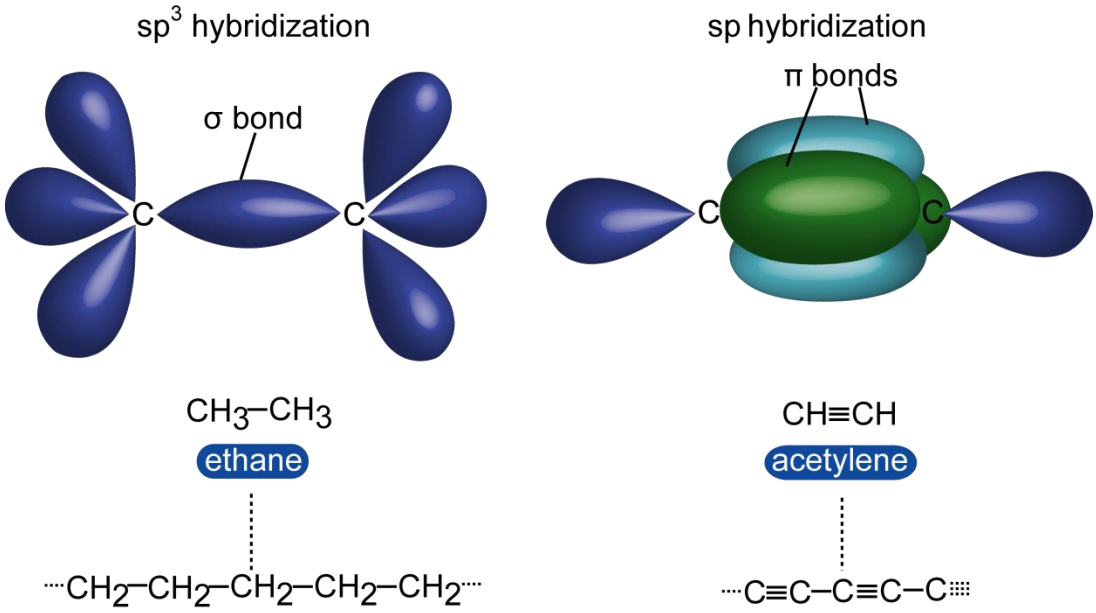

Figure 1.8 sp^3 hybridization and sp hybridization. Carbon atoms in ethane and the corresponding polymer (such as polyethylene) are linked by localized σ-bonds. In acetylene, two π-bonds and one σ-bonds (blocked from view) are formed. Alternation of single-triple bonds in the polymer leads to delocalization of the π-electrons along the conjugated backbone.

where one sigma bond and two pi-bonds form between the carbon atoms. Delocalized electron density above and below the conjugation plane of carbon atoms is established by electrons occupying the π-orbitals. These π -electrons are sufficient in determining the electrical properties of conjugated materials and are also a very important factor in the optical properties.

Extension of conjugated chains by linking additional unsaturated carbon atoms, for example through polymerization, further delocalizes electron density to the added units. Typical π -conjugated oligomers and polymers contain from several to thousands of conjugated units that are capable of forming delocalized π -bonds. The delocalization nature enables quasi-free π -electrons to contribute to the electrical conductivity. As a good example, doped polyacetylene shows 5.6×10^2 ohm^{-1} cm^{-1} electrical conductivity at

room temperature.[106] But polyethylene, consisting of only hydrogen saturated carbons linked by localized sigma-bonds (also shown in Figure 1.8), shows very low electrical conductivity. The latter, a plastic commonly used in plastic bags and bottles, is a very good insulator and shows no interesting optical properties.

To introduce the molecular orbital theory, a simple example of 1,3-butadiene is used as shown in Figure 1.9. Before excitation, electrons occupy the highest occupied molecular orbitals (HOMO), which are the bonding π orbitals. This is the ground state, S_0, of A_g symmetry. After excitation, an electron is promoted from the HOMO to the lowest unoccupied molecular orbital (LUMO) which is an anti-bonding π^*orbital. This one-photon allowed transition is referred to as a π-π^* transition, which excites the molecule to the $1B_u$ excited state (of B_u symmetry). Any one-photon forbidden $2A_g$ excited states (of A_g symmetry) requires the promotion of an electron from the HOMO to LUMO+1or from the HOMO-1 to LUMO or collectively promotion of two electrons from the HOMO to the LUMO. These processes are illustrated in Figure 1.9. The one-photon forbidden $2A_g$ states are the lowest excited states in pure polyenic organic molecules, like the highly conducting polyacetylene, which are nonemissive. The switching from pure polyenic to polyenic-aromatic backbone, like in the poly(*p*-phenylene vinylene) (PPV) type of polymers, lowers the $1B_u$ state relative to the $2A_g$ state. Consequently the $1B_u$ state becomes the lowest excited state and is strongly emissive,[107] which is the reason that primary candidates for polymer-based light emitting devices have mixed polyenic-aromatic backbones. Cross-linking of benzenes with alternating single-double bonds in the PPV type of polymers, or single-triple bonds in the poly(*p*-phenylene ethynylene) (PPE) type of polymers yields some of the most studied

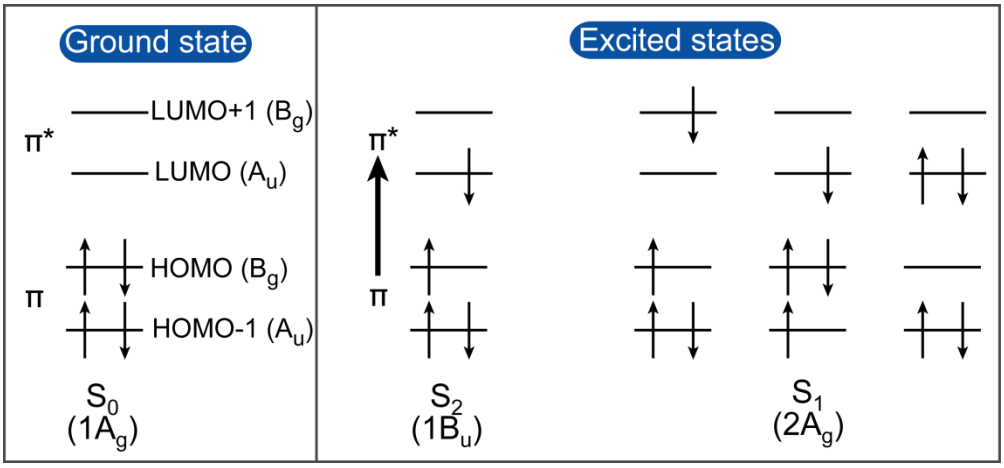

Figure 1.9 π-π^* transitions in 1,3-butadiene. In the ground state, all electrons occupy the HOMO levels. One-photon allowed π-π^* transition promotes an electron from the HOMO level to the LUMO level and forms an excited state of B_u symmetry that is emissive. Symmetry of each molecular orbital is indicated in the parenthesis. Excited states of A_g symmetry are formed by one-photon forbidden transitions, which are nonemissive.[107]

optoelectronic pi-conjugated materials, where benzene units and linear bonds form cross-conjugation along the backbone.[29,108-110]

1.2.2 Intrinsic Electrical Properties

Due to the molecular nature and the semiconducting electrical properties, the scientific community has been debating whether a molecular[111,112] or band-like model,[106] or even a model considering both,[113] would be more suitable to describe how pi-electrons determine material properties. It is difficult to find a coherent description of optoelectronic properties of conjugated materials. The molecular theory treats the excited state as localized excitons, while the band theory views it as delocalized free electron-hole pairs. Since only the lowest excited state is considered in describing the intrinsic properties of materials, the molecular orbital theory is used in this section.[107,113]

Excited state energy is roughly inversely proportional to conjugation length to the power of two. In conjugated polymers, even in the ideal chain, π-electrons are not

delocalized over the entire conjugated backbone. Instead, due to twist or defect sites, typical conjugation lengths only extend over 4-10 repeat units.[107,114,115] Each of these broken conjugation segments along the backbone is a single chromophore,[116] where electrically injected or optically excited excitons are localized. According to the particle-in-a-box model, electrons of mass *m* are confined in the one-dimensional potential well of length *L* with infinitely high boundaries at the ends of the chromophore. To zeroth-order approximation, the energy of the *n*th energy state is

$$E_n = \frac{(n\pi h)^2}{2m^2L^2} \tag{1.3}$$

where h is the Planck constant. 2N electrons in a chromophore fill orbitals to the E_N energy state according to the Pauli exclusion rule, forming the HOMO level or π orbital in molecular orbital language as shown in Figure 1.9. This HOMO level is the ground state of the chromophore. The next energy level E_{N+1} is the LUMO level, or the π^* orbital, which is the lowest excited state. In the semiconductor terminology, the energy difference between N+1 and N states ($\Delta E = E_{N+1}-E_N$) can be defined as the band gap.

Excitons are formed on a chromophore after optical excitation which causes a π-π^* transition. After absorbing a photon, an electron is excited into the LUMO level and leaves a vacancy (or hole) behind in the HOMO level. Coulombic interaction between the electron and hole binds the electron-hole pair together into an exciton in a localized configuration within the chromophore. The binding energy of the exciton is estimated as

$$E_b = -\frac{e^2}{4\pi\varepsilon\varepsilon_0 r} \tag{1.4}$$

where e is the charge of a single electron, ε_0 is the vacuum permittivity, r is the exciton Bohr radius, and ε is the dielectric constant. The exciton binding energy in pi-conjugated molecules is larger than that of inorganic semiconductors due to the three-times-smaller-dielectric constant in organic compounds. So-formed excitons are more tightly localized within a chromophore of size 20-25 Å via a process called exciton *self-trapping*.[117,118] During this process, excitons quickly relax through vibronic coupling from an absorbing state delocalized over the entire chromophore to a more localized emitting state, which finally generates excitons of 1-2 nm size.[117,119,120] Therefore, a tightly bound Frenkel exciton is formed in isolated pi-conjugated molecules, compared to the Mott-Wannier exciton formed in inorganic NCs.

This localized exciton model invokes the hopping nature of energy transfer from a high energy chromophore to the neighboring lower energy chromophore along the backbone as discussed in Section 1.3.2.[111,121] However, the Frenkel exciton model breaks down either by exciting the molecules into a very high energy state, or by strong electronic coupling that delocalizes the exciton over nearby chromophores.[4,113,122,123]

Aside from localized Frenkel excitons, polaron pairs or charge-transfer excitons are another frequently generated electron-hole pair type in π-conjugated molecules, which are loosely bound and easy to dissociate compared to excitons.[124] These charge carrier pairs are of great importance in organic photovoltaic devices as the goal there is to improve the efficiency of exciton separation. Polaron pairs are formed when the electron and hole are delocalized on different chromophores on the same or different polymer chains.[109,124] They are also believed to be the precursor states for excitons after charge injection in an electroluminescent device, like organic light emitting diodes

(OLED).[125,126] Due to the delocalized nature of polaron pairs, the Wannier exciton model is more useful in studying their properties.[105]

1.2.3 Intrinsic Optical Properties

Following the same molecular-orbital theory used in the previous sections, light absorption drives π-π* transition in π-conjugated molecules, which generates singlet excitons by exciting the molecule from the ground state S_0 to the excited state S_n (n=1, 2, 3…) as shown in Figure 1.10. Optical excitation does not generate triplet excitons since the optical transition operator–which is the electric dipole moment operator–only appears in the electronic parts of the wavefunction in perturbation theory. The total energy of a molecule is approximately the sum of electronic and vibrational energy by neglecting the rotational energy since it is relatively small. The origin of electronic energy has been introduced in the previous section, and the vibrational energy E_v comes from coupling of nuclei with electronic transitions, also known as the vibronic coupling of electron and phonon. Based on the Born-Oppenheimer approximation, there is an equilibrium potential energy surface associated with each electronic state with a set of vibronic levels, labeled ν= 0, 1, 2… representing ascending vibrational energy. As electronic transitions takes place in less than 10^{-15}s compared to the much slower nuclei reconfiguration time of about10^{-13}s,[105] the electronic transition from one electronic state to another is finished without change of nuclei position, which is denoted as the vertical transition in Figure 1.10, or a Franck-Condon transition. The excited state has a short lifetime and returns to the ground state within a few ps to μs depending on the dipole selection rule for a specific transition. For molecules that obey Kasha's rule,[127] radiative transitions happen from the lowest excited state after nonradiative internal conversion in less than a few fs from upper

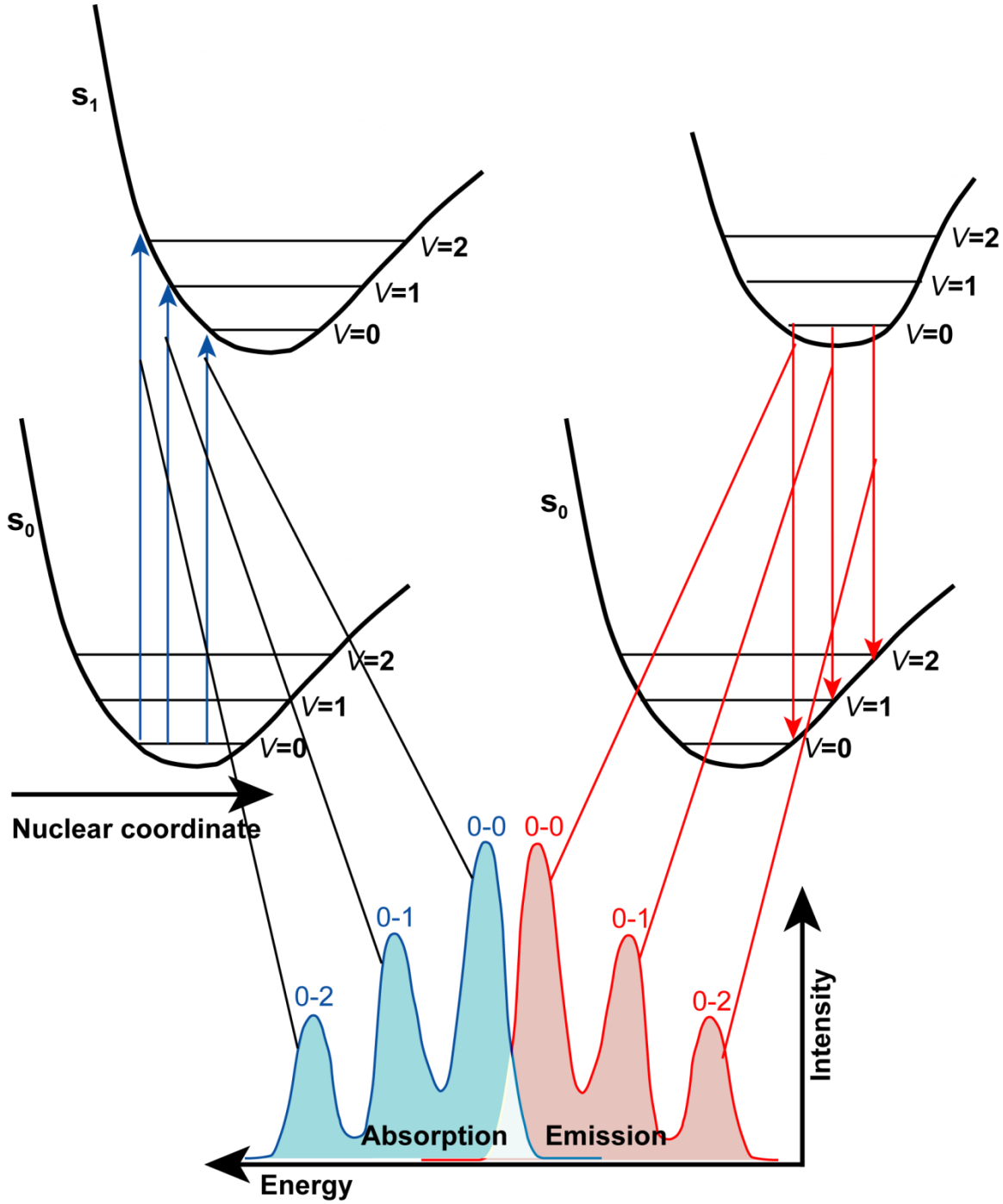

Figure 1.10 Schematic of the S_0-S_1 transition with vibrational levels. Each electronic state (S_0 or S_1) is associated with a potential energy curve in the nuclear coordinate. Besides the pure electronic transition (0-0), transitions from the vibrational levels (v=1, 2) result in vibronic peaks in the mirror-symmetry absorption and emission spectra.

levels, emitting a photon in the form of fluorescence, or radiating heat.[105]

The above processes all happen within the singlet spin manifold, however, strong emission from the forbidden triplet states is also observed in the form of phosphorescence in organic materials.[128] With the presence of heavy metal atoms,[129,130] phosphorescence is especially strong due to increased intersystem crossing between singlet and triplet spin manifolds. The triplet state constantly lies about 0.7 eV below the singlet state in nearly all homopolymers where singlet and triplet excitons are localized to the same extent.[131] However, in certain heteropolymers, the exchange gap can be reduced through delocalizing singlet excitons over localized triplet excitons.[128]

It is hard to overestimate the importance of spectroscopy in studying optical properties as can be easily seen from the symbolic spectrum drawn in Figure 1.10. All spectroscopic techniques involve detecting of a signal at certain energy, which can be optical as in all absorption and emission spectra, electrical like in the case of photocurrent measurement, or magnetic as in optically detected magnetic resonance (ODMR).[126] Each spectral peak in an optical spectrum corresponds to a transition between two energetic states. Unfortunately, assignment of spectral peaks can be complicated by the existence of defects,[132] dark states,[133] and thermal broadening, which is why different experimental techniques are performed jointly to probe the full parameters of the material properties for cross proof of conclusions.

1.3 Energy Transfer and Molecular Aggregates

1.3.1 Motivation of Using Model Systems

In the previous section, the intrinsic properties of organic π-conjugated oligomers and polymers in isolation from influences of the environment or other molecules were

summarized. Despite the successful demonstration of device concepts based on a single molecule,[134,135] it is the bulk organic films or single crystals that serve as the active areas in the majority of organic optoelectronic and photovoltaic devices.[136] In these bulk states, interchromophoric interactions between different conjugated segments of the same molecule or different molecules contribute largely to the final properties that a molecule presents.[29,137-139] Unfortunately, the poor understanding of the intra- and intermolecular interaction remains an obstacle to the construction or optimization of practical devices based on organic materials.[109]

The intramolecular interaction is especially important in individual polymer chains, where the constituent chromophores are statistically situated in a local environment varying strongly from one site to another. As shown in Figure 1.11, energy transfer is favored from chromophores of high energy to chromophores of low energy until reaching the nearby chromophore of lowest energy where emission takes place. This hopping process leads to a redshift of the ensemble emission spectrum within picoseconds, which can be resolved in time-resolved spectroscopy.[137,140] In addition, the fact that there are more absorbing chromophores than emitting chromophores suggests differences between the excitation polarization and the emission polarization and an energy transfer induced depolarization.[141-144]

The electronic and optical properties depend largely on the physical conformation of molecules and the way the molecules are packed together, which influence intermolecular interactions.[29,109] These morphological properties vary with processing conditions such as: solvents, thermal annealing, and concentration.[109] This vulnerability yields many controversial results in the literature.[109]

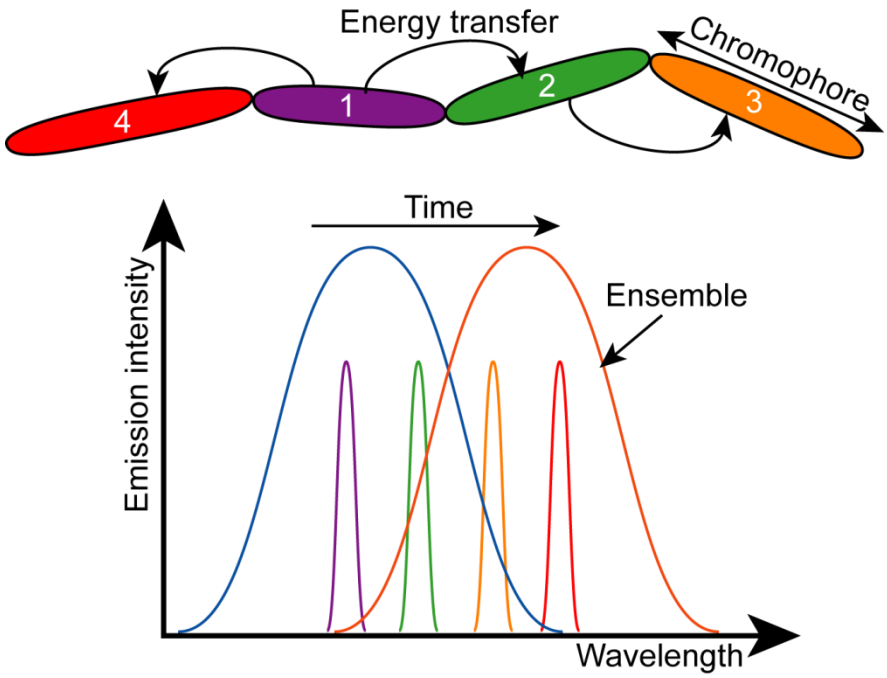

Figure 1.11 Energy transfer between chromophores along a conjugated polymer chain. Each chromophore shows a size dependent emission peak (narrow peaks). Energy transfer from the high energy chromophores to the low energy ones leads to a shift of the ensemble emission spectrum (broad peak) toward a longer wavelength with delay time after excitation.

Intermolecular interaction through excitation energy (or exciton) transfer is the key process for the device applications. Similar to the incoherent exciton hopping between chromophores along the polymer chain shown in Figure 1.11, excitons can also hop between adjacent molecules. In photovoltaic devices based on blended materials of different HOMO and LUMO levels, such as the well studied P_3HT/PCBM blend film used in organic solar cells,[124] efficient exciton hopping is crucial to achieve exciton dissociation at the boundaries of two material domains.[145] Coherent energy transfer is added to intermolecular interactions when the intermolecular distances are so close that strong electronic coupling results in direct excitation energy delocalization between molecules.[119,139,146] Different interchain species, such as aggregates and excimers,[109,138,147,148] are formed in this strong coupling regime depending on how the

molecules interact. The emission spectrum, decay lifetime and charge transport across the bulk are largely altered by the interchain species.[105,149]

To isolate these practical complications and gain insight into how molecules interact, model molecular systems are designed to mimic the intermolecular processes through intramolecular interchromophoric processes in controllable fashion. As illustrated in Figure 1.12, various model systems can be synthesized to contain chromophores arranged in different orientation and space. The use of model molecular system offers a toolbox to study the complex intermolecular interaction in (opto)electronic devices in a simplified and controllable way.

1.3.2 Incoherent Energy Transfer

Fluorescence resonance energy transfer (FRET) or Förster transfer refers to a radiationless transition of energy from an excited donor to an acceptor in the ground or

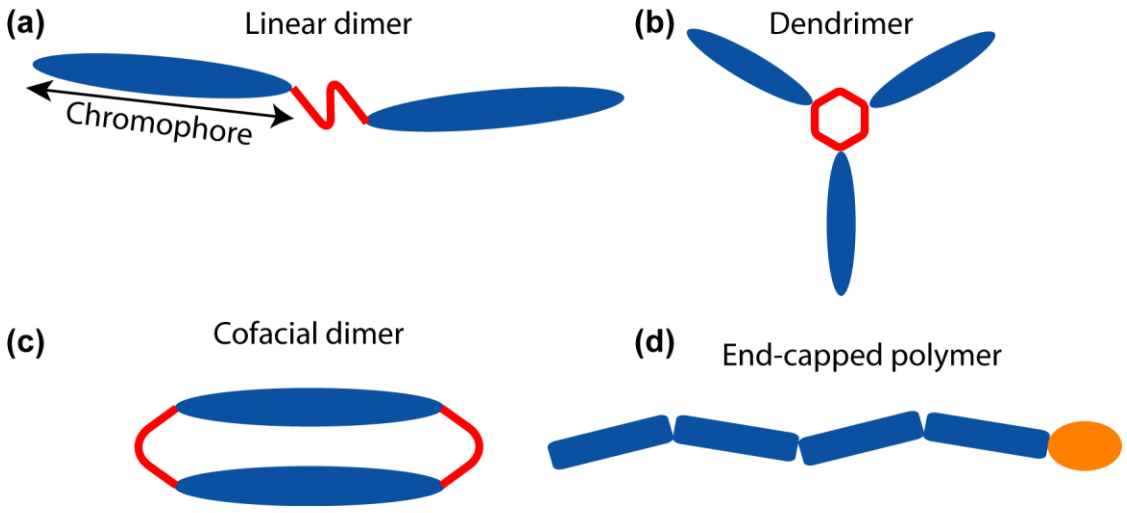

Figure 1.12 Four examples of model molecular systems. Identical chromophores (blue) are linked with various orientation and distances through covalent bonds (red) in linear dimers (a), dendrimers (b), and cofacial dimers (c). In the end-capped polymer (d), a different chromophore (orange) is added at one end of a polymer chain.

excited state. As the dominating long-range energy transfer mechanism, the electronic coupling in this regime can be approximated with only the coulombic interaction between the transition dipoles of donor and acceptor. The Förster theory is applicable to the weak coupling regime where the thermal equilibrium and internal relaxation finish before the transfer process occures.[150,151] Therefore, FRET is incoherent and irreversible. The dipole approximation is made valid by assuming the center-to-center distance between the molecules is much larger than the size or shape of molecules. Thus, according to theclassic electrodynamics theory of dipole-dipole interactions, the FRET rate κ scales with the inverse of distance R^6 between donor and acceptor:[152]

$$k = \frac{\emptyset_D}{\tau_D}\left(\frac{R_0}{R}\right)^6 = \frac{\emptyset_D}{\tau_D}\left(\frac{8.785 \times 10^{-25} I}{n^4 R^6}\right) \tag{1.5}$$

where Φ_D is the fluorescence quantum yield of the donor, τ_D is the decay lifetime of the donor in isolation, n is the refractive index of the medium, and I is the spectral overlap between donor emission and acceptor absorption.

R_0 being the Förster radius at which FRET efficiency drops to 50% is consequently written as

$$R_0^6 = 8.785 \times 10^{-25} \cdot I \cdot n^{-4} \tag{1.6}$$

The FRET is particularly suitable when dealing with energy transfer between non-identical molecules as spectral overlap between the donor emission $f_D(\lambda)$ and acceptor absorption $a_A(\lambda)$ is required. This term is defined as integral I

$$I = \int_0^\infty a_A(\lambda) f_D(\lambda) \lambda^4 d\lambda \tag{1.7}$$

The FRET rate is in the range of a few tens of ns^{-1} to a few hundreds of ps^{-1} depending on the distance between donor and acceptor.[150,151,153] Both spectral overlap between the donor and the acceptor and the refraction index of the dispersing medium can strongly affect the radius of FRET which is generally above 0.5 Å. Below this distance, FRET is beyond the weak coupling limit where Förster theory is no longer valid.[151]

The above theoretic descriptions of FRET indicate a clear dependence of the efficiency of energy transfer on the separation between molecules, or on molecule stacking in films and crystals. The energy transfer rate is increased by one order of magnitude in film compared to solution, which suggests a lower interchromophoric exciton hopping rate along the polymer chain than the interchain transfer rate in the film.[151] A recent modification was made to the Förster theory when the distance R is sensitive to the exact position of donor and acceptor, in which case averaging over coupling between wavefunctions should replace the traditional averaging over wavefunction, and subsequent coupling.[151-153] This modification is especially suitable for the intramolecular energy hopping between chromophores along a polymer chain where the donor and acceptor are arranged in the head-to-tail configuration instead of parallel configuration as shown in Figure 1.12a.

FRET can also act as one cause of fluorescence blinking. The specific pair of donor and acceptor is subjected to local field fluctuation, therefore their emission and absorption follows a subsequent change. In consequence, the spectral overlap $I(t)$ and FRET rate $\kappa(t)$ become time dependent, which causes a type of blinking that is correlated with the spectral diffusion.[141]

Förster's theory is applicable in limited cases under conditions like no energy transfer induced changes in lifetime, line shape or oscillator strength in addition to the requirement of the dipole-dipole approximation. Therefore a new theory is needed in cases of molecular aggregates when both absorption and emission spectra and decay lifetime are altered due to perturbation of the wavefunction of the interacting molecules. This effect is observed in closely bridged dimers as shown in Figure 1.12,[123,154] dendrimers, [155,156] and some interchain species in films and crystals. The last case leads to luminescence quenching in films forming ordered π-π stacking between molecules of a few Å spacing as a consequence of formation of weakly emissive interchain aggregates.[138,157] The next two sections will focus on this topic.

1.3.3 Coherent Energy Transfer

In contrast to requirements of spectral overlap for FRET in the weak coupling limit, coherent energy transfer in the strong coupling regime requires direct spatial overlap between the wavefunctions of donor and acceptor, which is similar to the condition of the strong quantum confinement of charge carriers in NCs. In this regime, the distinction between donor and acceptor becomes meaningless since the interaction is mutual among all interacting molecules or chromophores. Instead of being localized on one molecule, the excitation energy mixes and oscillates coherently between two molecules in a timescale as fast as intraband vibronic relaxation. Therefore, both the electronic and vibronic structures change in the strong coupling regime as shown in Figure 1.13b.

Using the dimer as an example for strong coupling between two molecules, the energy of the newly formed molecular system of mixed and delocalized electronic structure is derived using quantum mechanics as shown in Figure 1.13a. The sharing of

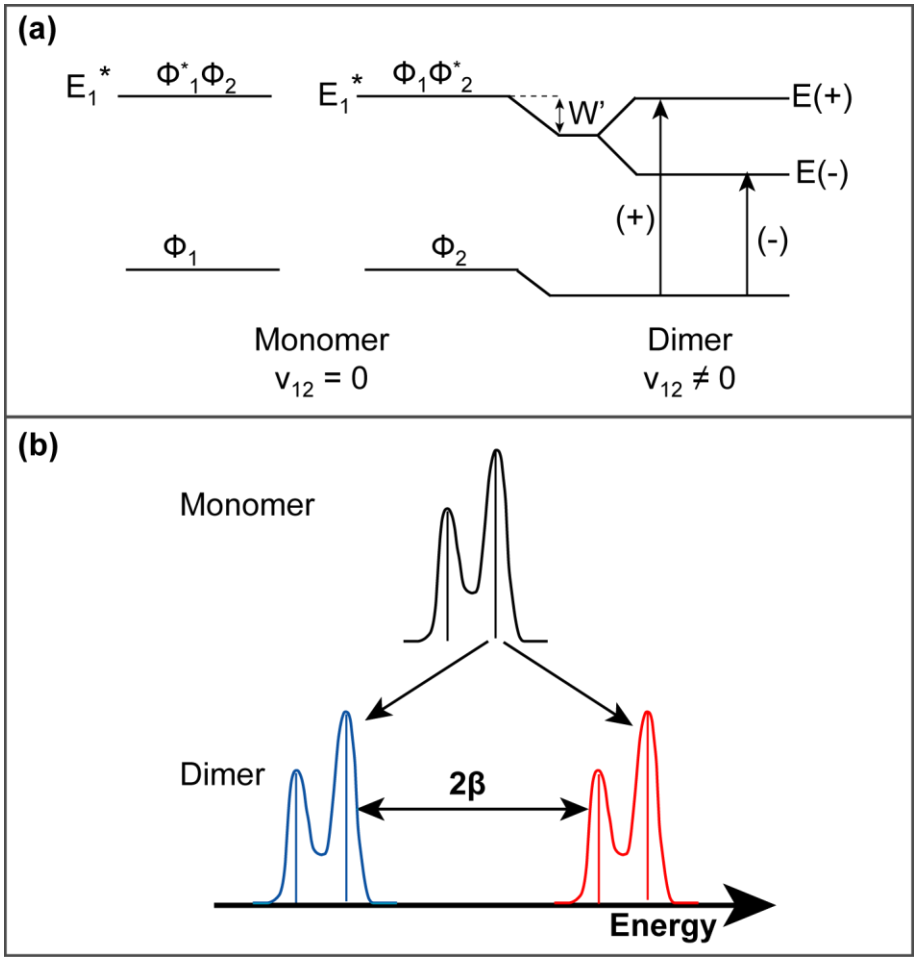

Figure 1.13 Splitting of excited state in the strong coupling regime. (a) When the interaction term V_{12} between the two monomers is nonzero, the excited state of the dimer shifts by W' and then splits into two levels E(+) and E(-). In this diagram, the resonance energy $\beta>0$. (b) Splitting of the absorption spectrum in the dimer (red and blue) with respect to that of the monomer (black).

excitation energy can be described by a wavefunction that is the linear combination of the unperturbed states of the constituent molecules (1 and 2) in the ground state (Φ_1, Φ_2) and the excited state (Φ_1^*, Φ_2^*). Thus the excited state of the dimer can be written as[105]

$$\Phi_E = c_1\Phi_1^*\Phi_2 + c_1\Phi_1\Phi_2^* \qquad (1.8)$$

In the case of dimers of identical molecules, the normalization coefficients are $c_1 = c_2 = 1/\sqrt{2}$, and the excited state energy of each molecule is equal ($E_1^* = E_2^*$). The splitting of dimer energies E(±) is given by

$$E(\pm) = E_1^* + E_2 + W' \pm \beta \tag{1.9}$$

where β is a resonance interaction energy that causes the splitting of the energy of the dimer:

$$\beta = \langle \Phi_1^* \Phi_2 | V_{12} | \Phi_1 \Phi_2^* \rangle \tag{1.10}$$

and W' is the coulombic energy of the interaction of the charge distribution of the excited state of molecule 1 with the ground state of molecule 2 (and vice versa):

$$W' = \langle \Phi_1^* \Phi_2 | V_{12} | \Phi_1^* \Phi_2 \rangle \tag{1.11}$$

V_{12} is the term representing the intermolecular interaction energy, which only represents the electronic interaction in β and W'. The exchange interaction that Dexter type of energy transfer is attributed to is neglected here and will be discussed separately at the end of this section. Figure 1.13a demonstrates how the energy of the dimer changes with respect to the monomer according to the above formulas.

Equation 1.9 indicates the splitting of excited state energy due to delocalization of excited state wavefunctions between molecules when the intermolecular distance R becomes small enough (typically R≤ 0.5Å) due to the resonance energy term β. This splitting of energy is observed as split of the absorption lines of linearly covalently bound

dimers, trimers and dendrimers as illustrated in Figure 1.13b.[4,139,153,158] Both experimental and quantum chemical calculations reveal the decrease of delocalization with increase of the intermolecular distance, angle, and the size of the bound molecules.[4,139,153] These trends cause a decrease of energy splitting (2β). Single molecule spectroscopy of linearly bridged dimers (shown in Figure 1.12a) and trimers shows correlated spectral shift and superradiance compared to the corresponding monomer, which adds further proof of electronic coherence.[123,159,160] In contrast to the above covalently bound chemical dimers, the physical dimers– which are formed in bulk films or crystals when molecules are close to one another–also cause a redshift or blueshift of excited state energy.[29,138,148] Compared to incoherent energy transfer, coherent energy transfer through direct delocalization of wavefunction is very fast. For example, the decay of fluorescence polarization anisotropy due to rapid coherent energy transfer always precedes that due to slower incoherent energy transfer (see Section 2.1.1).[161,162]

Quantum chemical calculations, such as the collective-electronic oscillator (CEO) procedure, can directly reveal the delocalization of charge density from one atom to an adjacent one. Therefore, it is particularly useful to study coherent energy transfer as mentioned above.[119,136] The CEO procedure calculates the linear absorption spectra and the relevant transition density matrices which connect optical response with the underlying electronic motion. Upon optical excitation, an electronic transition from a ground state to an excited state is represented by a transition matrix and contributes to one absorption line which closely reproduces the experimentally observed absorption spectrum.[119,139,158]

The Dexter exchange integral that contributes to energy transfer through electron exchange between two molecules, i.e., Dexter energy transfer,[163] decreases exponentially with distance. Therefore, Dexter energy transfer is short ranged and typically sets in at 1 nm.[118] In some extended polymer chains, the strong interchromophoric coupling leads to fast energy transfer, which is dominated by Dexter transfer.[164,165] Although spectral overlap is not required for Dexter energy transfer, coupling between the donor and the acceptor can be mediated by the intervening bonds or chromophores that serve as the bridge states to extend the exchange interaction to a longer range than the conventional Dexter transfer.[152,166,167]

The distinction between the long range energy transfer through spectral overlap and the short range energy transfer through wavefunction overlap is demonstrated in Figure 1.14. However, it is very common to find both types of energy transfer appearing at short and long timescales, respectively, in a single molecular system. [153,161]

1.3.4 Aggregate and Excimer Formation

Strong electronic coupling between molecules separated by a few Å in amorphous films, single crystals and even solution, populates a large collection of interchain species as introduced previously.[29,109,168] Among these interchain species, aggregates (H- aggregate of parallel geometrical arrangement as shown in Figure 1.15b and J-aggregate of head-to-tail geometrical arrangement as shown in Figure 1.15a) and excimers are particularly interesting because of the rich optical properties presented in them.[4,105,138]

The theory introduced in the last section on the basis of a dimer offers a generalized solution for both J- and H-aggregates without distinguishing the relative orientation of the transition dipoles of the participating molecules. The attractive (repulsive) interaction

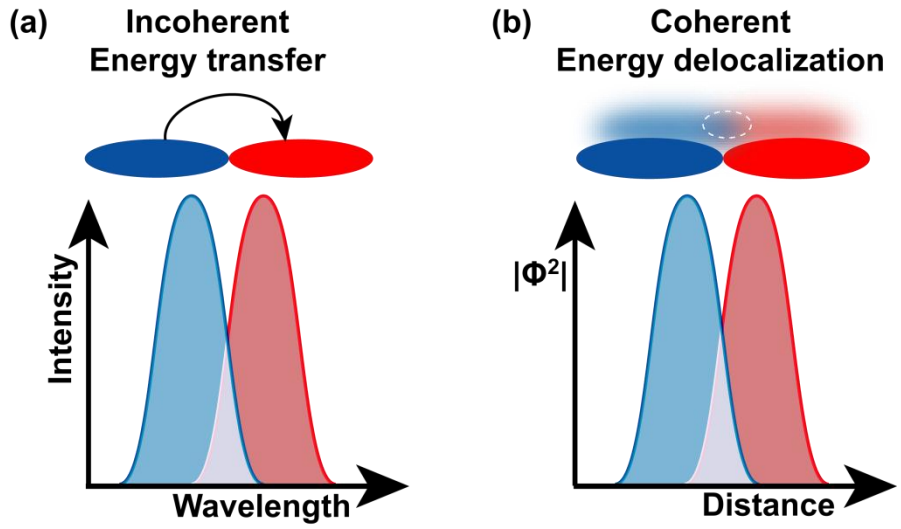

Figure 1.14 Comparison of incoherent and coherent energy transfer. (a) For incoherent energy transfer, a spectral overlap between donor emission (blue) and acceptor absorption (red) is required. (b) For coherent energy transfer, a direct spatial overlap between wavefunctions of the donor and acceptor is essential for excitation energy delocalization.

between the interacting dipoles selects the E(-) (E(+)) split energy level as the excited state for the dimer, while the selection rule of the absorption transition is determined by the vector sum of the transition dipoles in a specific arrangement. It turns out that only in-phase arrangement of the dipoles presents allowed transition (the solid arrow in Figure 1.15) since the wavelength of the excitation photon is much larger than the size of the molecules, thus molecules in a dimer absorb most effectively under simultaneous in-phase perturbation.[150] Due to this argument, the high energy transition E(+) is the allowed transition in the H-aggregate which shows blueshifted absorption and emission spectra compared to the monomer. H-aggregates also shows very slow decay rate as energy relaxes from the high energy E(+) state to the low energy forbidden state E(-) as shown in Figure 1.15b. In contrast, the low energy transition E(-) is the allowed transition in the J-aggregate which shows redshifted absorption and emission spectra and faster decay compared to the monomer as shown in Figure 1.15b. The oblique dimer yields split

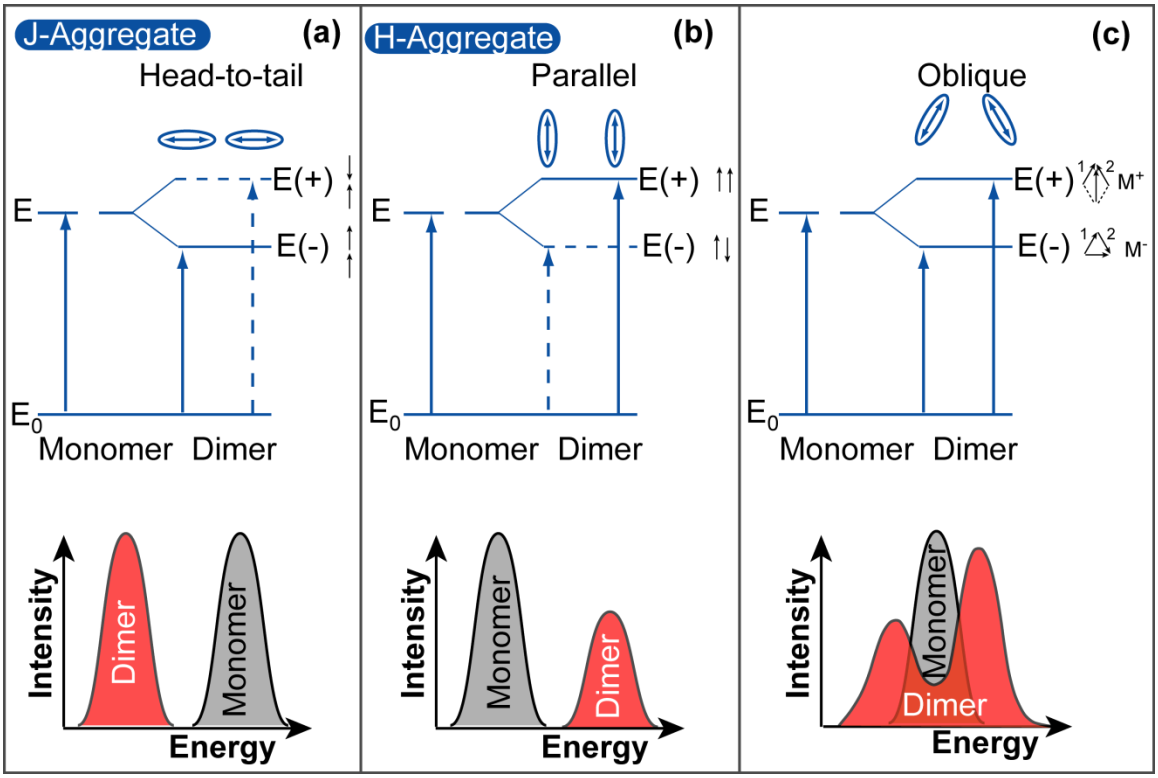

Figure 1.15 Comparison of three configurations in dimers and the corresponding emission under each configuration. Because the excitation wavelength is larger than the size of molecules, the allowed transition happens in the in-phase configuration of dipoles in the dimer. Therefore, in a J-aggregate (a), the allowed transition takes place between the low energy split state and the ground state, which shifts the dimer absorption to a lower energy with a faster decay rate compared to the monomer. In an H-aggregate (b), the allowed transition takes place between the high energy split state and the ground state, which shifts the dimer absorption to a higher energy with a lower decay rate compared to the monomer. (c) In an aggregate of oblique orientation between dipoles, both split energy states are allowed, which causes splitting of the dimer absorption.

energy levels of nonzero transition moments but mutually perpendicular polarization of light absorption ($M^+ \perp M^-$) as shown in Figure 1.15c. This configuration is frequently found in linearly bridged dimers that show split absorption peaks.[139,169]

An excimer is formed between a molecule in the excited state and another molecule in the ground state and only exists in the excited state. Therefore, the excimer exhibits the optical absorption characteristic to a monomer, but reveals a broad and structureless emission spectrum that shows characteristics of a dimer as shown in Figure 1.16b. The

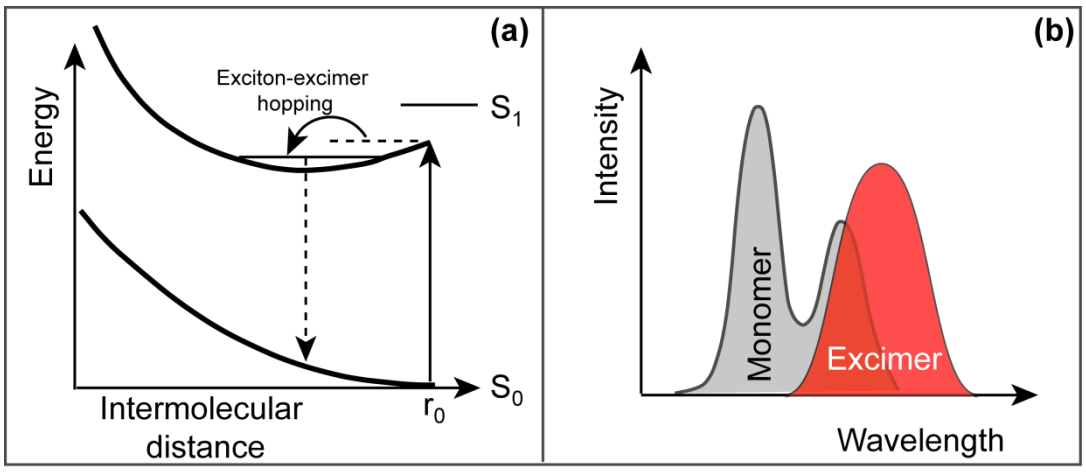

Figure 1.16 Diagram of ground-state and excimer potentials and the emission of the excimer. (a) r_0 is the ground-state distance between molecules (or monomers) that form the excimer. S_1 is the excited state of the monomers. Solid arrow indicates possible S_0-excimer absorption, while dashed arrow indicates excimer emission. The exciton-excimer hopping indicates transition from an excited monomer to an excimer. (b) Emission from the excimer with longer lifetime is broad and redshifted compared to the monomer.

ground state of the pair of molecules forming an excimer is dissociative, thus the ground state energy increases with decreasing distance as shown in Figure 1.16a, which explains the redshifted and broad emission of excimers.[170] The dashed arrow in Figure 1.16a represents the low quantum yield and slow decay rate of the excimer emission as also shown in Chapter 3.[138,147]

The study of aggregates on the microscopic level based on single molecule spectroscopy has yielded comprehensive results. Both J-aggregates and H-aggregateshave been experimentally identified as correlated spectral shift with decay lifetime as theory predicted.[122,123] Chemical dimers consisting of covalently bonded monomers of fixed separation and orientation show experimental results agreeing with theory and calculations.[4,136] Furthermore, the stepwise photobleaching of single dimers or trimers (as shown in Figure 1.18) shows correlation of the emission spectrum and decay lifetime with fluorescence intensity that changes collectively from a high level to a lower

level when one monomer is photobleached while the rest are still emissive.[159,160] This stepwise photobleaching represents an optically induced transition from aggregates to monomer. The observation of excimer on the single molecule level remains controversial due to complications from the keto defects.[132,171]

The study of aggregation in bulk films and crystals is much more complicated due to the number of parameters that affect aggregation (formation of interchain species, not agglomeration) and the number of aggregation species that coexist.[29,109] Aggregation is more commonly formed between chromophores on distinct polymer chains than on the same chain, which, as expected, increases with increasing concentration of polymers in solution used for film casting.[109] Similarly, aggregation in solution is increased when the solvent favors open coil over tight coil conformation.[168] The appearance of redshifted and broad emission is a typical signature of the formation of aggregation in bulk films when accompanied by changes of decay rate or quantum yield.[109,138,147,157] Rare cases of observation of H-aggregates are reported in crystals where some molecules can be periodically arranged in a cofacial fashion.[29,148]

1.4 Blinking, Spectral Diffusion and Photobleaching

1.4.1 In Colloidal Nanocrystals

Trap states play a key role in many aspects of the properties of NCs, such as fluorescence intermittency,[172] emission color,[173] carrier localization,[77] multiexcitons,[174] and intensity decay.[11] Ref. 66, Ref. 70 and Ref. 175[175] give a good review on both the experimental and theoretical progresses on the study of trap states and its impact on optical and electronic properties of NCs.

Trap states in NCs originate from several sources: one major type of trap state is the surface traps states originating from dangling anion and cation bonds, which act as electron and hole trap sites.[176] Due to the large surface to volume ratio, NCs are abundant of surface states. For example, a NC of 4 nm diameter has 30% of the constituent atoms at the surface.[177] In the early stages of the development of colloidal NCs, strong emission from the surface trap states appeared as a broad emission band that was red shifted compared to the emission of the band edge states. Significant reduction of this broad and red shifted emission band through surface passivation suggested its origin in surface trap states. [3,55] Good passivation of a NC surface with both organic ligands or an inorganic shell has been shown to largely remove these surface trap states,[3,55] but still there are remaining sites that affect more subtle effects such as blinking, fluorescence lifetime and exciton storage.[11,15,16] The second source of trap states is the impurity or dopant which might introduce a state in the band gap.[174,178] Implanting trap sites into NCs through doping has been a particularly hard task due to the small size of NCs since even doping of a NC with a single dopant would have exceeded the normal doping level in bulk semiconductors.[66] Successful doping of NCs with metal atoms has shown formation of trap states in or out of the band gap, which results in localization of excitons around these defects and controlled energy transfer from band edge states to the defect states.[19,174,178] The third type of trap states is the intrinsic gap state of semiconductors which originates from the Shockley-like surface state.[66] This type of trap state localizes on the surface in large NCs, but delocalizes to the entire volume in small NCs. In this section, only surface trap states will be focused on.

Trap states can affect properties of NCs on the ensemble as well as on the single particle level. In an ensemble of NCs, the delayed emission is dominated by direct trap emission or band edge emission through exciton transfer from the trap states.[88,179] The trap emission only shows up in delayed emission due to its long lifetime.[88,180,181] The energetic distribution of trap states results in different decay rates.[88,179] Consequently, the decay of the emission intensity of an ensemble of NCs follows a power-law function for delay times above 1 ns [182] and depends strongly on temperature.[11,88] With increased excitation density, the decay rate of NCs increases, too, as shown in Figure 1.7. This effect is attributed to increased fast nonradiative Auger recombination due to the presence of photogenerated charges that are localized at the trap sites.[183] The microscopic mechanism of this effect is the same as the blinking behavior observed on single NCs.

The blinking behavior observed in a single NC shows as intensity fluctuations over time between the "on" state of high intensity and the "off" state of low intensity,[32,61,70] which is often referred to as "fluorescence intermittency." The widely accepted charging model of blinking proposed by Efros and Rosen[13] is based on nonradiative Auger recombination of a single carrier charged NC which keeps the NC in the "off" state until the neutral state recovers. When a charged NC absorbs a photon which then generates an exciton, it becomes a three-particle system as shown in Figure 1.17a. Instead of emitting a photon, recombination energy of the exciton is transferred to the charge trapped on the NC through a rapid (~100ps) Auger process[70] that is faster than the radiative lifetime of the exciton (10 ns to 1us).[11] Therefore, a charged NC is a "dark" NC since it emits no light. The reasons for the blinking behavior being observed exclusively in NCs but not in bulk materials are enhanced Auger recombination resulting from strong coulombic

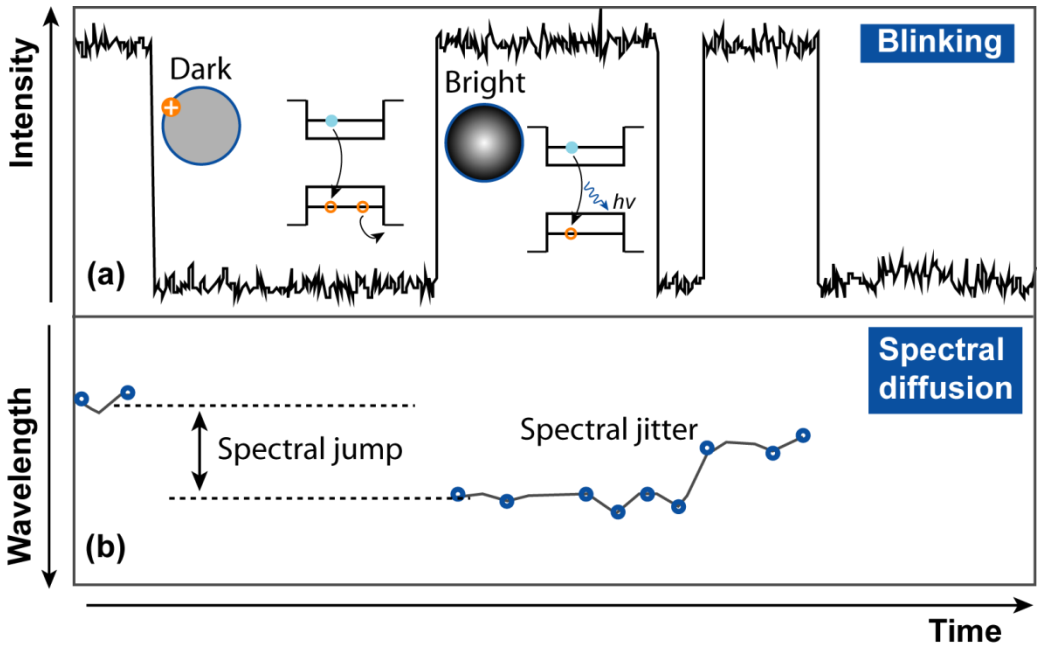

Figure 1.17 Correlated blinking with spectral jumps of a single nanocrystal. (a) Emission of a single NC jumps from low to high intensities, when the NC switches from charged "dark" state with a trapped hole (orange), to neutralized "bright" state.[70] (b) Two types of spectral diffusion in the emission of single NCs are shown here. A large spectral jump (from long to short wavelength) follows a "dark" period. Random spectral jitter happens during the entire "bright" period.

interaction between charge carriers and relaxed requirements of momentum conservation of Auger type processes at abrupt surfaces of NCs.[70] The charged NC becomes neutralized by obtaining a charge carrier of opposite sign from the surrounding matrix and becomes bright again. But the neutralization process might leave a net dipole moment in the NC which then causes a correlated spectral jump with blinking as shown in Figure 1.17b.

The "on" and "off" periods change from a few millisecond to minutes.[32,70] Regardless of composition, size, shape or surface of the studied NCs,[184-187] the probability of both "on" and "off" time distribution P(t) follows a universal power-law statistics as[188]

$$P(t) = t^{-\alpha} \tag{1.12}$$

where α is the power-law exponent. α is close to 1.5 for both "on" and "off" time distributions. However, the "on" time distribution does deviate from the power-law statistics at a time called the "truncation point." This stands in contrast to a persistent power-law functionality of "off" time statistics over the whole experimental time range.[186,189,190] The truncation point shifts to a shorter time with increase of excitation density and temperature or removal of passivation layer,[32,189] which is directly reflected as stronger blinking. Although blinking traces are usually collected from a single NC, a clear interplay between the slow decay dynamics of ensemble NCs with the single particle intermittency can be identified by investigating blinking statistics of a collection of NCs.[191,192] This interplay indicates the microscopic mechanism of the power-law like intensity decay of NCs, which is associated with the blinking behavior.

The independence of both the power-law statistics of blinking and its exponent on temperature, excitation density and NC morphology all suggests that the power-law statistics of "on" and "off" blinking is governed by a tunneling process. [186] To explain the power-law statistics, several models based on a distribution of trapping and neutralization rate were proposed.[186,188,193] The diffusion based model suggests that the trap state energy undergoes a random walk, with a transition from a bright state to a dark (trap) state happening when the energy of these two states is the same.[186] Therefore the blinking period is given by the diffusion time it takes for the trap state to drift in and out of resonance with this condition, which naturally assumes a power-law distribution.[186,188] This diffusion model is then further developed by Tang and Marcus through the diffusion-controlled electron transfer model.[194,195] The other model assumes a uniform spatial distribution of traps in the matrix around a NC and an exponential decay of

trapping and recovery rate with distance between the NC to a trap.[193] The deviation of the "on" time distribution from the power-law after truncation point indicates a secondary process involving on-to-off transitions that is temperature, excitation density and morphology dependent as discussed above. This process might be an optical or thermal charge ejection due to Auger ionization.

Another phenomenon that can be observed in single NC spectroscopy measurements is random jumps or jitter of the spectral position over time, i.e., spectral diffusion.[15,75,196] The spectral diffusion is found to be correlated with blinking events in a way that spectral jump follows recovery of intensity from an "off" event as shown in Figure 1.17b. [14,196] By placing a NC in an external electric field, the same spectral jumps are reproduced, which indicates that spectral diffusion is related to local field fluctuations.[14,15] The correlation relation found between emission intensity and spectral position of a single NC is of similar origin as the correlated intensity and spectral changes. Both correlation relations are induced by electric fields which leads to quantum confined Stark Shifts (see Section 1.5.1).[15,75,197] Therefore, qualitative models propose that the spectral diffusion and intensity fluctuation are due to local charges that are present on the surface of NCs. These charges exert a local electric field on the NCs which then changes the emission peak position and emission intensity as in the case of an applied external electric field.[14,197] Consequently, the observed correlation between spectral diffusion and blinking can be explained as an effect of spectral diffusion— an effect induced by the remaining electric field from the charging event that cause blinking.[70,196]

1.4.2 In π-conjugated Organic Molecules

As demonstrated in inorganic semiconductor NCs in the last section, the fluorescence of a single quantum emitter is subject to intensity blinking and spectral diffusion under continuous wave excitation, which is also observed in pi-conjugated organic molecules of single or multiple chromophores in a similar fashion.[121,198] One well-studied cause of blinking in organic molecules is the transition from an emissive singlet state to a dark triplet state through intersystem crossing.[133,199-201] Despite the presence of dark states of similar nature in semiconductor NCs, this type of blinking is hard to observe due to both the smaller singlet-triplet energy gap and shorter decay lifetime of the dark state (shorter than the experimental resolution) in NCs compared to that in organic molecules. The fast blinking due to the triplet dark state usually follows exponential statistics.[202] Besides this fast blinking, long-lived dark states with "off" time much longer than that of the triplet state have also been reported in organic molecules.[133,203] In the case of organic molecules, the formation of such dark states is thought to originate from the formation of reversible nonemissive photo-oxidation products,[204] electron tunneling processes, [203] charged molecules (radical anion or cation) after exciton dissociation.[202] Such dark states have led to power-law like blinking statistics of "on" and "off" time distribution as in NCs. Other sources of blinking such as energy transfer to defect sites[133] and exciton blockade of energy transfer to acceptor chromophore have also been reported in literature.[205]

Aside from the temporary loss of emission, single molecule spectroscopy also suffers from photobleaching, a photochemical reaction such as oxidation that yields nonemissive products.[204] Single molecule studies on stepwise photobleaching of a trimer demonstrates collective reversible "off" events due to the formation of charged radicals preceding the

irreversible photobleaching in most cases,[133] which suggests the cause of photobleaching as long lived radicals. Interestingly, the "off" time distribution extracted from a single molecule fluorescence time trace in this study also follows a power-law distribution of exponent -1.5 like in the semiconductor NCs, and a similar power-law distribution of "on" time is also reported.[202] This observation points to a close link between the fluorescence intermittency of organic and inorganic single quantum emitters with stochastic time dependencies.[199]

Single molecule spectroscopy of coupled multichromophoric molecular systems reveals important features of aggregates. As discussed in Section 1.3.4, the formation of J-aggregates shortens fluorescence lifetime due to a gain of oscillator strength through exciton delocalization between multiple units such as chromophores. This superradiance signature can be easily observed in correlated time traces of stepwise photobleaching and lifetime measurement.[159,160,200] This effect is illustrated in Figure 1.18 using a dimer for example. The drop of intensity is due to photobleaching of one chromophore when the other one is still emitting. Therefore, lifetime increases through the loss of the superradiance condition. The similar correlation is also observed in other molecular systems of coupled chromophores.[133,160] Other than this coherent intramolecular interchromophoric coupling that changes emission energy and lifetime, weak coupling through incoherent Förster type energy transfer (FRET) between chromophores can also be identified through single molecule spectroscopy. It is shown that only one chromophore is emissive when two chromophores are brought to be within the proximity of the FRET radius even if they are both excited.[206] In another words, the coupled multichromophoric system is a single emitter as proved by the photo-antibunching

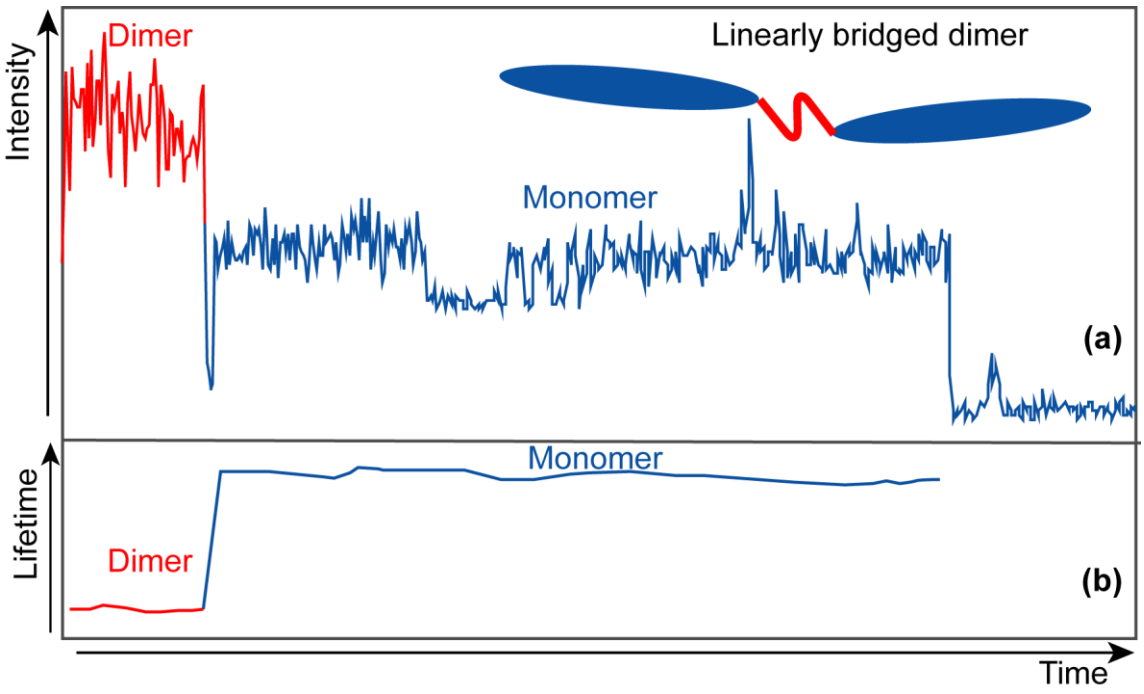

Figure 1.18 Stepwise photobleaching and correlated fluorescence lifetime of a single dimer. (a) Time trace of intensity initially shows a high level (red) from the dimer fluorescene. After photobleaching of a unit, the dimer becomes a monomer of lower emission intensity. The inset shows a representational molecular structure of a linearly bridged dimer.[160] (b) The fluorescence lifetime increases upon the switch from a dimer to a monomer.[160]

measurement.[200]

Spectral diffusion is another common feature observed in both single NCs and single organic molecules. As a direct probe of variation of energy gap, spectral diffusion can be caused by conformation changes by local heat dissipation and by nonradiative decay or excess energy dissipation through phonon-coupled relaxation. The other cause of spectral diffusion like in the case of NCs is local field fluctuation. Changes of local environment by charges sitting on the side chains cause a change of the local electric field which subsequently perturbs the energy level through the Stark effect and cause schange of emission energy.[28] Correlated blinking and spectral diffusion can be observed under the

energy transfer condition as spectral diffusion leads to a time dependent overlap between donor and emitting acceptor as discussed previously.

1.5 Electrostatic Manipulation of Electric and Optical Properties

As introduced in Section 1.1.1, state-of-the-art fabrication enables precise control of composition, shape and size of semiconductor NCs which show a large range of electronic structures. The electronic and optical properties of these interesting material systems are extensively studied for applications in various optoelectronic and photovoltaic devices.[20] It is only natural to study the impact of electric fields on spectroscopic properties of these materials. The manipulation of excitons–which are the carriers of optical and electronic information with electric field–is one important field that attracts considerable attention.[21,207] Concepts of devices for storage, read-out and transfer of excitons are explored using an electric field as manipulation force.[21,22,208-210]

The importance of manipulation of excitons is also applicable to pi-conjugated organic materials. Photoinduced charge carrier generation and transport are key processes underlying the application of organic semiconductors as the active materials of devices such as solar cells and diodes.[149] These processes largely determine the performance of the corresponding devices. The central interest is in understanding the mechanism that governs the surmounting of the coulombic barrier which leads to charge carrier photogeneration.

The manner in which to manipulate electronic and optical properties of semiconductor NCs and organic materials will be discussed in full detail in this section.

1.5.1 Stark Effect

The "Stark effect" is the shifting and splitting of spectral lines of atoms and molecules under the influence of a static external electric field. The Stark effect in systems of size where quantum interaction applies is often called quantum confined Stark effect (QCSE) and is largely enhanced compared to the bulk due to the increased carrier coulombic interaction. To the second order approximation, the shift of energy caused by the Stark effect can be written as

$$\Delta E = \mu\varepsilon + \frac{1}{2}\alpha\varepsilon^2 \tag{1.13}$$

where ε is the external electric field, and μ and α are the projections of the dipole and polarizability in the direction of the electric field. Empedocles and Bawendi reported the observation of the Stark effect in single CdSe spherical NCs as the shift of emission lines by as much as 75meV.[14] In single NCs, variations from linear to quadratic dependence of Stark shift on electric field are observed.[14,15] However, thus far, experiments on the electric field induced spectral shift of a single conjugated polymer chain reveal only a linear dependence of the Stark shift on the field, which is possibly due to the strong internal field of the molecules.[28]

Aside from spectral changes, PL intensity quenching, defined as the decrease of PL intensity when an electric field is on compared to the zero-field PL intensity, also arises when organic pi-conjugated materials and semiconductor NCs are under the influence of an external electric field.[197,211] This effect is caused by the separation of excitons, which reduces the overlap of electron and hole wavefunctions and consequently the oscillator strength. The separated but still weakly bound exciton is often referred to as indirect

exciton or polaron pair of smaller binding energy and slower radiative decay rate.[21,207,212,213] A linear increase of quenching with increase of electric field is observed in CdSe/CdS tetrapods in this work, but this dependence can change into other complicated functionality in different NCs[197,214,215] and pi-conjugated polymers.[213,216] The separation of exciton and intensity quenching also shows an opposite dependence on excitation density in NCs compared pi-conjugated materials, which will be given in detail in Chapter 3 and Chapter 4.

1.5.2 In Nanocrystals

The band structure of a bulk semiconductor dominate its optoelectronic properties since the interband transition is largely determined by the atomic-like Bloch parts of the wavefunction as introduced previously in Section 1.1.2. Thus it seems that strong interband transitions of short radiative lifetime are linked to the direct band gap semiconductors such as GaAs, while weak interband transitions of long radiative lifetime are associated with indirect band gap semiconductors like Si. Instead of manipulating the band structure in this momentum space which is hard to achieve practically, experimental approaches seek ways to achieve band-gap engineering in the physical space.

The initial attempts of band-gap engineering focused on quantum superlattices of alternating *n* and *p* types of doping regions for the separation of electrons and holes spatially into these two types of regions, respectively.[217] This method changed the electronic structure by manipulating composition and formed quantum wells of separated space charges. There were also attempts to manipulate the electronic structure through the application of electric-field waves across the sample to achieve spatial separation of

charge carriers which can be entirely controlled using a switch, unlike the former static method.[207,218]

The electronic structure of semiconductors can also be manipulated using an external electric field. This method is based on the tilt of the conduction and valence bands along the electric field and the subsequent shift of electron and hole wavefunctions to the opposite directions. To illustrate this mechanism, a single core/shell nanorod heterostructure is used as an example as shown in Figure 1.19. The applied external electric field ($\vec{E}$) tilts the conduction and valence band in the way that the electron wavefunction shifts along the opposite direction of $\vec{E}$ toward the CdS arm, while the hole wavefunction is still localized in the CdSe core due to the structure asymmetry. This increase of distance between electron and hole reduces emission intensity and increases

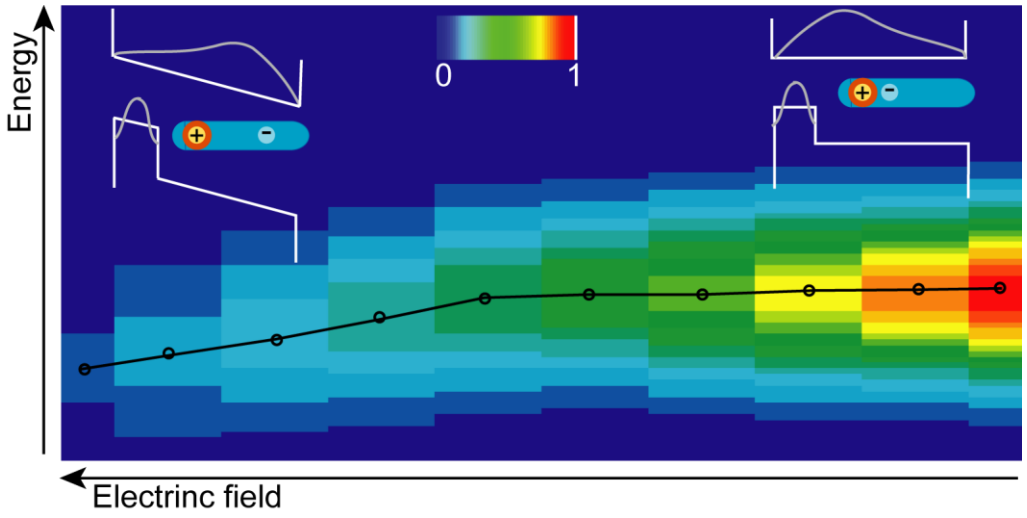

Figure 1.19 Stark effect in a single core/shell nanorod. Normalized PL spectra at different electric fields are plotted here. Both emission intensity and emission energy decreases with increased field strength (redrawn from Ref.197). The inset demonstrates how band structure and electron-hole wavefunction changes with the applied electric field.

the radiative lifetime.[16,197,212] As shown in Figure 1.19, the PL intensity of NCs when the electric field is on (red) is lower than the intensity without electric field (black).

The quenching of emission intensity is correlated with redshifted emission due to a large reduction of correlation energy when the electron and hole wavefunctions are separated.[15,197] This negative Stark shift is shown to be also correlated to emission linewidth broadening.[14,15] This observation can be explained by attributing electric fields as additional sources of local field fluctuations, which causes broadening of energy state. The shape of NCs can also affect the strength of electric field induced changes. For instance, NCs of elongated shape exhibit larger quenching and Stark shifts compared to spherical NCs.[14,15,197]

Increase of radiative lifetime through separation of the electron and hole wavefunction indicates an storage mechanism of excitons. An overshot of emission intensity immediately after the switch-off of the electric field can be observed as excitons stored in the electric field recombine.[16] The storage of excitons was first investigated in double quantum wells,[21] in which exciton excited into one quantum well was separated and the electron and the hole were stored in different wells. These processes are illustrated as "write" and "store" steps in Figure 1.20a and Figure 1.20b respectively. The application of a "read" electric pulse tilts the band structure to allow the electron and the hole to be present in the same well and recombine as shown in Figure 1.20c. The corresponding electrical and laser pulses are plotted in Figure 1.20d. The storage time can be seconds during which there is small loss of the stored signal through slow indirect exciton recombination and thermal activation or tunneling.[16,21,208] Optimization of this storage method, such as a reduction of response time,[22] polarization preserving light storage,[210]

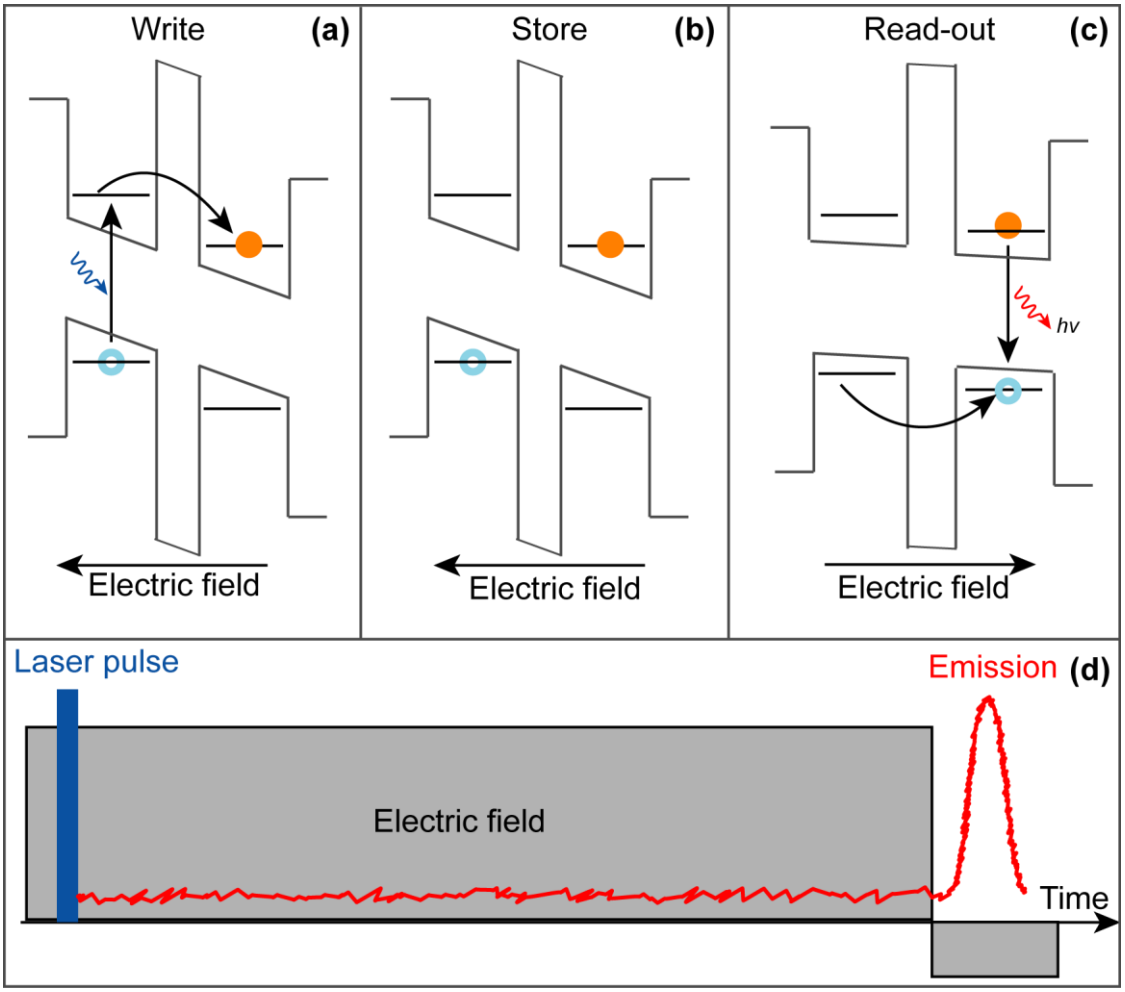

Figure 1.20 "write," "store" and 'read-out" of excitons in double quantum wells.[21] (a) The laser excitation pulse generates an exciton in the left quantum well, which is immediately separated by the electric field. The electron tunnels to the right quantum well, while the hole remains in the left well. (b) The electric field stores electron and hole in separated wells and prevents them from recombination. (c) Application of the read-out bias reverses the electric field. Therefore, the hole tunnels to the right well, where it recombines with the electron. (d) shows sequences of laser pulse, the electric field and the read-out signal in time.

and controllable exciton flow among different logic gates[209] are recent focuses in this field.

Exciton storage within isolated colloidal NCs was originally studied on CdSe/CdS nanorods in which the storage time was up to 100 microseconds.[16] The long exciton storage time indicates that the lifetime of the indirect exciton is too long to be entirely attributed to reduction of electron and hole wavefunction overlap.[197] In analogy to the case of double quantum wells, storage sites that provide an additional barrier to prevent charge carriers from recombination are needed for similar purposes as the high band gap material between the wells. These storage sites are attributed to long-lived trap sites in NCs.

The above arguments are based primarily on experiments at relatively low excitation density to avoid charging of samples. However, the impact of electric fields on interesting phenomena such as multiexciton generation and high-density exciton storage can be studied only at high excitation density. Therefore, a study of the dependence of field induced intensity quenching and exciton storage on excitation density was conducted and further discussed in Chapter 4.

1.5.3 In Organic Molecules

Two basic models are currently used to describe carrier generation in organic molecules. According to the direct carrier generation model based on the studies of PPV type of polymers, unbound electron and hole pairs are generated directly after photoabsorption.[219,220] The other two-step model introduces the generation of the polaron pair, i.e. weakly bound excitons, as the intermediate step before final photogeneration of charge carriers.[213,221,222]

Electric field induced singlet exciton dissociation and generation of polaron pairs were reported in numerous polymers which resulted in quenching of fluorescence intensity[137,213,216,223]. The applied external electric field provides excess energy required for the formation of polaron pair of higher energy compared to the exciton. Field induced quenching is not instantaneous but instead evolves on the picosecond time scale during which dynamical processes of exciton dissociation occur.[137] Gulbinas's work on poly(paraphenylene) (MeLPPP) using transient absorption demonstrates the electric field induced formation of charge carriers throughout the entire lifetime of S_1-S_0 transitions of a few hundred picoseconds.[213] The dependence of the yield of charge separation of less than 1% on electric field follows the Poole-Frenkel model.[213]

The efficiency of photogeneration of charge carriers can be increased by increasing excitation photon energy[224] or excitation density, which both supply excess of energy to overcome energy barriers of dissociation.[213,225] An increase of excitation density significantly increases the population of excitons and promotes interaction between them in a similar way as in semiconductor NCs shown in Section 1.1.4. Fast exciton depopulation through nonlinear singlet-singlet annihilation at increased excitation density was reported to contribute to the generation of charge carriers.[213,225] As illustrated in Figure 1.21, one singlet exciton (S_1) transfers its recombination energy to the other one and promotes the latter to a higher energy state S_n. Excitons at S_n states have increased an chance of exciton dissociation and an increased contribution of photogeneration of charge carriers similar to the scenario where samples are excited with photons of high energy.[224] The fact that intermolecular exciton species only appear at high exciton density also

indicates the increase of photogeneration of carriers through an increase of excitation density.[226]

The same study also demonstrates a dependence of field induced fluorescence quenching on molecular structures. It is shown that quenching increases with number of chromophores in the molecules. Similar results were also observed in MEH-PPV and its five-ring oligomers where quenching also was shown to decrease with decrease of chain length.[227]

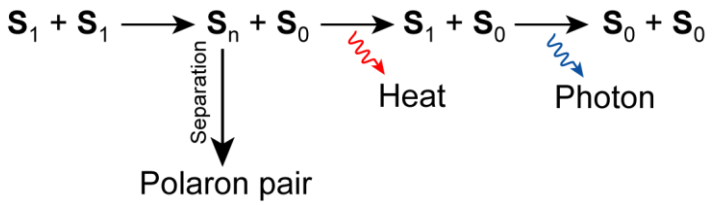

Figure 1.21 Schematic of singlet-singlet annihilation.

CHAPTER 2

EXPERIMENTAL METHODS

2.1 Concepts of Time-Resolved Spectroscopy

Time-resolved spectroscopy is an important experimental tool to study the temporal dynamics of materials after an excitation pulse. The difference between time-resolved spectroscopy and traditional spectroscopy is that the former probes spectra at varying delay time following a pulse of excitation and therefore reveals the temporal evolution of excited states. As an important characterization tool, time-resolved spectroscopy distinguishes materials based on the decay lifetime, which also reflects the nature of the excited state. Furthermore, the capability of time-resolved spectroscopy to "freeze" a moment in time enables the probing of the temporal evolution that a process undergoes. Since its development in the 1970s, time-resolved spectroscopy has been applied in studies of excited state lifetime,[63,212] energy transfer, [146,151,153] exciton transfer and storage,[16,74,76] emission depolarization,[142,143,228] phosphorescence,[128,130] dynamics of proteins and membrane[229] as well as several other fields.[124,178,230] Accurate timing of detection with excitation necessitates usage of temporally pulsed excitation (usually a pulsed laser) in time-resolved spectroscopy. The various time-resolved techniques can be divided into two groups according to the gating mechanism of the temporal signal: the pump-probe method and the time gated method. With the pump-probe method, samples are first excited with a narrow and intense pump pulse followed by a weak probe pulse at

a certain delay that probes structural and energetic changes initiated by the pump pulse. Popular pump-probe techniques include transient absorption,[231] time-resolved fluorescence upconversion,[162] three pulse photon-echo measurements,[232] and degenerate four-wave mixing.[233] In contrast, time-gated techniques utilize a similar excitation pulse scheme, while the temporal evolution is resolved through the gating of detection which controls both the length of detection and the starting time with respect to the excitation pulse. This technique has been successfully applied in streak cameras, gated ICCDs, and time-correlated single photon counting (TCSPC) apparatuses. Generally, the pump-probe methods have higher time resolution but short delay ranges compared to the time gated methods. Since temporal dynamics of emission over both a short and a long delay range is the focus of this study, time-resolved PL spectra are collected by a streak camera and a gated ICCD, respectively.

2.1.1 Gated Spectroscopy

Time gated spectroscopy measures emission spectra or intensity at varying delay times and reveals the evolution of emission due to excited state relaxation through mechanisms such as excitonic recombination or energy transfer.[63,137,160,234-236] The key function of time-resolved techniques is the assignment of a precise time tag or delay time to the measured spectrum or intensity with respect to the arrival of the excitation pulse, which occurs at time zero. For example, when using an external trigger with a gated detector, a pulsed laser fires an excitation pulse at the sample and sends a trigger signal to a delay generator simultaneously at time t=0. After delay time t, the delay generator sends a pulse of width t_{width} to the ICCD to turn on its intensifier for signal detection for the length of t_{width}. Therefore, signal $I(t)$ integrated from t to $t+t_{width}$ is recorded, where t is the

delay time or gate delay and t_{width} is gate width. Increasing delay time by step size t_{step} (gate step) to $t+t_{step}$, a new signal $I(t+t_{step})$ is recorded. The gate step does not necessarily need to be the same at all of the delay times. The operation principle of the gated ICCD is illustrated in Figure 2.1.

Measurement of decay lifetime is the basic function of gated spectroscopy. In this case, $I(t)$ is integrated intensity. A simple example of decay dynamics to start with is monoexponetial decay of an excited state. Then $I(t)$ after an initial emission intensity at t=0, $I(t=0)$ is

$$I(t) = I(0)e^{(-\frac{t}{\tau})} \tag{2.1}$$

where τ is the decay lifetime which is inversely proportional to decay rate κ ($\kappa=1/\tau$). However, more commonly, the recorded decay shows multiexponential or power-law

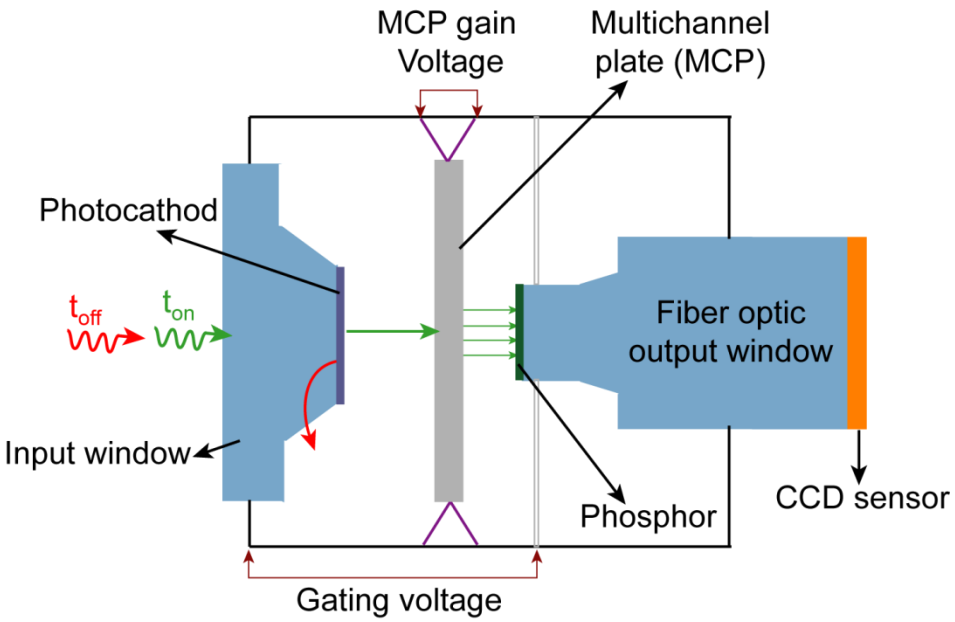

Figure 2.1 Schematic and gating mechanism of a gated ICCD. When the gating voltage is negative (gate on), electrons converted by the photocathode are drawn toward the MCP. When the gating voltage is positive, electrons cannot pass the gap.

functionality due to a distribution of states or decay rates that are involved in the relaxation processes, especially at long delay times.[64,182,216]

By combining a gated detector with a monochromator or a spectrometer, a time resolved intensity trace can also be spectrally resolved to record the evolution of both the population and constituent species of the excited state. Figure 2.2a shows a typical example of a time series of normalized emission spectra from dual-color NCs at different delay times recorded on a gated ICCD. The trace shows shifts of both emission peaks over the delay times in the range of 0-1μs due to energy transfer between the two emission states. The corresponding intensity decay shown in Figure 2.2b demonstrates a power-law decay over four orders of magnitude over the delay range.

The delay time can also be converted to a different quantity, such as charges stored in a capacitor as in a TCSPC apparatus, or a spatial position as in a streak camera. In the

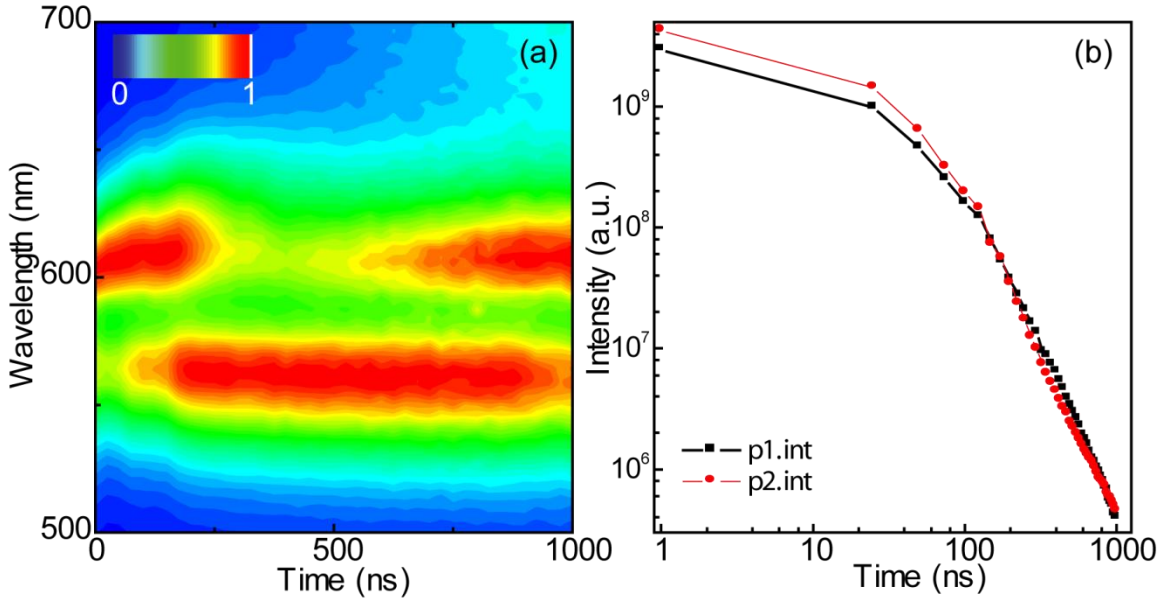

Figure 2.2 A time series of PL spectra and corresponding intensity decay of dual-color NCs. (a) Normalized PL spectra in delay time range of 1 μs to 1μs. The two emission peaks at 560 nm (p1) and 620 nm (p2) are shown to shift with delay time. (b) Corresponding decay intensities of p1 and p2 in log-log scale to show power-law decay.

latter system, spectrally dispersed light is converted by a photocathode to an electron beam which is then accelerated and passed through a time dependent electric field in the streak tube as shown in Figure 2.3. Depending on the arrival time of the photons at the entrance of the streak tube, the electrons strike different vertical position on the phosphor screen where they are converted back to light. This light is then detected at the corresponding position on the CCD camera. In this way, the light signal is spectrally resolved in the x-direction and temporally resolved in the y-direction.

A streak camera was used in measuring fluorescence anisotropy decays in Chapter 3. Anisotropy is a term that is used to define the degree of polarization of an emitter. Light emitted from a fluorophore (e.g., a fluorescent molecule) is polarized in certain directions defined by the transition dipole moment of the fluorophore, and the fluorescence anisotropy value r describes the inequality of fluorescence intensity from the fluorophore along different polarization directions. The temporal decay of anisotropy represents depolarization mechanisms such as excitation energy transfer, excited state delocalization, or the rotation of fluorophores in solution.[143,146,237] Figure 2.4 illustrates the setup for the measurement of fluorescence anisotropy decay in solution and an example of depolarization due to energy transfer and rotation of a linear dipole. To extract the anisotropy values, a λ/2 waveplate is used to rotate the excitation polarization to be either horizontal (H) or vertical (V), and the polarizer in the detection path selects emission light that is polarized either parallel or orthogonal to the excitation light. The anisotropy r is then calculated as

$$r = \frac{(I_{VV} - G \cdot I_{VH})}{I_{VV} + 2G \cdot I_{VH})} \tag{2.2}$$

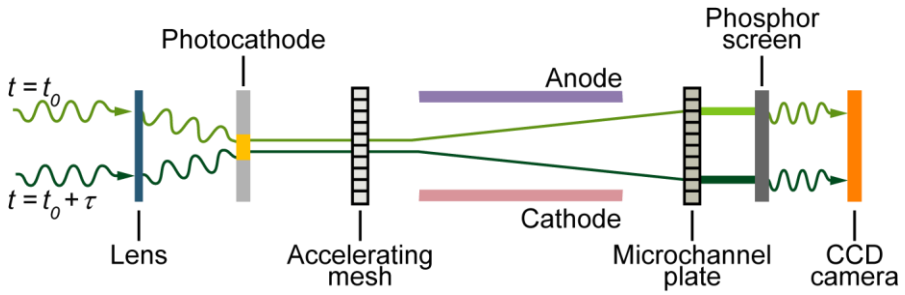

Figure 2.3 Schematic and operation principle of a streak camera.[238]

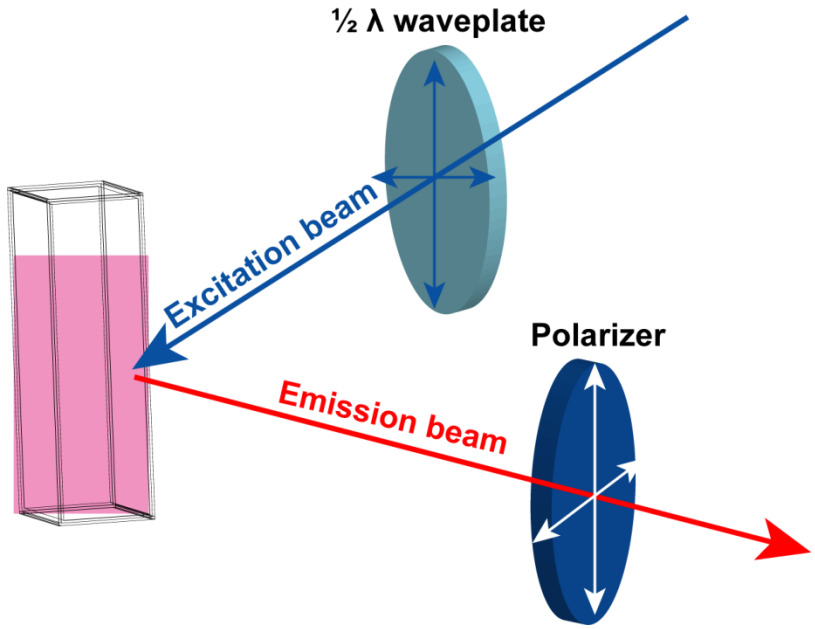

Figure 2.4 Setup for measurement of fluorescence anisotropy.

where G is the correction factor for the instrument response defined as $G = I_{HV}/I_{HH}$. G is between 0.9 and 1.0 in this study. I_{VV} (I_{HH}) is the intensity when excitation light and emission path are vertically (horizontally) polarized. I_{HV} (I_{VH}) is the intensity when exciton light is horizontally (vertically) polarized while the emission path is vertically (horizontally) polarized. The maximum anisotropy value is 1 (e.g., for an immobilized linear dipole),[239] and the minimum value is 0 for unpolarized emitters.[240] For randomly

distributed linear dipoles, the average anisotropy is 0.4 immediately after light excitation.[241]

2.1.2 Field Induced Intensity Quenching and Exciton Storage

Synchronization of additional stimulating pulses to the excitation and gating pulses enables the study of transient effects induced by the stimulation similar to that of pump-probe techniques. As discussed in Section 3.5, application of an external electrical field can modulate both emission intensity and emission color through the Stark effect.[16,28] Shifting the electric field (EF) pulse in time with respect to the excitation pulse and the detection window isolates different effects including quenching, storage and detrapping of the excited state carriers.

The EF pulse is synchronized to the laser pulse by triggering the pulsed laser with a synchronization signal sent at the same time as the voltage pulse (that is used to generate an EF pulse in devices) from the same delay generator. The sequence of laser, voltage and detection pulses under the detection of quenching, storage, or detrapping is illustrated in Figure 2.5a, Figure 2.5b and Figure 2.5c, respectively. Time t=0 is defined as the arrival time of the laser pulse in all three cases. For the quenching measurements, the laser pulse is applied within the EF pulse to ensure separation of excitons from the onset of excitation, while the detection window delay is varied from t=0 to the end of the EF. To measure excitation storage, the sequence of the laser pulse and the EF pulse is the same as the previous case, but the detection window delay is varied from the end of the EF pulse to longer times to detect delayed recombination of stored excitons as an overshoot of intensity. Finally, for the detrapping measurements, the EF is applied after

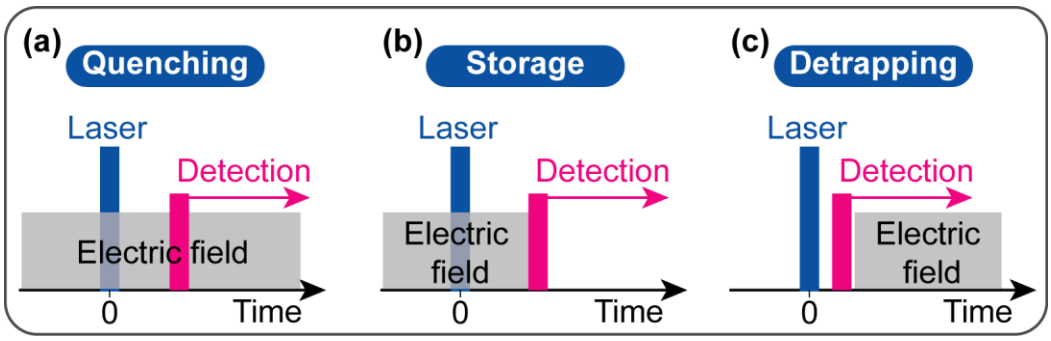

Figure 2.5 Schematic of pulse sequences to isolate different effects. a) quenching. b) storage. c) detrapping.

the laser pulse to prevent storage of direct rather than indirect (trapped) excitons. The detection window is applied at the same time as the EF to detect field induced detrapping which also causes an overshoot of intensity. The application of a continuous EF is much simpler since the EF is on all the time while the detection window delay varies.

To study the effect of excitation density in field induced quenching in both colloidal NCs and organic molecules, a fairly high excitation density is required.[63,213,221,225,226] A practical problem with using high excitation density is significant background luminescence from the host matrix and glass substrate. Therefore, optically inert polystyrene matrix and thin glass substrates are used in the devices to minimize this background emission. The thermal depositions of a SiO_x dielectric layer and an aluminum electrode also reduce the signal-to-noise ratio due to quenching of the emission from NCs and organic molecules. Therefore, a thick polymer layer in which the sample molecules or NCs are embedded is cast to reduce direct thermal deposition on the NCs or molecules. The samples were mounted in a closed cycle helium cryostat, where the samples were measured at low temperature (20K) and under high vacuum (4×10^{-5} torr) resulting in increased quantum yield of the luminescence.

2.2 Single Molecule Spectroscopy

Single molecule spectroscopy (SMS) is similar to conventional ensemble spectroscopy with the exception that only the emission from a single molecule (or a single NC) is collected. This exception provides SMS with the capability to view into the intrinsic properties of single quantum systems, which would not be possible on the ensemble level. The emission spectrum of a single molecule has a much narrower spectral linewidth compared to that of the ensemble counterpart due to the lack of ensemble broadening (see Section 1.3.2). The exact spectral position varies from molecule to molecule, but the histogram of spectral position of a large collection of molecules typically matches the ensemble emission spectrum as shown later.[114,116,132]

To be able to isolate a single molecule in conventionally far field optical microscopy, the spatial distance between molecules must be larger than the diffraction limit of light which is about half of the wavelength of the excitation light. This spatial isolation can be achieved by highly diluting the samples (typically 10^{-10} mol/L) in an inert polymer solution which is then spin cast onto a substrate creating an inert film with a very low density of analyte molecules.[118] The polymer (for example Polystyrene, PMMA, Zeonex[118]) acts as a matrix that suspends molecules so that they will not aggregate into large clusters. The small cross section of 10^{-15} cm^2 for single molecule absorption results in low photon fluxes from single-molecule fluorescence. Thus highly sensitive detectors are required and are now readily available in a variety of forms including CCDs and APDs.

The successful applications of SMS in the studies of structure-property relations [114,116,118,242] and energy transfer[122,123,160,200] motivate the study of structural properties

using SMS in Chapter 3. During this experiment, samples containing isolated molecules embedded in Zeonex are mounted in a 5 K cold-finger cryostat and excited by a pulsed laser at a wavelength where the molecules strongly absorb. Light that is collected by a microscope objective passes through a long pass filter to block any scattered laser light before entering an imaging spectrometer that is connected to a CCD. Due to the Stokes shift between absorption and emission, most of the emission is not blocked by the filter. Emission spectra from a large collection of isolated molecules have to be taken to gain enough statistics to indentify the significance of effects. Sometimes, careful inspection of the data is needed to discriminate emission from the matrix or a cluster of multiple molecules, which generally emit in a different spectral region or show different blinking behavior.

2.3 Materials

2.3.1 CdSe/CdS Tetrapods

In Chapter 4, colloidal CdSe/CdS tetrapods heterostructures are investigated for exciton separation, storage and detrapping in an external EF. The colloidal NCs are synthesized using wet chemical processes and generously provided by the group of D. V. Talapin at the University of Chicago. The uniqueness of this colloidal NC sample is the branched structure of four rod-shaped CdS arms that are grown around a spherical CdSe core in symmetric tetrahedral arrangement. Detailed synthesis, structural and optical characterization has been described in previous publications.[49,74,243]

As confirmed in the TEM image in Figure 2.6a, a single tetrapod consists of a CdSe core of 4 nm in diameter and 4 symmetrically grown CdS arms of 30 nm in length and 5 nm in diameter. The cartoon in Figure 2.6b illustrates the three-dimensional structure of a

CdSe/CdS tetrapod and the corresponding energy diagram of an arm based on studies of CdSe/CdS nanorods.[16,72,197,244] In this heterostructure NC, the holes are localized in the CdSe core while electrons are delocalized across the core and the CdS arms due to the quasi type-II band structure as discussed in Section 1.1.2. The absorption spectrum of the tetrapods taken in a toluene solution shows a sharp onset at about 500 nm corresponding to absorption of the CdS arms, which dominate the spectrum due to the larger volume of CdS compared to the CdSe. Therefore, the low absorption peak of CdSe at 560 nm is not apparent on a linear scale.[49] In contrast, the emission spectrum excited at 355 nm at low excitation density is dominated by the CdSe core emission at 645 nm. Therefore, the tetrapod provides an efficient model light-harvesting system, where light is harvested in the CdS arms, from which the excitons are transferred to the light emitting region at the

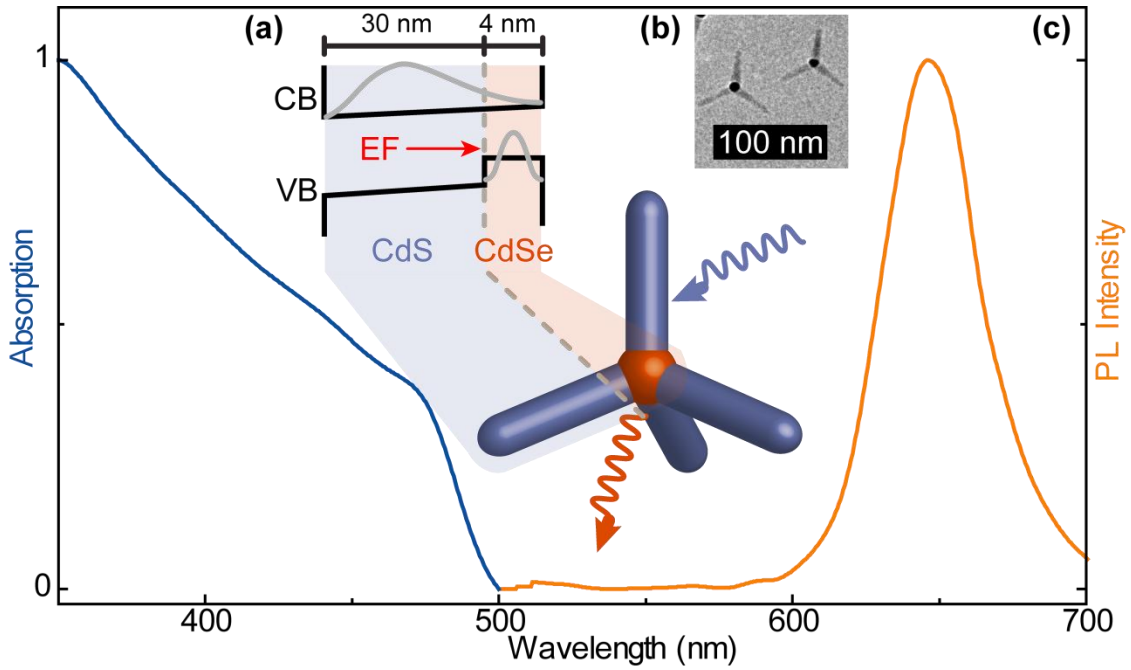

Figure 2.6 Properties of CdSe/CdS tetrapod heterostructures. (a) Cartoon of the tetrapod and the qualitative band structure under the influence of an electric field. The band structure tilts with the applied electric field. (b) TEM image of tetrapods. (kindly provided by Dr. Jing Huang). (c) Absorption (blue) and PL (orange) spectra of tetrapods.

CdSe core within 2 ps.[76] Additional excitonic bands, such as the triexciton and the arm exciton, also appear at high excitation density,[97,243] and are discussed in Section 1.1.4 .

2.3.2 Cofacial pi-Conjugated Dimers

In Chapter 3, a model molecular system containing of dimers of various interchromophoric distances and a macromolecule in the shape of a wheel with spokes are studied to investigate intermolecular interactions using time-resolved spectroscopy, single molecule spectroscopy, and field induced modulation. The systematic approach presented here provides a comprehensive route to probe subtle structural changes in molecules especially when conventional photophysical properties such as emission spectra and decay lifetimes do not show any difference.

The molecules were synthesized and provided after purification by Sigurd Höger's group at the University of Bonn. The synthesis procedure and structural characterization are listed in detail in the Supporting Information of Ref.143 and Ref.206.[143,206] To investigate the dependence of electronic coupling on intermolecular distance, the interchromophoric distances between monomers in the dimers (**2**-**4**) are masterfully tuned from 0.7 nm to 2.1 nm. The open dimer (**5**) is bridged at only one end to allow flexible arrangement between the two chromophores. The chemical structures of all these molecules is in shown in Figure 2.7. The monomer (**1**)–oligo(phenylene-ethynylene-butadiynylenes)–is the primary building block of these structures. The alternating single and triple bonds that linearly link the aromatic rings together form the conjugated backbone of the molecule. The side groups are added to increase solubility. The absorption spectrum of the monomer in chloroform shows a broad peak at 425 nm, and

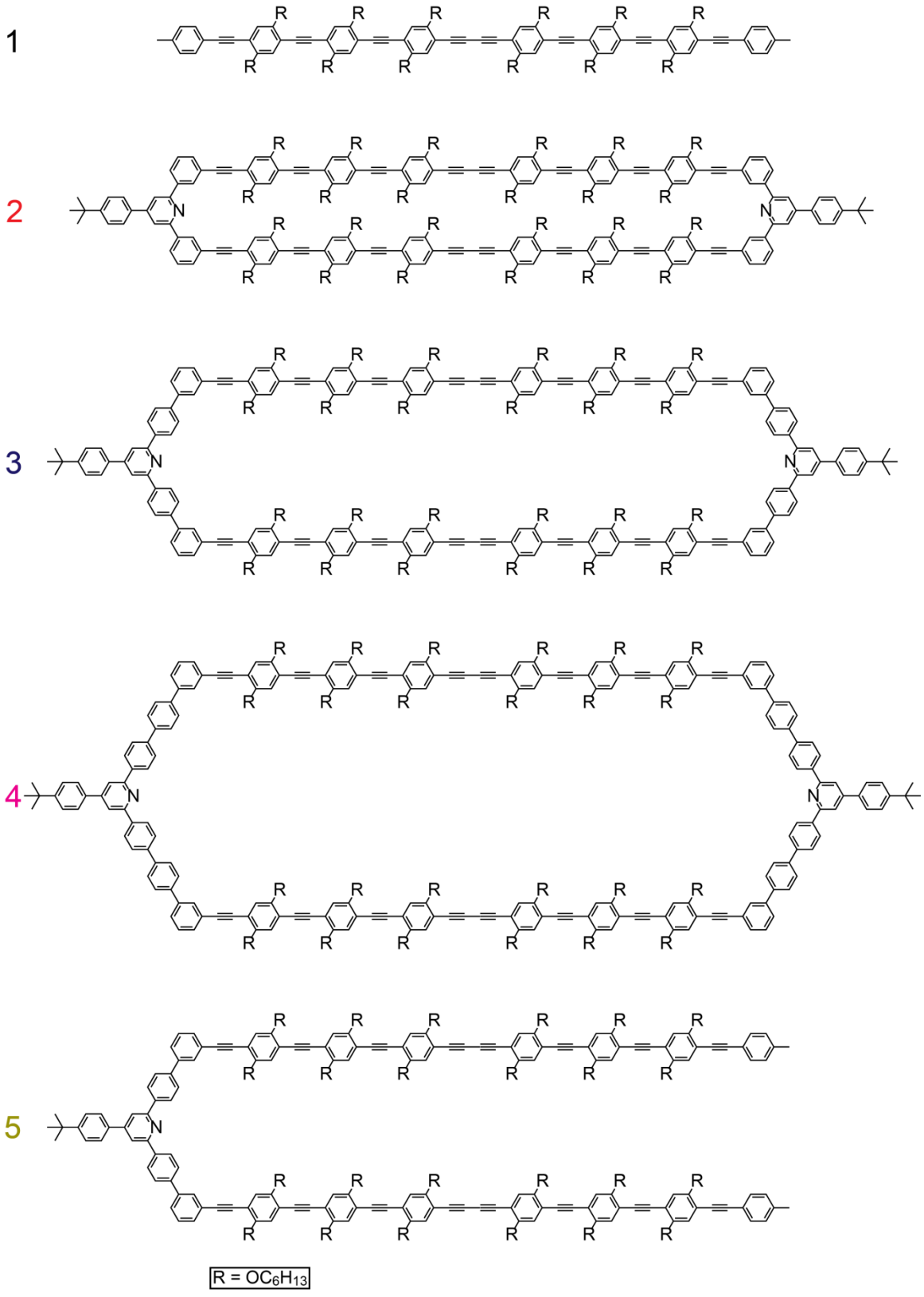

Figure 2.7 Chemical structures of the monomer (**1**), the closed dimers (**2**-**4**) and the open dimer (**5**).

the PL spectrum excited at 430 nm shows a 0-0 transition at 470 nm and the vibronic progression at 500 nm. The vibronic peaks are clearly resolved in the single molecule spectrum as shown in Figure 2.8. The other molecules show similar absorption and emission spectra. The overlap between the absorption and the emission spectra leads to reabsorption and a red shift of the emission spectrum in the concentrated solution and film. Therefore, to avoid interactions between molecules, films used for the study of field

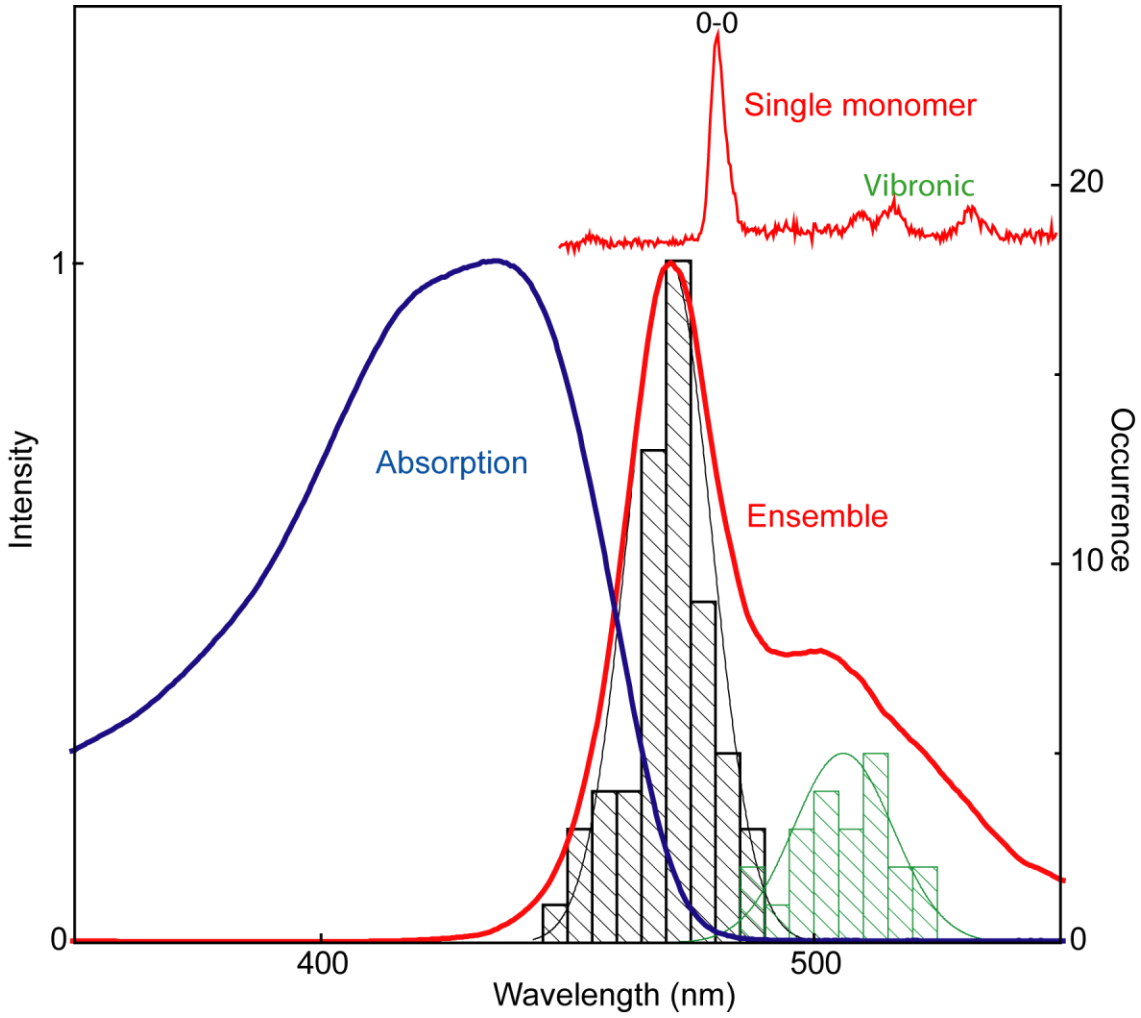

Figure 2.8 Properties of the monomer. The ensemble absorption (blue) and emission spectra (red) were taken in toluene solution. A typical single monomer PL spectrum at 5K is given at the top. The histograms give distributions of the 0-0 (black) and the vibronic (green) emission peak positions of 62 single monomers at 5K.

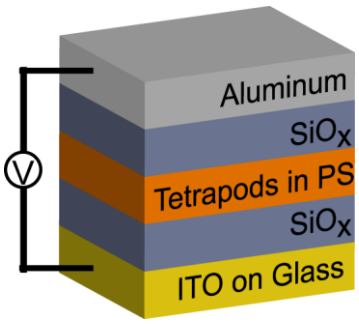

Figure 2.9 Cartoon of the layer structure of a capacitor device.

induced quenching are cast from diluted solutions of molecules mixed with a polystyrene matrix. A histogram of emission peak positions of 62 single molecules at 5 K is also plotted which closely matches the ensemble PL spectra.

2.4 Sample Preparation

2.4.1 Capacitor Device for Field Induced Effects

As mentioned previously, the EF is applied in a capacitor device containing a film of tetrapods or organic molecules embedded in a polystyrene matrix that is sandwiched between dielectric layers and electrodes. Figure 2.9 illustrates the layer-by-layer structure of this capacitor-like device which is constructed from the bottom-up with layers of glass, ITO, SiO_x, samples in polystyrene, SiO_x, and aluminum, in that order.

The received ITO coated glass substrates[1] are patterned by removing all the ITO except for a 12 mm stripe at the center that was covered with Scotch tape during etching substrates are cleaned following the standard cleaning procedure[2] and then baked in a

---

[1] *SPI supplies;* West Chester, PA, USA; 30-60 Ohm sheet resistance 22×22 mm^2 ITO coated coverslips.

[2] Cleaning procedure: (1) ultrasonication for 10 min in acetone. (2) ultrasonication for 10 min in isopropanol. (3) Rinsing with ultrapure water 3 times (4) ultrasonication for 10 min in ultrapure walter. (5) ultrasonication for 5 min in ultrapure water. (6) Blow-dry with nitrogen gas.

UV-Ozone cleaner[3] at 20 °C for 15 min. The bottom SiO_x dielectric layer with a thickness of 20-30 nm is deposited on the cleaned ITO substrate at a constant rate of 0.6 Å/s by thermal evaporation of a mixture of Si and SiO_2 powder[4] in a vacuum of about 2×10^{-6} mbar. The relative dielectric constant of the SiO_x layer is between 2.5 to 6.[245] Tetrapods or organic molecules are diluted in a solution of 15-30 mg/mL of polystyrene in toluene, from which a film is spin cast on the first SiO_x layer on top of the ITO substrate. The thickness of this sample layer depends on spin speed and is about 80 nm (1500 RPM) or 200 nm (at 500 RPM). The second SiO_x layer is deposited in the same way as the first one. Finally, six aluminum electrodes with thicknesses of 150 nm are deposited through thermal evaporation from a mask at a rate of 5 nm/s at the same vacuum as before. Each electrode forms an individual capacitor with the underlying ITO. The EF is created with a voltage source by connecting the ITO electrode (positive) and the aluminum electrode (negative) with a C.W. source meter[5] or a pulse generator[6]. The pulse sequence illustrated in Figure 2.5 represents the ideal case where the RC time constant of the device is zero. However, due to the finite capacitance and resistance of each device, the RC circuit gives a rise- and fall- time of about 500 ns after the applied voltage pulse is turned on or off as shown in Figure 2.10. This RC time constant has to be taken into account for the timing of the excitation and detection. To fabricate quickly responding devices with reduced RC time constant, smaller capacitors of reduced resistance and capacitance have to be constructed. The glass-ITO side of the device

[3] *Novascan Technologies, Inc*; Ames, IA, USA; Digital UV ozone cleaner, Model *PSDPro series*.

[4] *Super Conductor Materials, Inc* ; Suttern, NY, USA; SiO power, 99.9% purity, -200 mesh.

[5] *Keithley Instruments, Inc*; Cleveland, OH, USA; Broad purpose source meter, Model *2400*.

[6] *Agilent technologies*; Santa Clara, CA, USA; High power pulse generator, Model *8114A*

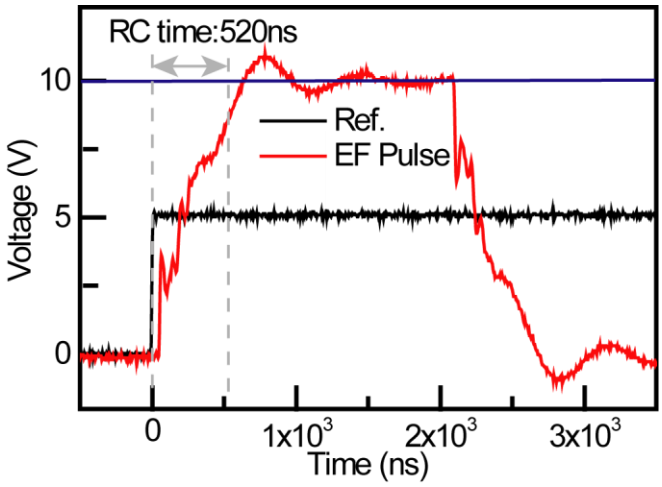

Figure 2.10 RC time constant of capacitor device. The ref. signal (black) is synchronized to the applied electric field pulse, while the EF pulse (red) is the response of the device. RC time constant of the device is defined as the rising time of the response signal.

provides a transparent window for both optical excitation and emission collection.

2.4.2 Single Molecule Sample

The two most important factors for the successful preparation of samples for SMS are cleanliness and dilution. The cleanliness requires careful cleaning of substrates and labwares, purified molecules, spectroscopic grade polymer matrix and solvents, and careful handling of the samples to prevent post-preparation contamination. Detailed preparation techniques are presented in the Ph.D. thesis of M. J. Walter. [118]

For the SMS studies here, molecules are embedded in thin films of Zeonex[7] and spin cast on quartz substrates,[8] which show minimal fluorescence. The 7.5 mm^2 quartz substrates are cleaned following the standard cleaning procedure[2] and then baked at 450 °C for 30 min to remove and decompose any organic contaminants. The glass wares used

[7] *Zeon Chemicals L.P.*; Louisville, KY, USA; cyclo olefin polymer *Zeonex 480R*

[8] *Chemglass Life Science;* Vineland, NJ, USA; 0.15- 0.25 mm thick coverslips

for the dilution steps, except for the vials that are only baked, are cleaned following the same procedure. To prevent background emission from the sample holder and the silver paste used to glue the samples to the holder, an aluminum layer of about 150 nm is deposited at the back of the cleaned substrates. The organic molecules in Chapter 3 are diluted in 10 mg/mL solution of Zeonex in toluene. Zeonex is a transparent matrix that is known to have low autofluorescence.[118] To find a suitable concentration, a few dilution steps are taken and samples are checked under the microscope for the appropriate spatial density of molecules. The final molecular concentration used in this study is less than 10^{-7} mol/L. This solution is spin cast on the back coated substrates at 5000 RPM to form smooth thin films of about 30 nm thickness. To prevent contamination and oxidation from air, samples are mounted into the cryostat immediately after preparation.

2.5 Experimental Setup

2.5.1 Setup for Measurement of Field Induced Effects

To perform the experiments on field induced effects discussed in Section 2.1 and 2.2, a setup consisting of a gated ICCD[9], a spectrometer,[10] a closed-cycle helium cryostat,[11] a solid state pulsed laser,[12] voltage sources[5,6] and other associated parts was constructed jointly with group member K. J. van Schooten. Figure 2.11 shows a detailed diagram.

---

[9] *Andor Technology plc*; Belfast, Northern Ireland; Gated Intensified CCD camera, Model *iStar*; 18 mm gen 3 intensifier tube

[10] *Andor Technology plc*; Belfast, Northern Ireland; Model *SR303i imaging spectrograph*; UV-Vis mirror, 150 I/mm (1.57 nm resolution) and 1200 I/mm (0.17 nm) gratings were installed.

[11] *RG Hansen & Associates*; Santa Barbara, CA, USA; Cryostat, Model; *ADP cryogenics*; Allentone, PA, USA; Helium compressor, Model *HC-4;* Expander head, Model *DE-202*

[12] *CryLaS GmbH*; Berlin, Germany; Dye Laser with DPSS-Pump-Laser, Model: *FTSS 355-50*

The pulsed laser system delivers 700 ps long laser pulses of maximum 118 μJ of energy per pulse at 355 nm. The laser repetition rate can be tuned from 1 Hz to 200 Hz through either an internal or external trigger. The large pulse-to-pulse jitter necessitates the use of a photo diode to synchronize the laser system with the gated ICCD. 10% of the laser beam is reflected by a coverslip onto the diode to trigger the ICCD with every laser pulse. An optical density (OD) filter wheel is inserted to attenuate the excitation density over 6 orders of magnitude. The excitation density is measured by a photodiode-based

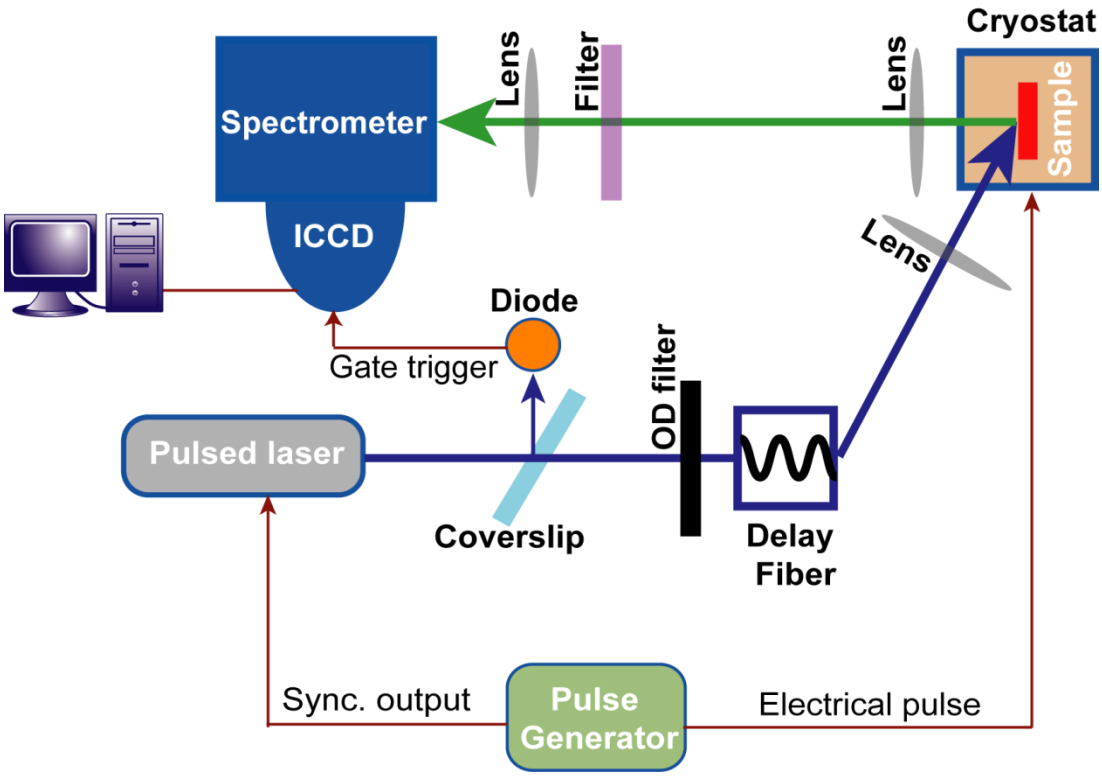

Figure 2.11 Diagram of the setup for measurement of quenching effect.

power meter[13]. To compensate for the 23 ns insertion delay in the ICCD, the remaining 90% of the laser beam is coupled into a 100 m long multimode optical fiber[14] with a diameter of of the coupled-in laser light to the opposite end. The loss is due to strong absorption of UV light in the fiber. Taking into account the 1.46 refractive index, the fiber gives a 49 ns delay between the excitation of the sample and the triggering of the ICCD. Therefore, the prompt emission is detected at a delay time of 26 ns in the ICCD. The coupled-out laser light from the fiber is collimated and focused to a 365 μm diameter spot onto the samples mounted on the sample holder inside the cryostat. The dye laser mode allows tuning of the wavelength from 400 nm to larger values depending on the dyes and dye concentration. The laser system is connected to the lab PC through optical fibers and controlled by software developed by CryLas.

The cryostat is pumped to a vacuum of 5×10^{-8} torr by a mechanical pump and a turbo pump. Excitation light comes in from one side of the vacuum chamber through a quartz window at an angle of about 63° with respect to the normal direction of the sample. Emission light is collected at the normal direction of the sample through the other window. The sample holder is cooled to about 20 K by a helium compressor.[11] One of the electric sources is connected to the sample rack with 7 electric pins to contact with the 6 aluminum electrodes and 1 ITO electrode on the capacitor device through the electric feed-through of the cryostat. To measure and control temperature at the sample holder, a

[13] *Ophir-Spiricon, LLC*; North Logan, UT, USA; Power meter, Model *Vega color display;* Detector model, *PE9-V2 & PD300*

[14] *Thorlabs*; Newton, NJ, USA; Multimode optic fiber, Model *BFH-365*

temperature controller[15] is connected with a Chrome/Au thermal couple and a resistor heater.

Emission is collected by a 60 mm lens and focused into the spectrometer[10] by a 50 mm lens to match the 0.6 NA of the spectrometer. A long pass filter is inserted between these two lenses to block the scattered laser light. There is a mirror and two gratings of 300 g/mm and 1200 g/mm installed in the spectrometer, for imaging or recording low spectral resolution and high spectral resolution spectra, respectively. The gated ICCD is mounted on the spectrometer, which is cooled to -15 °C during data acquisition. A synchronization signal from the diode is sent to the ICCD through the external trigger input which triggers the charging of the intensifier and the opening of the gate. Between the arrival time of the external trigger and the opening of the gate, there is a 23 ns insertion delay which is the minimum delay between triggering of the ICCD and excitation of the sample to detect prompt emission at zero delay. The integrated digital delay generator (DDG) inside the ICCD controls the delay time, gate width and gate steps. Both the spectrometer and the ICCD are connected to the lab PC and controlled by software provided by Andor.

To apply a C.W. EF, a continuous voltage is applied to the device with a C.W. source meter[5] and no further consideration of the timing of the voltage signal with respect to the laser pulse and gating pulse is needed. However, for a pulsed EF, a square voltage pulse is applied with a pulse generator.[6] The sequence of the voltage pulse, the laser pulse and the gating pulse need to be checked on an oscilloscope[16] to tune the delay time and the width of the voltage pulse. For the detrapping measurement, the DDG is triggered by the

[15] *Lakeshore Cryogenic, Inc;* Westerville, HO, USA; Autotuning temperature controller, Model *321*

[16] *Aglient technologies*; Santa Clara, CA, USA; 1GHz signal oscilloscope, Model *06104A;* 1GHz

synchronization signal from the gate ICCD to temporally align the EF with the detection window. With these additional electronics, optical and electrical pump-probe functionality is realized in the capacitor devices. All the measurements of field induced effects reported in this study were performed on this setup.

2.5.2 Single Molecule Microscopy and Streak Camera Spectroscopy

The single molecule spectroscopy in this work was performed on a home-built microscope. It was designed and built as part of the Ph.D thesis of M. J. Water with assistance from N. J. Borys and K. J. van Schooten. For time resolved measurements requiring a higher time resolution (~5 ps), a streak camera was integrated into this setup to measure the spectral evolution of an ensemble of colloidal NCs and organic molecules. The spectra of single molecules and photophysical data from solutions in Chapter 3 and Chapter 4 were collected in this setup. Figure 2.12 shows a diagram of this setup. Detailed descriptions of this setup can also be found in the Ph.D thesis of M. J. Water[118] and N. J. Borys.[238]

Briefly, the illumination source is a pulsed Ti:sapphire laser[17] (140 fs pulse width at 80MHz) of tunable wavelengths varying from 680 nm to 1080 nm. Directing the output beam to an optional autotracking SHG unit[18] can double the frequency and make the wavelength range of 340-540 nm accessible. Along the excitation path, λ/2 or λ/4 waveplates can be inserted to adjust the light polarization direction or change light from linearly polarized to circularly polarized, respectively. The latter was used to excite

---

[17] *Coherent Inc*.; Santa Clara, CA, USA; Model *Chameleon Ultra II*

[18] *APE GmbH*; Berlin, Gemerny; Model *fs-SHG for Chameleon with Autotracker*

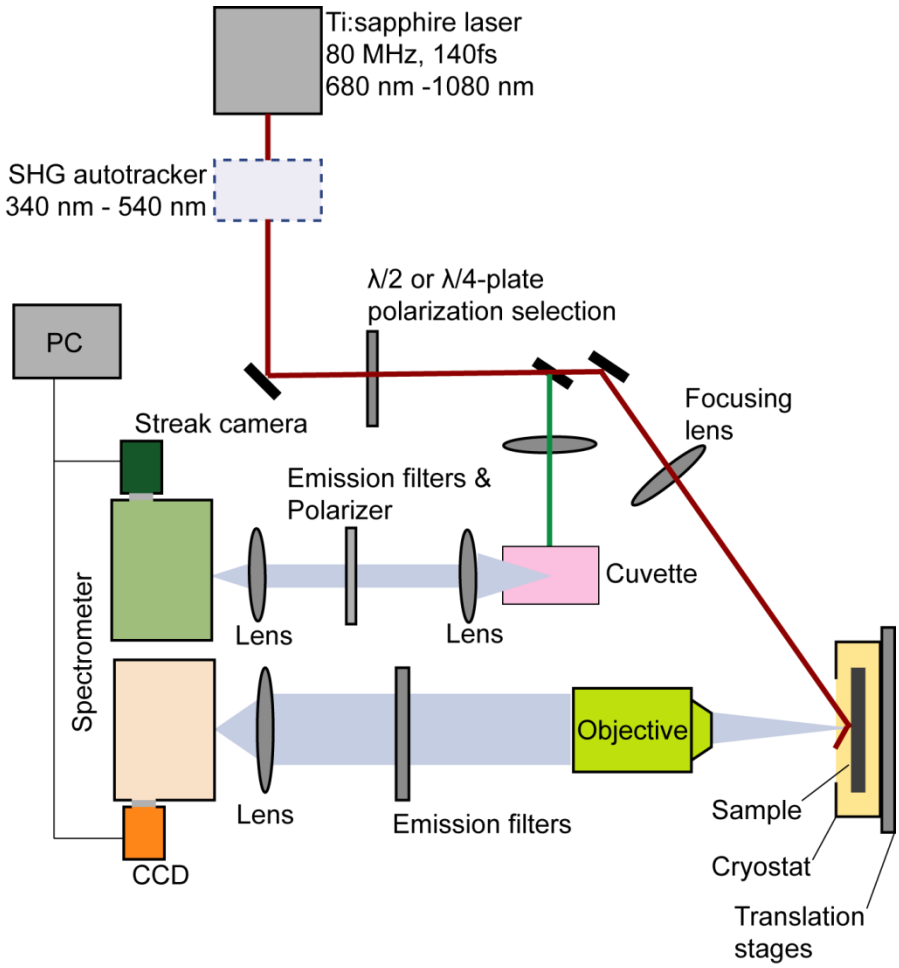

Figure 2.12 SMS and streak camera setup. The red path directs excitation light to the cryostat to excite single molecule samples.[238] The green path directs excitation light to the sample solution that is contained in the cuvette.

cryostat[19] under vacuum (~10^{-6} mbar) and cooled to cryogenic temperature (~5 K) through continuous liquid helium flow. The cryostat sits on a translation stage with sub-micrometer precision to scan samples in x- and y-directions. The excitation light entered the cryostat at a 60° angle relative to the normal direction of the sample and forms a spot of about 150 μm in diameter after being focused by an achromatic lens.

[19] *Janis Research Company Inc.*; Wilmington, MA, USA; Model *ST-500*; Temperature controller model *331S*

The emission was collected by a long working-distance microscope objective[20] with a collar to correct aberrations introduced by the quartz window of the cryostat. As the objective working-distance is larger than the film thickness (~30 nm), molecules embedded in the matrix film are in the same focal plane. High quality interference filters[21] were used in the collection path to isolate the emission light from scattered laser light. An achromatic lens finally focused light into the entrance slit of the spectrometer,[22] which also served as an aperture to select a region of interest on the sample. Depending on whether a grating (150 g/mm) or a mirror was used to reflect or disperse the emission light, an image or spectrum, respectively, from the sample was detected on a cooled (-30 °C) CCD[23] with a high quantum yield and low noise level.

A second path (green) optionally directed the excitation beam to solutions of the samples that were contained in a semi-micro quartz cuvette[24] that were 2 mm wide. Emission light was collected by a lens in the orthogonal direction to the propagation of excitation light in order to avoid the laser directly entering the streak camera. A polarizer was optionally inserted in the collection path to select emission light of a certain polarization direction. An interference filter[21] was inserted in front of the spectrometer to isolate the emission light. Then an achromatic lens focused the emission light into the

[20] *Olympus America Inc*; Melville, NY, USA; Model *SLCPlanFl, 40*×, NA=0.55, *infinity corrected, corrective collar 0-2.6 mm*

[21] *Chroma Technology Corp*.; Rockingham, VT, USA; and *Semrock*; Rochester, NY, USA

[22] *Princeton Instruments/Acton*; Trenton, NJ, USA; Model *SpectroPro SP-2556 Imaging spectrograph*; 500 mm focal length

[23] *Princeton Instruments/Acton*; Trenton, NJ, USA; Model *CoolSNAP:HQ2*; Sony ICX285 interline CCD, 1392×1040 pixels, 6.45×6.45 μm^2 pixel

[24] *Starna Cells, Inc*; Atascadero, CA, USA; Micro Fluorometer, Model *spectrosic 10 mm*

entrance slit of the spectrometer attached to the streak camera.[25] The spectrally dispersed light then entered the streak tube, which provided the time resolution. A silicon photo diode[26] was illuminated by a fraction of the excitation light to trigger the streak camera before entering the SHG unit. Two-dimensional images of fluorescence spectra at different delay time are recorded by the CCD camera with the emission wavelength as the x-axis and delay time as the y-axis.

---

[25] *Hamamatsu Corporation*; Bridgewater, NJ, USA; Model *C5680*

[26] *Hamamatsu Corporation*; Bridgewater, NJ, USA; Model *C1808*

CHAPTER 3

COHERENT AND INCOHERENT INTERACTIONS BETWEENCOFACIAL Pi-CONJUGATED OLIGOMER DIMERS IN MACROCYCLE TEMPLATES

With sufficient background knowledge introduced in the previous two chapters, the investigation of a series of pi-conjugated organic oligomers of macrocyle structure was conducted using various spectroscopy tools. The molecules under study in this chapter were synthesized to contain one (monomer) or two chromophores (dimer) that are covalently bound in parallel configuration among which the interchromophoric distances change from 0.7 nm to 2.1 nm based on the macrocyclic templates. Therefore, this molecular system provides a scaffold to study interactions between pi-conjugated molecules in bulk films that serve as the active regions of organic optoelectronic devices, which motivated this study of the relationship between properties and the structure. In this chapter, both photophysical characterizations and STM images reveal that dimers bound at both ends differ in emission and morphology from the dimers bound at one end. And the field induced quenching also increases in multichromophoric structures compared to the monomer.

This chapter is partially based on a manuscript submitted to a peer-reviewed scientific journal and is coauthored by John M. Lupton and Nick J. Borys. The molecules are synthesized by Daniela Schmitz, Stephen-S. Jester and Sigurd Höger (both: Kekulé-Institut für Organische Chemie und Biochemie der Universität Bonn), who are also coauthors of this manuscript. Subheadings are inserted for structural purpose and are not part of the submitted manuscript.

3.1 Abstract

The interactions between two pi-conjugated oligomers templated in molecular scaffolds are revealed as a function of separation and orientation, providing models of intermolecular interactions in bulk organic semiconductor materials. For a variety of dimer geometries (acyclic and macrocyclic) of the same model oligomer, no change in fluorescence spectra, fluorescence dynamics, or single-molecule emission characteristics is observed. A small red-shift and slowing of fluorescence in the most closely-spaced macrocyclic dimer structure is thought to arise due to an intramolecular solvatochromic shift as well as from weak intramolecular excimer formation. No corresponding effect is observed in bulk films of the acyclic model oligomer, implying the absence of intermolecular excimer formation due to random relative dipole orientations. The largest effect of intramolecular geometry of the model dimer structures is seen in transient fluorescence depolarization, where an open ring geometry leads to rapid depolarization, compared to the corresponding macrocycle, due to the presence of a range of molecular transition dipole moment orientations. Self-assembled monolayers of the molecules on HOPG investigated by single-molecule scanning-tunneling microscopy further illustrate the conformational variability of the open dimers in contrast to the fixed conformation of

the closed dimers. The efficiency of field induced quenching increases with excitation density due to enhanced nonlinear singlet-singlet annihilation, which is particularly obvious in multichromophoric molecules.

3.2 Introduction

One of the greatest puzzles in organic electronics relates to the emergence of bulk-like properties from individual molecular building blocks.[228,246,247] The electronic characteristics of individual molecules are reasonably well understood on a microscopic level,[122,158,234,235,246,248] and sophisticated empirical models exist to describe the function of bulk materials in devices, such as the creation, migration, recombination and dissociation of charges and excitons.[29,109,124,136,151,157,168,222,247] Yet few attempts have been made to go beyond the level of an individual molecule to begin to construct the bulk material from the bottom up.[123,139,154,160,169,249] With present advances in the synthesis of complex organic functional materials by means of structural templating, for example through rigid macrocyclic scaffolds,[143,228,250] routes are emerging to precisely control the relative spacing and orientation between individual conjugated segments to assess how cooperative and collective effects emerge on the way from the individual unit to the bulk.[4,247] Interactions between individual units may occur either in the weak or in the strong coupling regime.[123,139,152,153,160,234] In the former, resonance energy transfer (FRET) can occur,[152,234] which, given suitable orientations of the transition dipole moments, can be revealed by means of fluorescence depolarization spectroscopy.[142,143,152,228,234] In the latter regime, a coherent delocalization between excited states arises which modifies both the transition spectrum and lifetime.[4,139,148,156,160] Depending on the relative dipole orientation of the chromophores,

oscillator strength may add to or subtract from the lowest-energy transition, leading to a rise or a decrease of radiative rate.[122,123] Such coherent interactions will generally modify the spectra, whereas incoherent interactions will leave the spectra unchanged.[123,152] While there have been several studies on controlled interactions between individual conjugated units *within* a molecule,[4,139,151,234] most commonly in oligoacene derivatives, and attempts have been made to tune interactions between building blocks within the bulk,[109,148] it is much harder to create molecular frameworks in which the coupling of larger units such as the electronically-active segments of a conjugated polymer chain can be investigated.

Both incoherent and coherent electronic coupling suggests that it is possible to manipulate excitation density between conjugated segments through external electrical stimuli. Field induced modulation of photoluminescence (PL) and electroluminescence (EL) intensity were intensively used to investigate optoelectronic properties of conjugated polymers and oligomers.[28,213,227,251] Over 30% of field induced quenching of PL intensity of MEH-PPV film between parallel electrodes was observed in our apparatus as reported in the literature.[252] Serious debate in the literature regarding mechanism of field induced quenching of intensity was focused on two models. One favors the exciton dissociation and direct generation of charge carriers based on the fact that femotosecond transient absorption measurement rule out instantaneous quenching due to reduced oscillator strength,[251] while the other proposes the existence of intermediate state of separated but still weakly bound exciton, i.e., polaron pair, of low radiative lifetime before final exciton dissociation.[211,213] Regardless of the actual steps it takes to achieve exciton dissociation, application of electric field has proved to be an effective way to modulate emission and photogeneration of charge carriers.[28,213] Few results have been

reported in the field induced quenching of intensity on small oligomers due to relatively small effect in these small molecules compared to the polymers.[227] Linear decrease of quenching efficiency with the inverse of chain length has been observed in MEH-PPV and its oligomers of various chain lengths.[227] This dependence reveals a mechanism of intrachain exciton separation that is confirmed by experiment on polymer chains of deliberately interrupted conjugation lengths.[211] However, the unavoidable question regarding contribution of exciton separation between conjugation segments on the same chain or distinct chains was partially answered.[252]

Therefore, controlled interaction between conjugation segments is a timely requirement for the investigation of photophysical and electrical properties under the influence of surrounding molecules. Here, we focus on a material system based on oligo(phenylene-ethynylene-butadiynylenes) of defined oligomerization degree, which closely resembles a typical conjugated unit, the chromophore, as is formed in a polymer chain. By tuning the spacing between intramolecularly connected parallel units, and their relative orientation, coherent coupling and incoherent energy transfer can be differentiated. Enhancement of exciton dissociation from interchromophoric interaction is also revealed.

3.3 Results and Discussion

3.3.1 Photophysical Characterization and Self-Assembly

Figure 3.1 shows the structures under investigation. The synthesis and a full characterization of the compounds **1**, **2**, **4**, and **5** can be found in the Supplementary

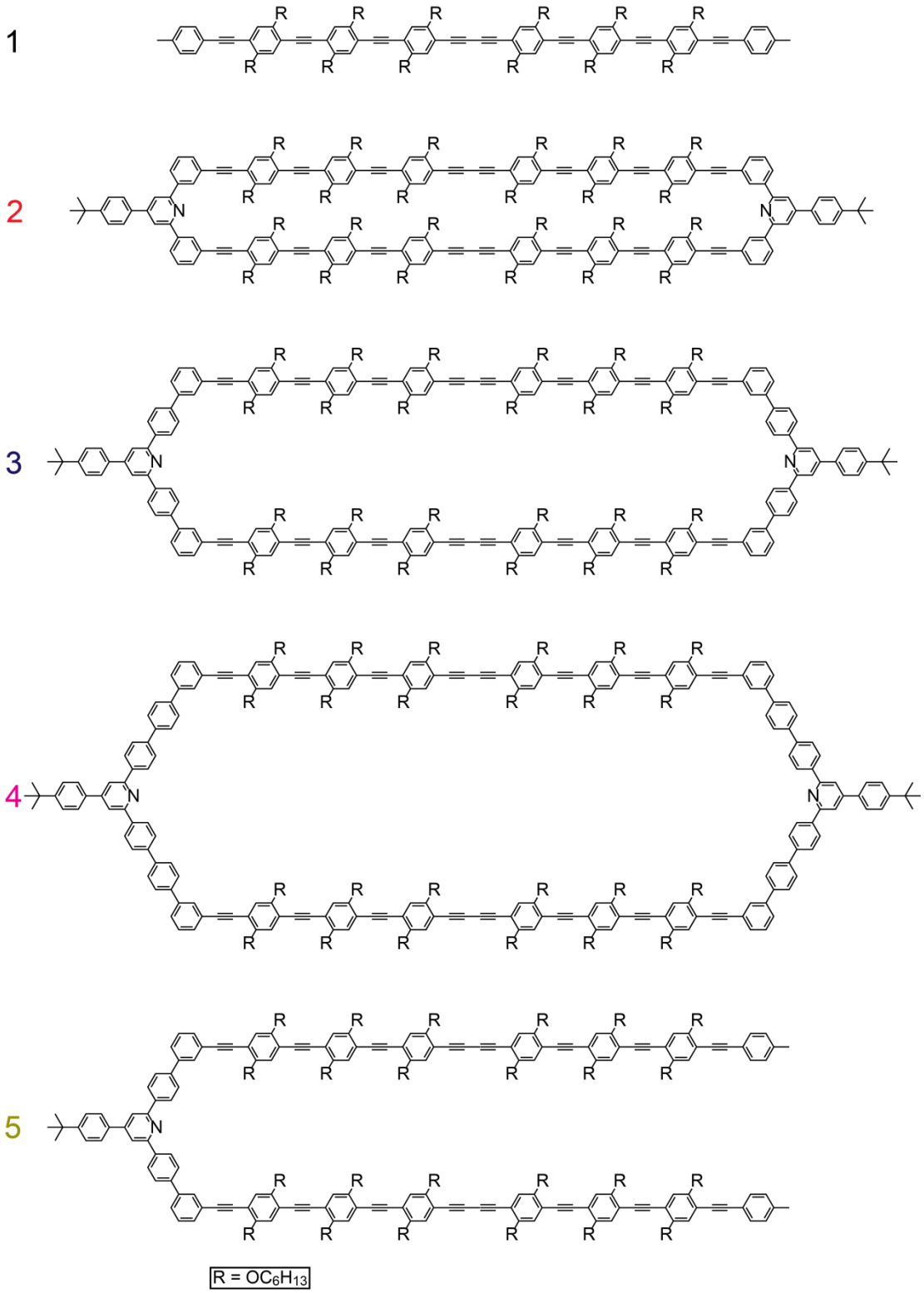

Figure 3.1 Structures of the phenylene-ethynylene-butadiynylene oligomer **1** and dimers **2-5**.

Information of Ref. 206.[206] The synthesis of macrocycle **3** was recently described.[250] All cyclic structures are built up by placing two monodisperse conjugated oligomers in a parallel configuration with a defined distance. The distance of the two chromophores is determined by two rigid aromatic clamps: 0.7 nm (**2**), 1.4 nm (**3**) and 2.1 nm (**4**). To evaluate the effect of the parallel chromophore alignment on the photophysical properties of the compounds, **5** was prepared in which the chromophores are still covalently connected but can adopt different relative orientations (see below). Monomer **1** is investigated as a reference, constituting the basic building block of the cyclic and acyclic model compounds. The basic optical properties of the materials, obtained at room temperature in dilute (10^{-7} molar) chloroform solution are summarized in Figure 3.2.

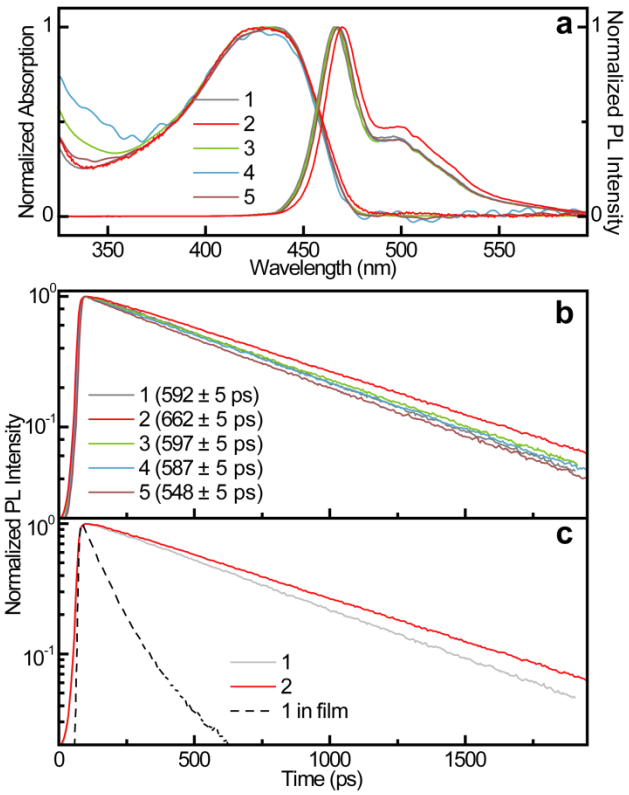

Figure 3.2 Photophysical characteristics of compounds 1-5. a) Absorption and fluorescence spectra in dilute chloroform solution. b) Fluorescence lifetime. c) Comparison of a film fluorescence decay of 1 to the solution emission decay of 1 and 2.

Based on their parallel arrangement, intramolecular H-aggregate formation between the two chromophores on the dimers is an intuitive expectation. Such aggregation should be evident both as a hypsochromic shift in absorption and as a decreased decay rate compared to the monomer, since the lowest-energy transition of the split excited state loses oscillator strength.[105,154] However, the absorption and emission spectra (panel a) are virtually identical for all five compounds, except that a small red-shift is observed in the absorption and emission spectra of the most closely spaced dimer **2**. In the absorption spectrum, the shift of the red-tail by 1.2 nm with respect to the monomer 1 is close to the resolution limit, but in emission the intramolecular interchromophoric interaction accounts for a bathochromic shift of 4 nm. At the same time, the intensity of the vibronic structure around 500 nm increases with respect to the monomer 1. The fluorescence decay of the solutions is given in Figure 3.2b), recorded with a picosecond streak camera under excitation at 430 nm by a frequency-doubled femtosecond laser. Within measurement accuracy, the fluorescence lifetimes of the monomer 1 and the more widely-spaced dimers **3** and **4** are identical. The closely-spaced dimer 2 displays an increase in fluorescence lifetime of 10 %, the open dimer a reduction in lifetime of 7 %. The combination of increased lifetime and red-shifted emission in **2** bears signatures of an excimer,[138,147,148,154,253] a dimer which only exists in the excited state. Since the ground state of such a dimer is repulsive, the transition lifetime is increased with respect to the monomer and the emission spectrum broadens and shifts to the red.[105,170]

There has been extensive debate in the literature about the possible emergence of excimers or other aggregate species by intermolecular interactions in conjugated polymers.[109,148,168] The underlying problem in any spectroscopic approach is that both

spectral and lifetime changes in a heterogeneous bulk system may have a range of origins. For example, emissive chemical defects may also be present, whose role can be dramatically amplified by energy transfer in the solid.[132] Given this tentative conclusion of weak excimer formation in **2**, it is tempting to search for excimeric signatures in the bulk film of the monomer 1, where even closer cofacial packing should be possible than in the dimer **2**. However, the decay of the fluorescence from the film of **1** is significantly accelerated with respect to the solution-based measurements of **1** and **2** as shown in Figure 3.2c). Thus, the film-based fluorescence decay measurement does not reveal any signatures of possible excimer formation in the film of **1** on the level of that seen in the intramolecular aggregate **2**, implying that spontaneous cofacial ordering of the oligomers does not occur in bulk films. Full inspection of the fluorescence spectra and decay characteristics of bulk films created from each molecular system is available in Section 3.5.

Strong dipolar interactions between adjacent chromophores leading to a splitting of energy levels and an energetic redistribution of oscillator strength are not the only interchromophoric effects which can arise. Many nominally unpolar π-conjugated systems display a substantial solvatochromic response which can be amplified by the presence of polar backbone substituents,[28] such as the alkoxy groups used in the present case. The slight red-shift in the absorption of **2** may therefore arise due to a small modification of the effective solvent shell surrounding the individual chromophore due to the proximity of the two chromophores – effectively constituting a solid-state solvatochromic effect within an isolated molecule.[254] We discuss this possibility in detail in Section 3.5. The formation of excimers should not be sensitive to solvent polarity.[253]

To assess the solvatochromic effect, we performed time-resolved spectroscopy in four solvents with different polarities, and found that the molecules demonstrate obvious solvatochromism. In all cases, **2** shows the most red-shifted spectra and the slowest PL decay compared to the other compounds. We conclude that both excimer formation and intramolecular solvatochromism are most likely responsible for the observed distinctive difference of **2** with respect to the other compounds.

The slight acceleration in fluorescence decay of the open dimer 5 may be interpreted as an indication for the occurrence of intramolecular FRET.[143,151,152] The two chromophores in the dimers have (nearly) identical transition energies and lifetimes. Coupling between the two in the form of FRET should therefore modify neither the emission color nor the fluorescence kinetics substantially. However, the open dimer **5** is by design less rigid than the other dimers so that the chromophores are only accidentally aligned in parallel with respect to each other.[250] This absence of rigidity is readily visualized by directly comparing the molecular self-organization on highly ordered pyrolytic graphite (HOPG) by scanning-tunneling microscopy (STM) for closed (**3**) and open (**5**) dimers. The STM images in Figure 3.3a) and b) show that **3** spontaneously orders into regular structures.[250] The cyclic nature of the molecular building blocks can be clearly visualized. The two-dimensional crystal structure is illustrated in the associated molecular models. In contrast, as shown in panel Figure 3.3c), the 2D crystalline domains of **5** are of limited lateral dimensions, and separated by amorphous regions. After adsorption from the solution (and thus restriction to planar structures), three distinct conformers of **5** with different orientations of the rigid rod units relative to the rotatable clamp unit can be distinguished, which are denoted in the schematic in panel d) as N, U,

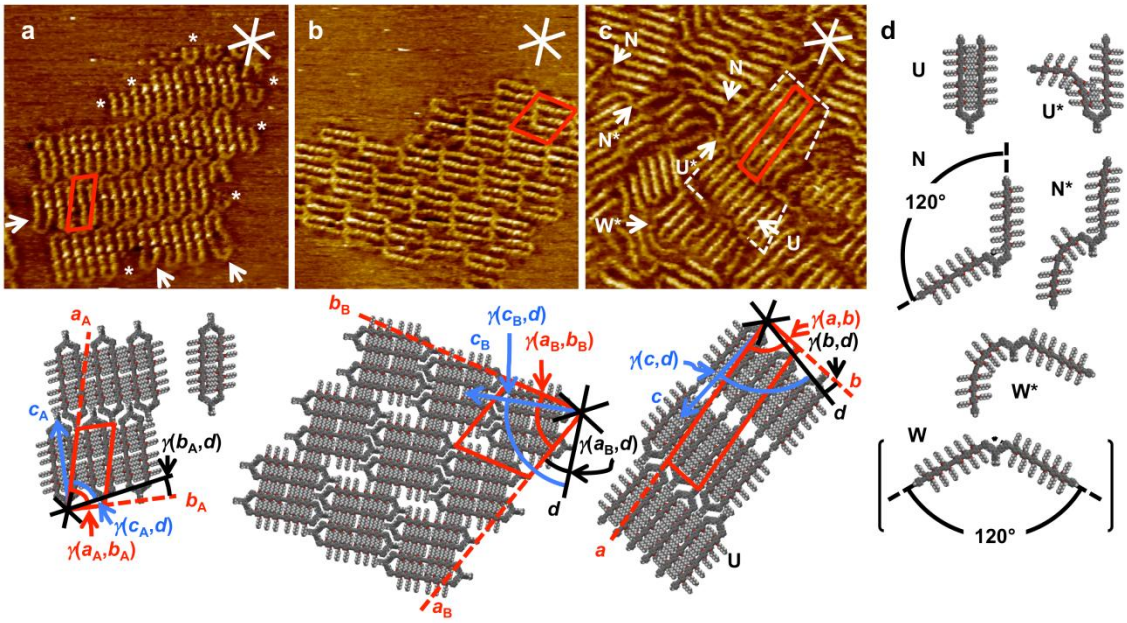

Figure 3.3 STM images and molecular models of self-assembled adsorbate layers of the closed dimer 3 (panels a, b) and the open dimer 5 (panels c, d) on highly ordered pyrolytic graphite (HOPG). The associated sketches illustrate the observed molecular packing. For the open dimer 5, different packing is possible due to the variable molecular conformations, as summarized in panel d. U, N, and W indicate distinct planar conformers of 5 after rotation of the rigid rod units around the clamp unit, and U*, N*, and W* illustrate similar conformers where additional bending of the rod units occurs. (a: 35.1×35.1 nm^2, V_s = -1.0 V, I_t = 10 pA, unit cell: a_A = 6.3 ± 0.3 nm, b_A = 2.9 ± 0.2 nm, □(a_A,b_A) = 77 ± 2°; b: 41.1×41.1 nm^2, V_s = -0.8 V, I_t = 6 pA, unit cell: a_B = 6.5 ± 0.3 nm, b_B = 6.3 ± 0.3 nm, □(a_B,b_B) = 74 ± 2°; c: 37.1×37.1 nm^2, V_s = -1.0 V, I_t = 6 pA, unit cell: a = 12.5 ± 0.3 nm, b = 2.9 ± 0.2 nm, $\gamma(a,b)$ = 83±2°. Red, blue and white (black) lines represent unit cells, directions of the linear rigid rod units, and HOPG main axis directions, respectively. Asterisks in (a) indicate partly imaged molecules. See also the Supplementary Information in Ref. 37.

and W (the ideal geometries with rigid oligomer units); and as N*, U*, and W* (which including bending of the rod units). Such a variety of structural conformers is observed in the images in Figure 3.3c). Further details of this structural analysis are given in the Supplementary Information of Ref. 206.

To test for the influence of this intramolecular conformational disorder in intramolecular FRET, we measured the depolarization of fluorescence as a function of time. The

polarization anisotropy in emission can be defined as $r = (I_{\parallel} - I_{\perp})/(I_{\parallel} + 2I_{\perp})$, where the intensities $I_{\parallel}$ and $I_{\perp}$ refer to the fluorescence polarized parallel and orthogonal to the incident laser, respectively. *r* is expected to decrease with time as the molecule tumbles in solution, starting from an initial value of 0.4 as expected for an isotropic distribution of linear transition dipoles in space.[143,255] Fig. 3.4 exhibits the transient anisotropy for the five model compounds. There is no difference between the rigid dimers 2, 3, 4, suggesting that these molecules have a similar effective hydrodynamic radius (and therefore the same rotational diffusion coefficient).[228] Fluorescence of the monomer 1 depolarizes more swiftly, since the molecule is smaller and rotates faster in solution. The open dimer 5, however, displays a rapid drop in anisotropy in the first 200 ps, followed by the same depolarization dynamics as found in the closed rings. See Section 3.5.3 for a direct comparison of anisotropies of all five compounds, where the anisotropy decay curves are all plotted in the same graph.

Given that the fluorescence spectrum and lifetime of **1**, **3** and **4** are identical to that of **5**, it is remarkable that such a large difference exists in the fluorescence depolarization kinetics. The depolarization can be explained only by the existence of a range of different conformers of the open dimer, with a large angular distribution of the two chromophores with respect to each other.[235] Although one may expect a significant degree of freedom to rotate around the phenylene bonds linking the two chromophores in **5**, with both chromophores remaining in the same plane, the results imply the possibility of bending of the molecule in three-dimensional space with the two chromophores twisting out of the molecular plane and opening up like a pair of scissors. The isolated dimer therefore behaves somewhat like a disordered bulk film, with acceptor sites of different orientation

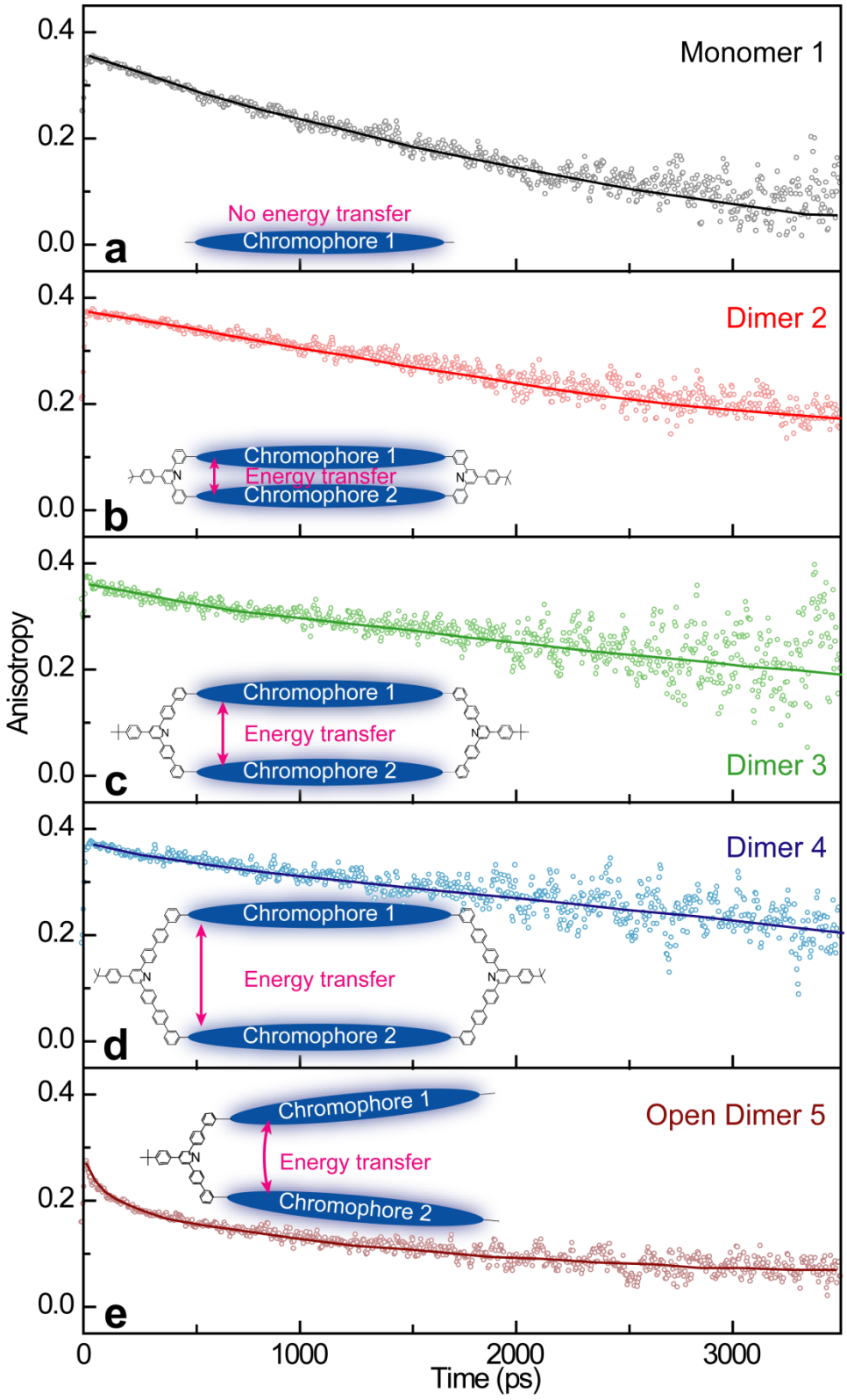

Figure 3.4 Fluorescence anisotropy decay for the monomer **1** (panel a), closed dimers **2-4** (panel b-d) and the open dimer **5** (panel e) in dilute solution.

available so that FRET can drive depolarization.[143,146,155,228]

In the rigid dimers, the parallel arrangement of the chromophores should imply that coupling by FRET is efficient, even if there is no immediate experimental path to prove this assumption since the chromophores are nearly isoenergetic (i.e., there is no spectral shift) and no FRET depolarization occurs. An indirect way to test for coupling is to examine the number of chromophores detected in a low-temperature single-molecule experiment. We have previously demonstrated that rigid polyphenylenes are especially prone to the formation of distinct chromophoric units with well-defined spectroscopic signatures.[248] These units can be differentiated by their transition energy, which effectively scatters over the inhomogeneously-broadened ensemble spectrum. The number of distinct spectral peaks, i.e., chromophores, scales with molecular weight of the polymer,[116] so we may expect to see multiple peaks in single-molecule spectra due to the multiple chromophores present in the dimers. Single-molecule fluorescence spectra were measured at 5 K by isolating individual molecules in a Zeonex® matrix and recording the emission in a microscope setup as described in earlier work.[144] Figure 3.5 shows two examples of the temporal evolution of single-molecule emission for **5**, where the intensity is color-coded and plotted as a function of time and wavelength with 5 s resolution. In the upper panel, we display an example where only one single transition is observed. The intensity and wavelength of the single emitter fluctuate over time, due to blinking and spectral diffusion. The bands at longer wavelength, e.g., at 530 nm and 545 nm in Figure 3.5 a, correspond to the vibronic progression of the electronic transition. The lower panel shows an example where two transitions are seen, one at 470 nm and one at 490 nm. In

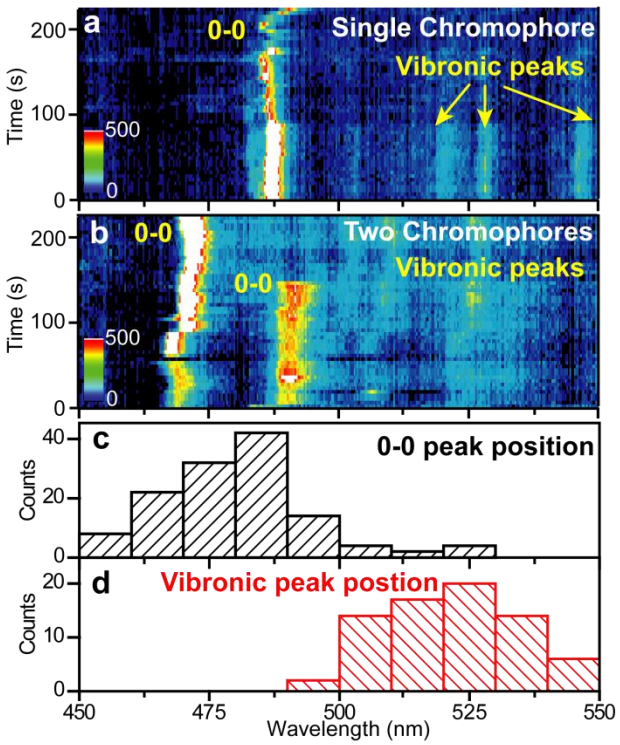

Figure 3.5 Low-temperature (5 K) single-molecule luminescence spectra as a function of time for a single dimer **5** exhibiting a single dominant peak (a) or two dominant peaks (b). The peaks are attributed to chromophores. Vibrational modes in the fluorescence are also seen, e.g. at 520 nm, 528 nm and 545 nm in a). The peaks scatter from molecule to molecule as shown in the histogram. c) and d) show histograms of the peak positions of the 0-0 transitions and vibronic progressions, respectively.

the course of the experiment we investigated a number of molecules. The scatter of the peak positions between different single molecules is shown in the histogram: different individual units exhibit different transition energies. Consequently, different units should be detectable within a single bichromophoric molecule. However, virtually all single molecules showed only single chromophore emission, whereas previous work on single polymer chains often showed multichromophoric emission with multiple peaks in the PL spectrum.[116] For **1**, where single-peak emission is to be expected, 434 molecules showed one 0-0 peak with one molecule showing two. For **2**, **4**, and **5** the numbers were 195, 0; 59, 1; and 130, 2, respectively. If the chromophores did not couple within the molecule,

we would expect to see many more cases of dual-peak emission in the dimers. Since this is not the case, we conclude that energy transfer occurs within the dimer to the lowest-energy unit so that only one emission peak is observed. The conclusion is subject to the assumption that there is no long-range correlation between the two chromophores, i.e., that the scatter in energy between chromophores within a molecule is identical to the scatter between different molecules as shown in the histogram. The four events of double-line emission recorded out of 818 single-molecule spectra may signify a rare situation of FRET blockage, e.g., due to particularly weak dipolar coupling between chromophores with weak vibrational coupling and correspondingly narrow spectral resonances and an absence of spectral overlap between donor and acceptor; or else could arise due to two molecules being present within the diffraction-limited focal spot of the microscope. Interestingly, no difference is seen between compounds **1**, **2**, **4** and **5** on the single-molecule level in terms of the spectrum, blinking, brightness and spectral dynamics, implying that efficient incoherent interchromophore coupling to a lowest-energy state also occurs in the most distantly-spaced aggregate **4**. The efficiencies of FRET of different dimers are a useful piece of information to interpret the similarity between the dimers presented here. However, due to the small quantities of materials, the molar extinction coefficient of the molecules, which is needed to calculate the Förster radius, could not be collected. Therefore, the efficiency of FRET cannot be estimated.

3.4 Field Induced Quenching

As mentioned in Section 1.5.2, an increase of exciton density has been shown to increase interactions between excitons which causes the generation of biexciton and ultrafast nonradiative decay of excitons through singlet-singlet annihilation.[225,226] The

latter effect is believed to increase exciton separation and photogeneration of charge carriers.[213]As pointed out by Kersting et al.,[137]quenching becomes increasingly difficult when excitons relax to states deep into the density of states, which indicates that excitons of higher energy generally have a higher rate of dissociation. This effect has been demonstrated by increase of field induced quenching with increase of excitation photon energy.[224] In the case of high excitation density, the acceptor exciton gains sufficient energy from the donor exciton through singlet-singlet annihilation as illustrated in Figure 1.20.

Figure 3.6 shows the molecular structure of molecule **6**. The synthesis of **6** was recently described.[143]This molecule with the shape of a spoked wheel consists of 12 chromophoric conjugated segments which are arranged as rims and spokes. The conjugation between the rims and spokes is interrupted. Side groups on the rims are removed to reduce repulsive forces. Each rim or spoke forms an absorbing and emitting chromophore. Capacitor devices containing **1**, **3** and **6** were fabricated for field induced quenching measurement following the procedure described in Section 2.4.1 and excited at 337 nm with a N_2 laser of 20 Hz repetition rate. The PL spectrum of **6** is plotted in Figure 3.6. The PL spectra of **1** and **3** in capacitor devices are the same as those shown inFigure 3.2. A shift in the PL spectrum of **6** to higher energy compared to those of **1**-**5** is observed due to the smaller size of chromophores in **6**.[227]

A DC voltage of 30 V was applied to generate an electric field of about 1.5 MV/cm in the capacitor devices of **1**, **3** and **6**. The concentration of molecules suspended in the polystyrene matrix was kept at a low level to avoid any intermolecular effects. This was

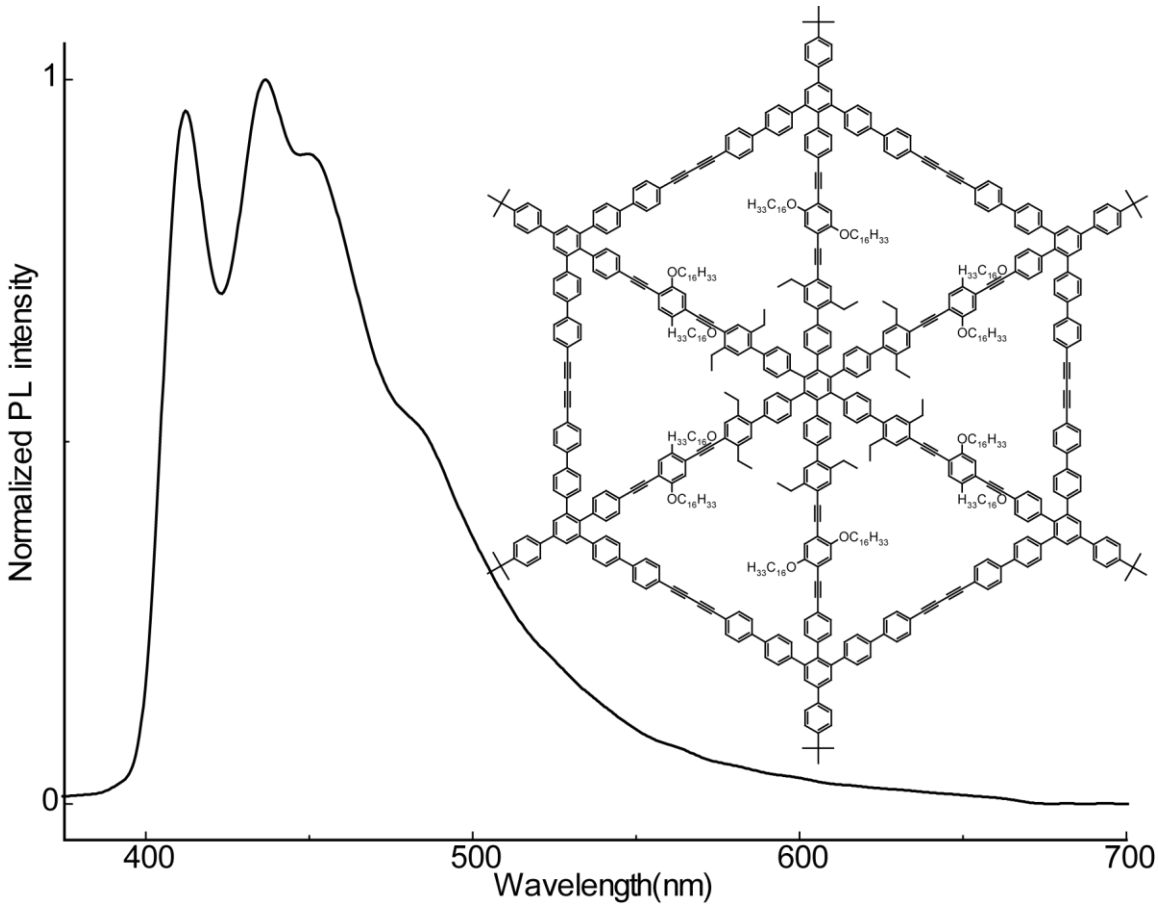

Figure 3.6 Molecular structure and PL spectrum of **6**.

confirmed by the same PL spectra in the film as in diluted solution. Therefore, all the effects present here arise from intramolecular processes. The dependence of PL quenching efficiency (as defined in Chapter 4) of **1**, **3** and **6** on excitation density is plotted in Figure 3.7. To compensate the intensity quenching due to photodegradation, the zero field intensity is an average of intensities that were taken before and after the application of the electric field. The quenching of monomer **1** is close to zero at our experimental resolution of 0.6% imposed by photodegradation at the excitation density used here. The dimer **3** shows similarly low quenching efficiency as monomer **1** below 10 $\mu J/cm^2$. A significant increase of quenching can be observed above this excitation density to approximately 3%.

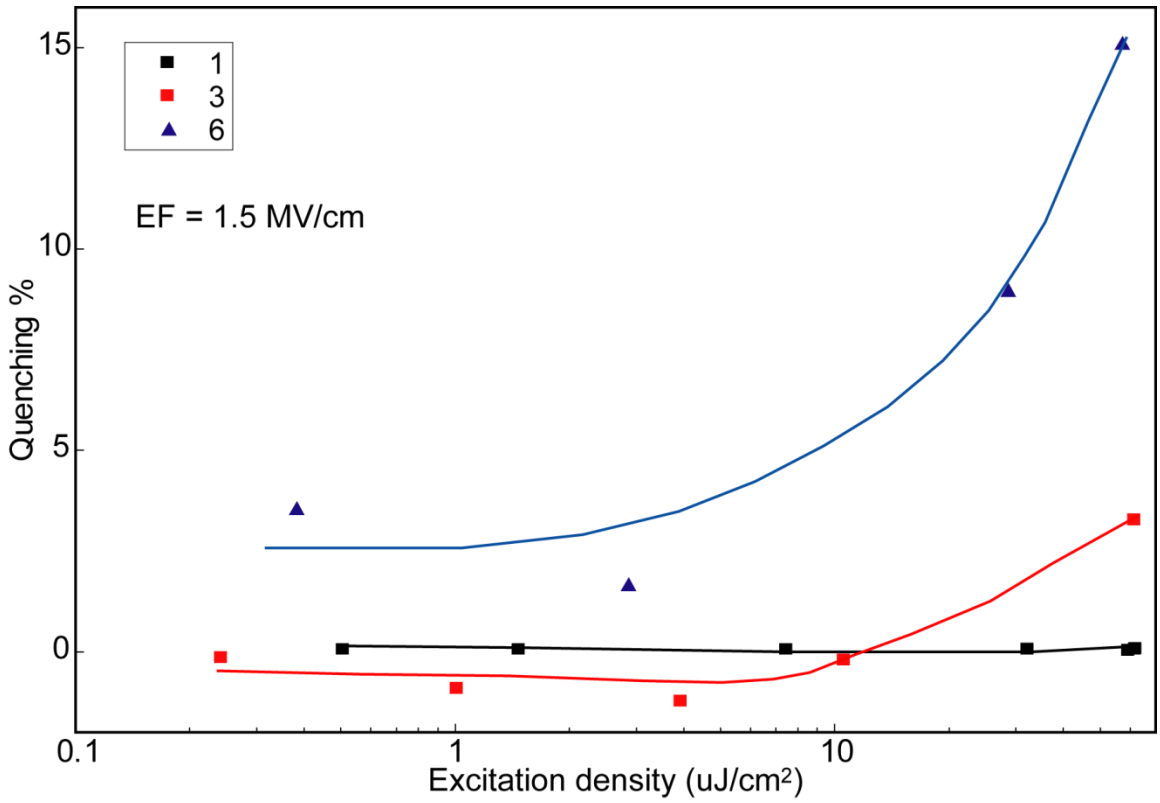

Figure 3.7 Dependence of quenching on excitation density of **1** (black), **3** (red), and **6** (blue) at 20 K. The applied electric field strength is 1.5 MV/cm.

The fact that quenching of **3** below 10 μJ/cm^2 has negative values is due to strong photodegradation of the molecules. The largest quenching effect is observed in **6,** which is above 2% through all excitation densities.

The apparent dependence of quenching on excitation density, especially in **6**, indicates an increase of quenching through exciton-exciton annihilation at high excitation densities.[200,213] The dominant case of single chromophore emission in the dimers observed in Figure 3.5 suggests the existence of efficient Förster-type energy transfer between 2 identical chromophores within a dimer. And the same energy transfer from the donor to the acceptor chromophore is also possible in multichromophoric molecule **6**.[143] At high energy density, both the donor and acceptor chromophores are in the excited

state. Energy transfer from the donor to the acceptor, also referred to as exciton-exciton annihilation,[200]promotes the exciton on the acceptor to a higher energy state of increased rate of separation and dissociation before it relaxes to a lower energy state.[213] Intramolecular interchromophoric energy transfer starts to appear in a dimer molecule like **3** and is enhanced in multichromophic molecules such as **6** or polymers. Thus a increase of quenching is observed at increased excitation density, which is accompanied by a dependence on molecular structure.

The observed quenching efficiency in the three oligomers presented here is lower than the values reported for MEH-PPV or other polymers.[28,252,256] The conjugation length does not seem to be the primary reason for the difference in quenching among **1, 3** and **6**. In that case the quenching in **6** of the shortest conjugation length should be the smallest among the three compounds.[211,227] Instead, the quenching shows a correlated increase with increased number of conjugated segments which increase from 1 in **1** to 12 in **6,** even at low excitation densities with negligible amount of exciton-exciton annihilation. Therefore, intrachromophoric exciton separation can be excluded from being the dominating factor that results in the differences in quenching observed among **1**, **3** and **6**. The correlation can be explained through interchromophoric (or interchain) exciton separation between different conjugated segments or chromophores.[252] The twelve symmetrically arranged conjugated chains in molecule **6** assure the exciton separation between two chains regardless of the direction of the applied electric field with respect to the orientation of the molecule. Thus, the capacitor structure of macromolecule **6** shows the largest quenching, while the capacitor structure f monomer **1** shows close to zero quenching.

3.5 Conclusion

In summary, we have performed a range of optical and electrical studies on open and closed pi-conjugated bichromophoric systems as model systems for interchromophoric interactions in organic electronic materials. The spectral properties and emission lifetime are remarkably resilient under structural variations. Introduction of intramolecular disorder by removal of one of the macrocycle clamps revealed interchromophoric intramolecular FRET in terms of an accelerated decay of polarization anisotropy. The occurrence of FRET in the open dimers implies that it must also arise in the closed dimers, even though it can only be inferred indirectly, for example by the low-temperature single-molecule emission characteristics. Interchromophoric interactions, and especially light-harvesting phenomena, are usually visualized by means of a change in fluorescence spectrum, lifetime or polarization anisotropy. The systematic approach presented here, by constructing conformationally-controlled dimers from individual building blocks, illustrates that interchromophoric interactions may even arise when no immediate observable is available since neither lifetime, spectrum nor polarization changes in the parallel closed dimers. Realizing the presence of such interactions is crucial for understanding limitations in quantum efficiency of the material, since interchromophoric coupling can promote migration of excitation energy to quenching species. At the same time, large aggregates of parallel chromophores in macrocyclic templates could pose excellent systems for fluorescence quenching-based sensing, with superior interaction cross sections when compared to conventional linear polymers. Field induced intensity quenching increases with the increase of excitation density in the multichromophoric molecules. Interestingly, the macromolecule of twelve symmetrically

arranged conjugated segments shows a quenching efficiency that is comparable to that of large polymers, which reveals the importance of interchromophoric interactions for exciton separation.

3.6 Supporting Information

3.6.1 Photoluminescence of Bulk Film

As stated in the main text, numerous reports have claimed to observe the formation of excimers in conjugated polymers due to either cofacial stacking between molecules, or self-folding of single chains.[29,168] Since dimer **2** shows signatures of an excimer in the solution measurements, we probed the possibility of cofacial stacking when the molecules are cast into a bulk film. If the cofacial stacking is favored in the bulk film, signatures of excimer emission should be readily observed with optical excitation.

Bulk film samples were prepared by drop casting concentrated solutions of different molecules (>10^{-4} molar concentration) in chloroform onto glass substrates, which were first allowed to dry in air, and then were mounted under vacuum (<10^{-6} mbar) in our microscope. The film samples were excited at 430 nm by the same laser source as used for the solution measurements, and the emission was collected by the same streak camera system, as described in the experimental methods.

The spectra in the bulk films are red-shifted compared to the spectra in solution, but the distinct vibronic peaks remain easily identifiable. The two peaks at 520 nm and 545 nm belong to the same vibronic progression identified in the single molecule fluorescence spectra. As their relative intensities increase in the solid state, these peaks have previously erroneously been attributed to aggregate formation. Although excimer emission should indeed be red-shifted compared to the isolated monomers as is the case

in Figure 3.2, the emission should also be broad without distinctive vibronic peaks due to the repulsive nature of the ground state in an excimer with the associated lack of a vibronic manifold. This is not the case here. Excimer formation should also be observable in the PL decay dynamics through a decreased decay rate as compared to that of the monomer. The bulk films of the monomers and the dimers all show multiexponential decay for both the high and the low-energy peaks. During the 800 ps time range displayed in Figure 3.8b, the bulk films show faster fluorescence decay compared to the solutions where the molecules are highly isolated, illustrating that the decay dynamics of the bulk film emission also lack any observable signatures of excimer formation. The acceleration of fluorescence decay that is observed in the bulk film most likely arises from enhanced migration to fluorescence-quenching defect sites. We therefore conclude that spontaneous cofacial dimer formation to spontaneously yield geometries comparable to **2** does not occur in the bulk film; instead, the molecules are oriented randomly with respect to each

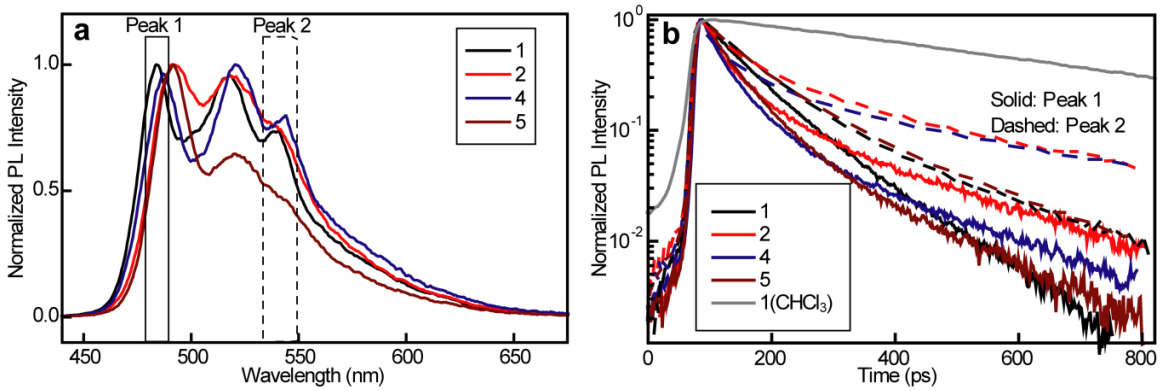

Figure 3.8 PL spectra and time-resolved luminescence of molecules **1, 2, 4,** and **5** in bulk films. a) PL spectra integrated from 0 to 100 ps after excitation. Peak 1 (solid box) and peak 2 (dashed box) mark regions integrated to acquire the intensity decay shown in b). b) Intensity decay of peak 1 (solid) and peak 2 (dashed) in bulk films. The decay curve of the monomer **1** (gray line) in chloroform solution is also plotted for comparison.

other. This conclusion is in contrast to the properties of **2** reported in the main text, wherea small red shift and a slowing of the PL decay is observed in solution, indicative of the formation of a weak intramolecular excimer.

Further inspection of the luminescence decay curves presented in Figure 3.8b reveals that the four compounds can be divided into two groups depending on their slow decay behavior. The initial fast decay is hard to distinguish, and is likely due to intermolecular energy transfer, while the subsequent slower decay shows two distinct behaviors: the closed dimers **2** and **4** show slower decay, which is close to that in solution, while the monomer **1** and the open dimer **5** have relatively higher decay rates. This structurally-related difference indicates that the rigid closed dimers tend to stay in the same configuration as in solution when deposited in the bulk. The configuration of the monomer and the open dimers, which have a more flexible structure, is more likely to be influenced by mechanical interactions with adjacent molecules in the bulk, leading to changes in excited-state lifetime. This change may be a signature of a distortion of the pi-electron system.

3.6.2 Solvatochromism

Side groups were added to the conjugated backbone of the molecules as a means of increasing solubility by slightly increasing the molecular polarity.[28] When two monomers are brought closer and closer, like in the case of dimer **2**, the dipole moment induced by the side groups from one molecule will start to affect the peak position of the emission from the other molecule, and vice versa, constituting a form of intramolecular "solid-state" solvatochromism.[254] This effect could potentially serve as an alternative mechanism for the observed spectral red shift and slowed decay in the dimer **2**.

To investigate this possibility further, we dissolved molecules **1, 2, 4**, and **5** in three additional solvents with varying polarities aside from chloroform. The emission spectra in hexane, THF and chlorobenzene were recorded in the same way as those in chloroform, as described in the main text. Solvatochromism was clearly identified for all four compounds under investigation as each spectrum shifts from blue to red when the solvent is changed from nonpolar hexane to polar THF, chlorobenzene or chloroform as shown in Figure 3.9. Changes of the PL decay rate occur within ~10 % but do not appear to follow a systematic dependence on solvent polarity, unlike the PL spectra. The spectrum of the small dimer **2** is red-shifted compared to other compounds regardless of solvent, and the decay lifetime of **2** is also higher by more than 15% in all four solvents compared to the monomer. We therefore conclude that excited-state interactions must account for at least some of the spectral changes of **2** with respect to the monomer or the

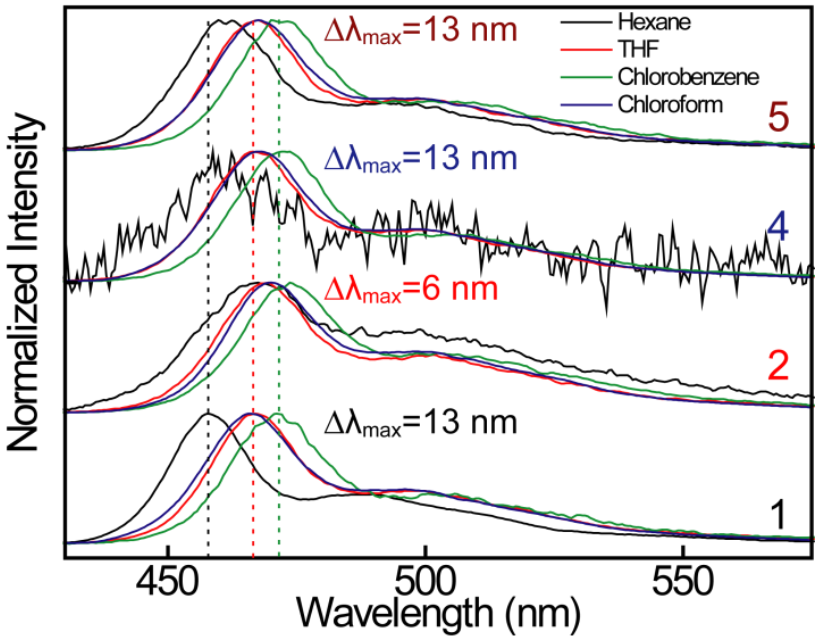

Figure 3.9 Normalized solution emission spectra of molecules **1, 2, 4, 5** in hexane (black), THF (red), chlorobenzene (green) and chloroform (blue).

larger dimers.

We note that **2** shows a smaller overall solvatochromic effect than the other compounds. There are two ways to interpret this observation. First, the delocalization in the excited state associated with the formation of the excimer could reduce the overall molecular polarity, thus lowering the solvatochromic effect. Secondly, the local fields of the side groups responsible for dipole formation interact with each other, leading to a decrease in dipolar anisotropy and thus a reduction in the overall dipole of the molecular dimer. At present, we see no obvious way to disentangle these effects, and therefore conclude that both "solid-state" (i.e., intramolecular) solvatochromic effects and excimer formation occur at the same time. We note that the mechanism of intramolecular solvatochromism, i.e., the change of effective molecular dipole by interaction with polar entities nearby, is usually ignored in the discussion of intermolecular interactions, such as those occurring in high-pressure spectroscopy, where pressure is found to induce a red shift and broadening in the emission of conjugated polymers.[257]

3.6.3 Fluorescence Depolarization

For direct comparison of the anisotropy decays of the five compounds under study, we plotted the decay curves together in Figure 3.10. It is obvious that monomer **1** shows the fastest rotation induced depolarization due to its smaller size and thus faster rotation in solution.

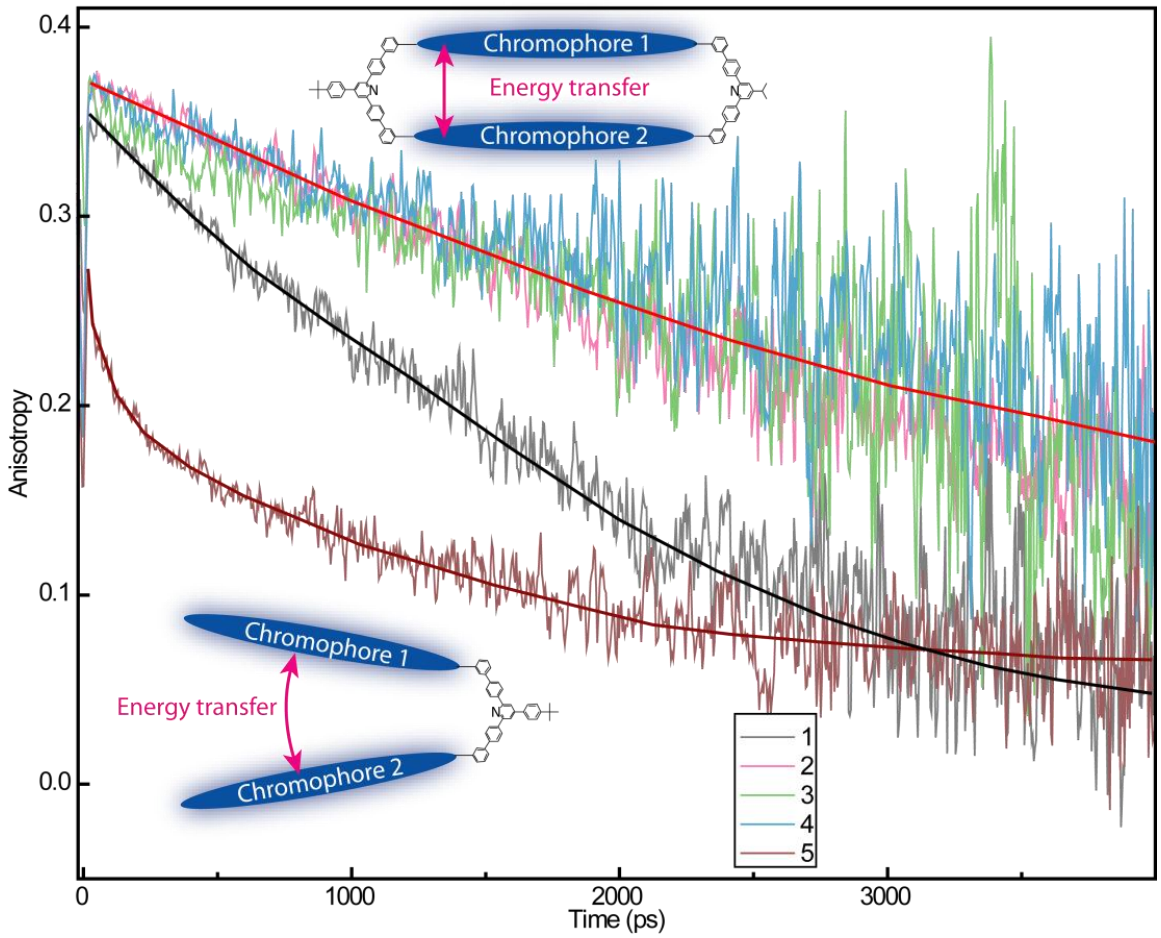

Figure 3.10 Fluorescence anisotropy decay for dilute solutions of the monomer **1**, closed dimers **2-4** and the open dimer **5**.

3.6.4 Experimental methods

The solvents and Zeonex were used as received without further purification. Sample solutions were prepared by dissolving molecules in reagent-grade chloroform ($<10^{-7}$ molar concentration) for absorption and time-resolved spectroscopy measurements at room temperature.

UV-Vis absorption spectra were recorded by a Perkin Elmer spectrophotometer. PL was excited by a frequency-doubled Ti:Sapphire laser source (Coherent Chameleon Ultra II) at 80 MHz repetition rate of pulses with 140 fs width at 430 nm. The PL spectra,

lifetime, and anisotropy decay were recorded with a streak camera system (Hamamatsu C5680) with a maximal time resolution of 4 ps. The anisotropy decay measurements were performed by tuning the polarization of the excitation beam in the horizontal and vertical direction using a λ/2 plate and collecting emission in the parallel and orthogonal polarization with respect to the excitation beam.

Single-molecule samples were prepared by spin-coating a diluted toluene solution ($<10^{-9}$ molar) blended with Zeonex on thin quartz substrates. The spectra were obtained in a home-built microscopy setup operating at 5K.

3.7 Acknowledgements

Collaborative funding by the Volkswagen Foundation is appreciated. We acknowledge financial support by the DFG (especially through the SFB 624) and the Fonds der Chemischen Industrie. JML is indebted to the David & Lucile Packard Foundation for providing a fellowship.

CHAPTER 4

EXCITON STORAGE IN CDSE/CDS TETRAPOD SEMICONDUCTOR NANOCRYSTALS: ELECTRIC FIELD EFFECTS ON EXCITON AND MULTIEXCITON STATES

Colloidal nanocrystals are known to exhibit electric field induced intensity quenching through the quantum confined Stark effect. Consequently, excitons are separated and stored in nanocrystals with an external electric field. As efficient model light-harvesting systems, heterstucture nanocrystals are ideal for population of multiexcitons at high excitation density. In this chapter, the decrease of field induced quenching of emission of CdSe/CdS tetrapod nanocrystals with increasing excitation density is revealed. Saturation of trap states which are the storage sites of excitons is proposed to cause the saturation of quenching at high excitation density. No field induced effect is observed on multiexcitons with fast decay rates, such as the biexcitons and triexcitons.

This chapter is based on a manuscript submitted to a scientific journal, which is coauthored with Nick J. Borys, Jing Huang, Dmitri V. Talapin and John M. Lupton. Subheadings are added for structural clarity and are not part of the submitted manuscript.

4.1 Abstract

CdSe/CdS nanocrystal tetrapods are interesting building blocks for excitonic circuits, where the flow of excitation energy is gated by an external stimulus. The symmetry of the

nanoparticle along with the electronic structure which favors electron delocalization between the two semiconductors suggests that all particles should adopt an orientation relative to an external electric field so that excitons can be dissociated and stored, to be released at a later time. While this approach, in principle, works and fluorescence quenching of over 90 % can be achieved electrically, we find that discrete trap states within the CdS are required to dissociate and store the exciton. These states are rapidly filled up with increasing excitation density, leading to a dramatic reduction in quenching efficiency. Charge separation is not instantaneous on the CdS excitonic antenna in which light absorption occurs, but arises from the relaxed exciton following hole localization in the core. Consequently, whereas strong electromodulation of the core exciton is observed, the core multiexciton and the CdS arm exciton are not affected by an external electric field.

4.2 Introduction

Semiconductor nanocrystals are frequently cited for their versatile optoelectronic properties,[20] yet surprisingly little is known about the excited states and their dynamics in the presence of an external electric field. In general, these states can be categorized as either quantum confined band states, or localized states, commonly referred to as traps, which are typically attributed to nanocrystal imperfections such as crystal defects and surface states. In particular, due to the large surface to volume ratio, nanoparticles are susceptible to the influence of surface defects, such as dangling bonds, which are capable of localizing charge.[15,75,258-260] Such charge localization can influence the electronic structure of the particle, to a first approximation by the quantum-confined Stark effect,[14,15,197,261] and may also play a role in more subtle effects contributing to

fluorescence intermittency.[13-15,75,215] One of the unresolved issues is how surface charge and surface traps in quantum dots relate to the underlying mechanism of blinking.[13,15,90,91] It has generally been assumed that digital blinking arises as a consequence of charging of the nanoparticle and an associated increase in the nonradiative Auger recombination rate.[13,183] The strong reduction of blinking in larger particles, most notably in vapor phase-grown self-assembled structures,[46] appears to support this conclusion, as does the sensitivity of fluorescence intermittency to surface modification and the environment.[34,262] Yet recent experiments have challenged a direct link between Auger recombination and blinking, since the dark quantum dot state does not necessarily exhibit the dramatic reduction in fluorescence lifetime indicative of increased nonradiative decay.[91] Clearly, surface traps can play a crucial role in quantum dot emission, which is readily visualized by considering the long-time luminescence decay dynamics.[88,182] Much like in the case of amorphous organic semiconductor films,[263] these transients in ensemble systems tend to follow power laws of the same exponent as the intermittency histograms recorded for single particles,[191,192] suggesting a direct link between blinking and trap filling.

We recently demonstrated that the charge-separated state in semiconductor core-shell nanorod structures can be exploited to electrostatically store excitation energy for over 10^5 times the fluorescence lifetime by spatially isolating the electron and hole of the exciton.[16] The storage mechanism can be described as a reversible transition between a direct radiative and an indirect nonradiative exciton state.[21,207,209,212,264] This nonradiative state is more reminiscent of spatially charge-separated excitations in coupled quantum well structures than of dipole-forbidden excitations such as the dark exciton in CdSe or

triplet excitons in molecular semiconductors.[64,83,130] Given the common assumption that charge separation should lead to charging of the quantum dot core, making it nonemissive by the Auger mechanism,[13] it is not clear how the proposed electrostatic formation and long-timescale storage of charge-separated excitons arises. Here, we describe a detailed study of exciton storage in CdSe/CdS tetrapod structures, with the aim of identifying the effects of the electric field on the excited state thermalization and the consequences for both the light-harvesting process from the tetrapod arms, as well as multiexciton formation and relaxation in the nanocrystal. Exciton storage is found to be due to discrete localized states (i.e., trap sites), which fill up with increasing excitation density. However, the external electric field is unable to store multiexciton states, thus suggesting that the electrical manipulation of the excited state carrier location within the nanostructures is not an instantaneous process and is slower than the relaxation time of multiexciton states. This control mechanism of carrier location and single exciton lifetime offers routes to designing building blocks for excitonic circuits and opens a direct spectroscopic window to surface trap states which play a crucial role in the photophysics of these materials.

4.3 Results and Discussion

4.3.1 Dependence of Quenching on Excitation Density

A transmission-electron micrograph of the CdSe/CdS tetrapod nanocrystals used in this study is shown in Figure 4.1a alongside a one-dimensional schematic depicting both the quantum confined band states and a distribution of traps states of a CdSe/CdS nanocrystal with and without an external electric field applied. The tetrapod structures are composed of a 4 nm diameter CdSe core that is surrounded by a CdS shell consisting of

four arms of ~30 nm in length and are particularly appealing for investigations of the effect of electric field manipulation. The bulky arms effectively prevent aggregation between cores, which cannot be fully excluded in the CdSe/CdS sphere-rod structures studied previously.[16] With the tetrapods, one can therefore be certain that electric field effects arise purely from the intraparticle electronic structure, and not from bulk-like interactions between particles. Secondly, the absorption cross section of the CdS arms in the UV, where optical excitation occurs, is over 300× larger than that of the CdSe.[49] Efficient relaxation of excitons generated in the arms to the core therefore enables the generation of very high excitation densities within the cores,[76,77,99] leading to the formation of emissive multiexciton states.[81,97,99,265,266] In addition, the greater level of symmetry of the tetrapods compared to nanorods suggests that tetrapods should be more facile for separating the electron and hole of the exciton: only nanorods with preferential orientation in the electric field will allow exciton storage, whereas for the tetrapods, all electric field orientations should lead to carrier separation.

We studied the nanosecond to microsecond photoluminescence (PL) dynamics of the tetrapod nanocrystals with and without an external electric field applied. Measurements were conducted under vacuum at both room temperature and 25 K. Figure 4.1b displays the basic capacitive device geometry employed, as described previously,[16] consisting of two electrodes with insulating layers to prevent charge injection, and a spin-coated dispersion of the nanocrystals in polystyrene. We note that great care has to be taken when choosing deposition rates and the overall thickness to prevent the formation of pinholes which can lead to current breakdown of the device. In addition, the high pulse energies of the exciting laser necessitate the use of very thin (200 μm) glass substrates to

minimize background emission from the glass. The luminescence of the device was excited by a pulsed solid state laser operating at 355 nm with 700 ps pulse lengths and variable (typically 200 Hz) repetition rate and pulse energy (up to 100 μJ). Electric fields were applied to the device either by static (Keithley 2400 source meter) or by a pulsed voltage source (Agilent 8114A pulse generator), and the emission was dispersed with a spectrometer and recorded with a gated intensified charge-coupled device camera (Andor iStar). Figure 4.1c shows the relative change in emission intensity, or quenching efficiency, as a function of electric field. The quenching efficiency is defined as the field-induced reduction in PL emission normalized to the unperturbed emission intensity ($\Delta I/I = 1 - I_{E\neq0}/I_{E=0}$). For low fields, the fluorescence quenching appears to follow a linear relationship, in contrast to the parabolic dependence reported for CdS nanocrystals.[214] This different functional dependence on field strength may arise from both the intrinsically different electronic structure of the heterostructure, as well as the different geometry of the tetrapod. Above 0.5 MV/cm the quenching efficiency begins to saturate and reaches a maximum of 95 %. Thus, at most, only 1 in 20 tetrapods are not affected by the external electric field, suggesting that suitable carrier separation and electrostatic control of photoluminescence is possible in nearly all of the individual nanocrystals. The quenched PL can be recovered in part by removal of the electric field in a pulsed experiment, which can be seen in Figure 4.1d where the luminescence decay is plotted on a double-logarithmic representation following a laser pulse at time zero. The black curve shows the emission decay at zero field, which follows the expected power-law dependence.[182] Under application of an electric-field pulse up to time 100 ns, the power-law dependence is unperturbed, but the delayed recombination is quenched by

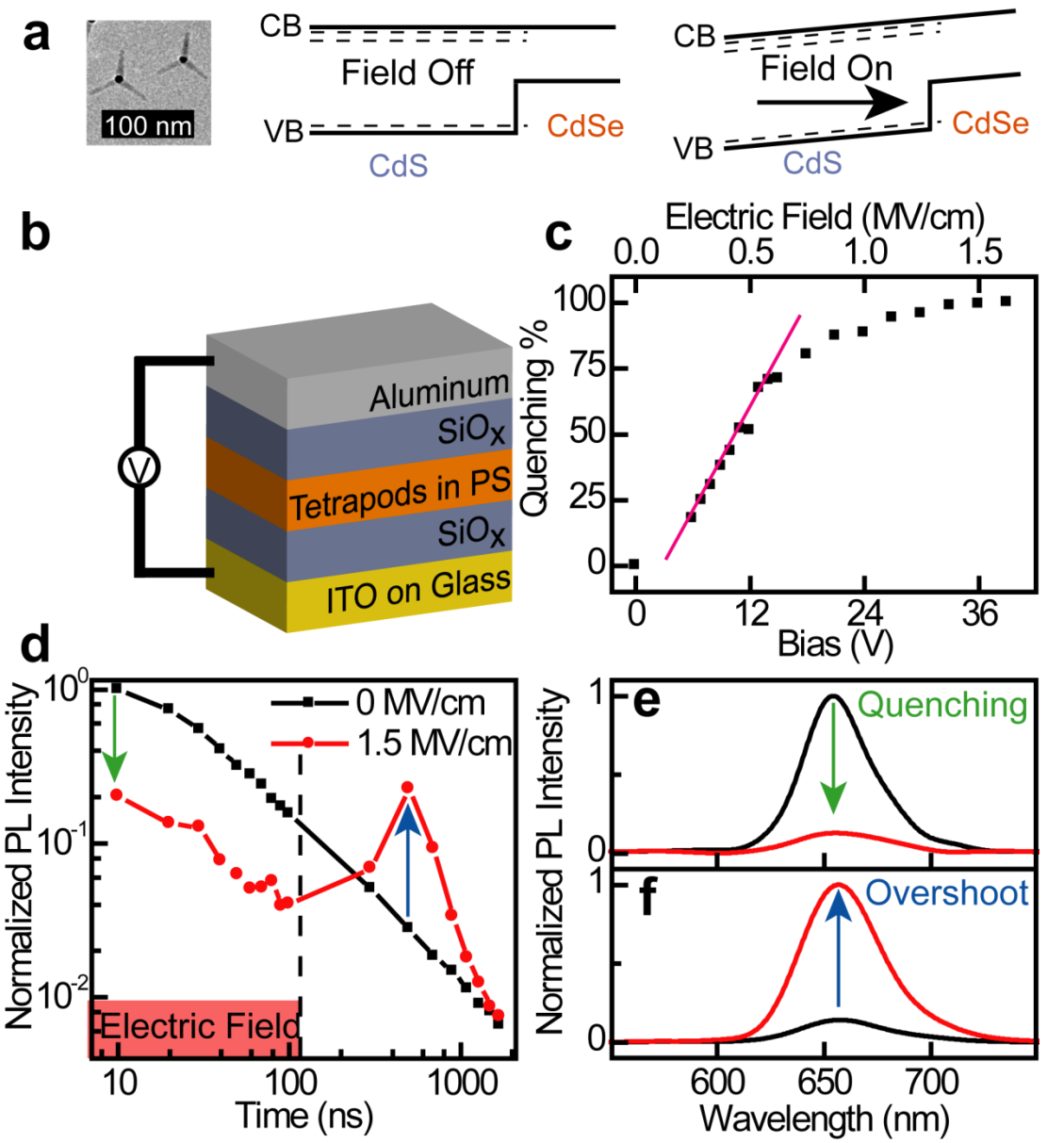

Figure 4.1 Separation and storage of excitons in an electric field. (a) Transmission electron micrograph and schematic of the electronic structure of CdSe/CdS core-shell tetrapods in and out of an external electric field where the dashed lines represent localized states while the solid lines depict the quantum-confined band states. (b) Structure of the device enabling time-resolved electromodulation of the fluorescence. (c) The PL quenching efficiency as a function of applied external electric field (i.e., device bias) shows an initial linear dependence followed by saturation. The pink line serves as guide of eye of a linear relationship. (d) The time-resolved PL within the electric field shows substantial quenching but the same power-law decay dynamics, followed by an intensity overshoot upon removal of the external field. (e), (f) Corresponding emission spectra of quenching and overshoot (black: unmodulated, red: modulated).

almost an order of magnitude. Removal of the field at time 100 ns leads to a recombination burst as separated charge carrier pairs stabilized in the external field can now recombine: excitons can be stored electrostatically in the tetrapods. The corresponding emission spectra under quenching and overshooting are shown in Figures 4.1e and 4.1f, respectively, and do not exhibit any dramatic difference to the unperturbed emission spectra, demonstrating that emission in all cases arises from the same quantum-confined CdSe excitonic species.

To gain better insight into the electronic states involved in the exciton storage process, we probe the effect of excitation density on the quenching efficiency of the CdSe core emission as shown in Figure 4.2. We find a strong dependence of the electrostatic fluorescence quenching efficiency on the excitation density per laser pulse. Figure 4.2a shows the PL intensity as a function of excitation density under different external field strengths. For all external fields, the PL intensity follows the expected linear dependence on excitation density over two orders of magnitude. Above 10 $\mu J/cm^2$, the dependence assumes a sublinear functionality which arises from the formation of multiexcitonic states and the associated increase in nonradiative Auger recombination.[18,97,243,266] Figure 4.2b plots the quenching efficiency in the 2 ns window following the laser pulse as a function of excitation density for three different field strengths. While the field strength affects the initial, maximum quenching amplitude, all three curves show the same functional dependence. Small excitation densities below 2 $\mu J/cm^2$ have a negligible effect on the quenching efficiency. Above this excitation density, however, the quenching efficiency of the device logarithmically approaches a minimum of almost 0 % over nearly 2 orders of magnitude in excitation density. Even though the PL intensity still increases with

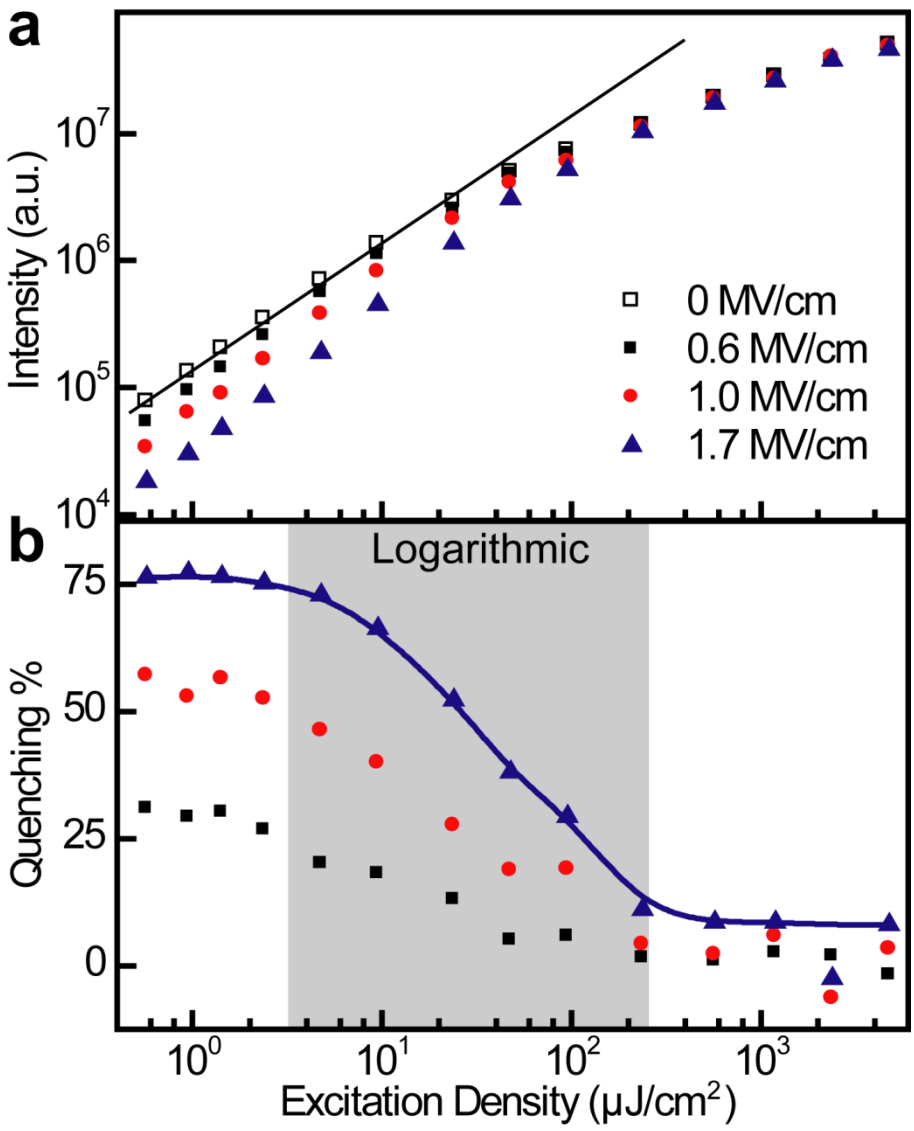

Figure 4.2 Dependence of PL intensity and quenching efficiency on excitation density at different external electric field strengths. (a) PL intensity dependence of the tetrapods on excitation density in the presence of different external fields where the black line depicts a linear relationship. (b) The PL quenching efficiency of the same device in corresponding external electric fields shows a logarithmic decrease with increasing excitation density to a uniform saturation point.

excitation density (Figure 4.2a), the quenching efficiency saturates at this minimum value. Furthermore, the saturation point of ~200 μJ/cm^2 is ubiquitous for all three of the external field strengths suggesting that it is an intrinsic property of the tetrapod ensemble and that significant quenching of the exciton can no longer occur, regardless of the electric field strength. We did not observe any significant change of the quenching functionality with temperature (from room temperature down to 25 K) or laser repetition rate thus excluding the possibility of quenching through the formation of local space charge that shields the external field. Furthermore, while only one representative device is shown here, such a logarithmic dependence of the quenching efficiency on excitation density was seen in all of the devices tested. We therefore conclude that the quenching efficiency for tetrapod CdSe/CdS nanocrystals is dependent on the excited state carrier population, and propose that each nanocrystal has a distinct threshold population of excited state carriers above which additional excitations can no longer be quenched.

By delaying the electric field pulse with respect to the optical excitation, we are able to differentiate the contributions to the exciton storage effect of delocalized band states from those of localized trap states. Accordingly, we reverse the experiment and apply an electric field pulse following the laser pulse at times exceeding the exciton lifetime, thus specifically probing any long-lived trapped charges. In this way we can drive trapped charges, which are created due to spontaneous ionization of the exciton, to recombine,[15,183,259,267] assuming that they have preferential orientation with respect to the electric field. Figure 4.3a plots the transient PL intensity for a device with and without an electric field pulse applied between times 1000 ns and 1800 ns after laser excitation. The transient luminescence decay follows the common power-law dependence. At the onset

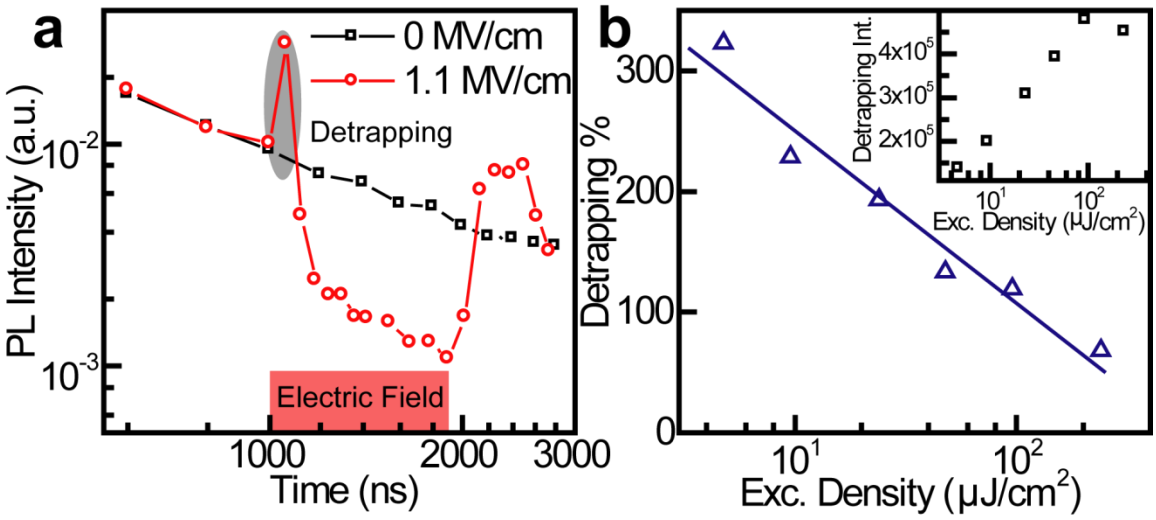

Figure 4.3 Transient luminescence of a device for which the electrical pulse is applied after excitation by a laser pulse. (a) The recombination rate of intrinsically-generated trapped excitations is initially increased by the electric field pulse which promotes charge detrapping of carrier pairs with dipoles parallel to the electric field. (b) The relative intensity of the electrically-induced PL burst decreases with increasing excitation density due to the limited population of trap states in the individual nanoparticle. Inset in (b), the absolute area of the PL burst grows logarithmically with excitation density until it appears to saturate at large excitation densities.

of the electric field pulse the luminescence rises by a factor of three, only to be quenched subsequently by an order of magnitude. After removal of the electric field, the usual overshoot occurs. The overshoot at the *onset* of the pulse can only result from detrapping of charges in the nanocrystal that is then followed by formation and relaxation of core excitons. As shown in Figure 4.3b, the relative area of the detrapping peak decreases logarithmically with excitation density in a similar fashion to the quenching of the luminescence (Figure 4.2b). Further, the absolute area of the detrapping peak shows a logarithmic *growth* which appears to also saturate at large excitation density as shown in the inset of Figure 4.3b. The remarkably similar dependence of the detrapping overshoot peak on excitation density to that of the PL quenching strongly suggests that the observed exciton storage effect is mediated through long-lived localized states of the nanocrystal.

Consideration of the dynamics presented here for tetrapods in addition to our past work on nanorods,[16,197] leads us to propose that the primary states responsible for the formation of these charge-separated excitons in the presence of an external electric field are the localized trap states,[15,178,259,267,268] as opposed to the quantum-confined band states of the nanocrystal. The conduction and valence band offsets of CdSe and CdS are such that, to a first approximation, a quasi type-II heterostructure is formed (Figure 4.1a),[12] where the excited electron state spans the two materials while the hole state is confined in the lower-gap CdSe. Intuitively, one would therefore expect an external electric field to simply shift the center of the electron wave function out of the CdSe and into the CdS, thus reducing overlap with the hole and lowering the radiative rate and emission strength. One would also expect such an effect to depend on excited state carrier population due to increasing Coulombic repulsion with increasing population.[81,97,99] However, careful consideration of the reduced overlap of the delocalized states in the presence of an electric field for nanorods of similar aspect ratio shows that this effect alone is unlikely to account for exciton storage on timescales orders of magnitude longer than the unperturbed exciton lifetime.[16,197] Rather, the timescales presented here and in the nanorod work strongly suggest that localized defect or trap states with small oscillator strengths and long lifetimes are a crucial ingredient in the exciton storage effect reported for these CdSe/CdS systems.

It is known that such localized states, or traps, can be present on the surface of CdS.[56] For example, a signature of these localized states is the increase of direct CdS exciton recombination in tetrapods of increasing arm length.[243] In addition, it has been suggested that an interfacial barrier can be formed in the conduction band between the CdSe and the

CdS due to the strain arising from the lattice mismatch and the associated internal electric field.[12] Such traps are apparently crucial for enabling long timescale electrical exciton storage through the electrostatic separation of the excited state carriers. This situation is equivalent to the case of exciton storage in coupled quantum wells.[21,22,209] Furthermore, virtually all of the tetrapods must have such trap sites since, at low excitation density, the relative fluorescence quenching tends towards 100 % (Figure 4.1c). Once all of the suitable CdS trap sites are filled within an individual nanocrystal, any further excitons generated during the excitation pulse can no longer be stored; the CdSe core radiates unperturbed as it would in the absence of an external field. Strikingly, this observation also indicates that the separated carriers do not increase the nonradiative recombination pathways such as Auger recombination. Thus, it appears that neither the external electric field nor the separated carriers greatly affect the primary exciton states with short lifetimes.

4.3.2 Impact of Electric Field on Multiexcitons

To further probe the quenching and storage process on primary excitons, we address the question of the influence of the electric field on multiexciton states and the underlying relaxation mechanism from the arm to the core. Under conditions of sufficiently strong pumping, emission can result from CdS rod excitons[243] or from CdSe core multiexcitons,[81,97,265,266] in addition to the regular CdSe exciton. Due to the competition with nonradiative Auger processes, multiexciton states typically decay within a few hundred picoseconds.[18,81,95,97,99] Figure 4.4 summarizes the electromodulated luminescence spectroscopy of the tetrapods at high excitation density. Multiple excitons can be generated either at once within one arm, or in multiple arms of the tetrapod, as

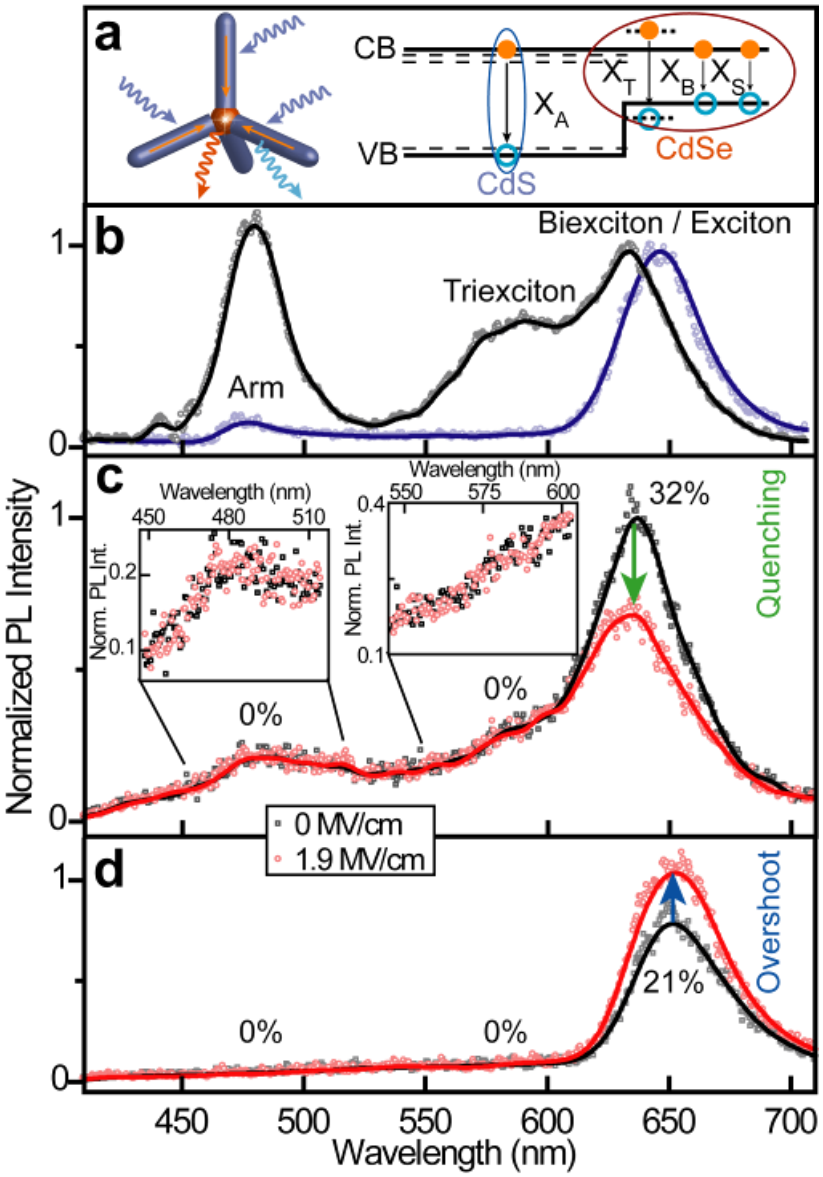

Figure 4.4 Multiexciton emission from tetrapods at high excitation densities. (a) Simultaneous absorption of multiple photons in an individual nanoparticle can lead to emission either from the arm (X_A), the core (X) or multiexciton states in the core such as the biexciton (X_B) and triexciton (X_T). (b) Comparison of gated picosecond luminescence spectra of nanocrystals in toluene solution (excitation with a 140 fs laser pulse, detection in a 0-40 ps time window) at high (black curve) and low (blue curve) excitation densities clearly reveals the spectral signatures of the multiexciton states. (c) Electric field quenching in devices is only observed in the core exciton channel, not for the arm exciton, biexciton, or triexciton. (d) Consequently, the stored excitation energy after removal of the electric field pulse returns solely as single exciton core emission.

sketched in Figure 4.4a. Emission may then either occur directly from the arm (labeled X_A, light blue), or from the core (orange) as a regular exciton (X) or a multiexciton state such as the biexciton (X_B) or the triexciton (X_T).[95,97,265] The four intraparticle species are clearly observed in time-resolved fluorescence spectra. Due to the fast decay of the multiexcitons, we employed a combination of femtosecond laser excitation with picosecond streak camera detection to clearly resolve the different features. Using pulsed excitation at 400 nm (pulse length 140 fs, repetition rate 80 MHz), Figure 4.4b illustrates the spectral signatures of the multiexciton states by comparing the PL spectrum of the tetrapods in a toluene solution in a 40 ps time window after excitation at high excitation density (9 $\mu J/cm^2$) to the spectrum at low excitation density (0.2 $\mu J/cm^2$). The PL spectrum at high excitation density shows three notable differences to that at low excitation density: (1) the main luminescence peak shifts ~10 meV to higher energies which is attributed to the Coulombic repulsion present in the biexciton formed;[81,97] (2) a luminescence peak appears at ~580 nm which is assigned to the triexciton state;[97,266] and (3) a luminescence peak at ~480 nm arises due to radiative recombintation in the CdS arms.[243] The three visible peaks display the characteristic power dependence: linear for the arm emission, linear to sublinear for the core exciton, and quadratic for the core triexciton (data not shown). The small protrusion at 450 nm arises due to Raman scattering from the solvent.

The same spectral features are visible in the nanosecond PL spectra of the thin-film devices, albeit with reduced amplitudes of the multiexcitons due to the longer optical gate length of 2 ns in detection using the intensified camera rather than the streak system. To test for the influence of the electric field we chose the lowest excitation density for which

triexciton emission could be clearly resolved, and sufficiently high electric field pulses to ensure substantial quenching. As Figure 4.4c reveals, application of the field only reduces the intensity of the main luminescence peak. All of the signatures of the multiexciton states (the CdS arm emission, the triexcition emission, and the spectral shift of the main peak due to the biexcition) remain. In contrast, upon removal of the electric field, the spectrum of the fluorescence overshoot (Figure 4.4d) loses all signatures of the multiexciton states and returns to the form seen under low excitation density. We therefore conclude that neither the arm exciton nor the core multiexciton states, which all have lifetimes less than a few hundred picoseconds, can be quenched or stored electrically. This observation further indicates that the quenching induced by carrier separation requires trapping of the excited carriers in localized states on timescales that exceed those of ultrafast carrier thermalization and multiexcition recombination.[76,99] Consequently, the excition storage is not an instantaneous electrostatic effect, in contrast to, for example, the quantum-confined Stark effect.[269] Rather, the external field promotes the eventual localization of carriers to long-lived nonradiative states without drastically changing the ultrafast thermalization dynamics.

We have demonstrated that the quenching and storage of excitons in CdSe/CdS nanocrystals arises from the presence of nanocrystal trap states which can be reversibly filled and emptied by the application of an electric field. Formation of such a charge separated state within the particle does not necessarily render it nonemissive, or else the saturation of electric field quenching at high excitation densities would not be discernible. In the context of unraveling the underlying mechanisms of quantum dot blinking it is therefore crucial to develop a deeper understanding of metastable charge

separated states within the single particle, which can reversibly feed the core exciton and can constitute a dominant mechanism for the recombination dynamics.

4.4 Acknowledgments

JML acknowledges funding by the VW Foundation. JML and DVT are fellows of the David & Lucile Packard Foundation and express gratitude for support.

CHAPTER 5

CONCLUSIONS

5.1 Summary of Scientific Contribution

The rapid progress in nanofabrication powers numerous new devices from relatively mature organic solar cells[24] and quantum dot laser,[270] to purely conceptual single molecule transport junctions[271] and nanocrystal based integrated circuits.[209] The aim of these novel concepts is to demonstrate the capability of newly developed materials in achieving certain functions that might be used in future electronics. The application of organic pi-conjugated molecules and inorganic semiconductor NCs in various (opto)electronic devices requires the understanding of their properties under practical operating conditions in certain devices. Two of the conditions are investigated in this work: the presence of surrounding molecules and an external electric field. The results gained from this work should provide some guide to the future choices of materials and fabrication strategies of devices.

5.1.1 Intramolecular Interchromophoric Interaction

To study coherent and incoherent interactions between organic pi-conjugated molecules, an investigation is performed on a model molecular system consisting of dimers of various interchromophoric distances and orientations to mimic the actual intermolecular interactions in organic devices. A weak coherent interaction is observed in a small dimer of a cofacial interchromophoric distance that is 0.7 nm, which shifts the PL

spectrum to the red and slows the PL decay rate due to the formation of an excimer between two chromophores.[138] In dimers of larger interchromophoric distance, only incoherent interaction is observed. Despite the much closer intermolecular distance that is accessible in films, no signature of excimers is observed, which shows that the random cofacial stacking of molecules in films as reported in literatures is not likely to lead to formation of excimers or aggregates.[109,148,168]

The incoherent interaction between molecules through FRET is useful for the probe of subtle changes in molecular structure when no immediate observables such as spectral shift or lifetime changes are available. A single dimer shows emission from only one chromophore, also in the case of a monomer due to incoherent energy transfer between the constituent chromophores, which indicates that an incoherently coupled dichromophoric molecule acts as a single emitter as confirmed by photon antibunching.[200] When the geometric arrangement of the two chromophores in a dimer changes from parallel to unparallel, incoherent energy transfer results in depolarization. The systematic characterization shown here provides a comprehensive approach to probe molecular structure.

5.1.2 Field Induced Effects

Application of electric fields modifies the thermalization of charge carriers and generates indirect excitons that are electrostatically stored at the trap sites in colloidal NCs, which cause a reduction of emission intensity. Upon removal of the electric field, the quenched excitons can be partially recovered after being stored for several μs, which causes an overshoot of intensity due to recombination of the stored excitons. The relative quenching percentage increases linearly with increase of strength of electric field until

saturation. At low excitation density, nearly 100% quenching of emission intensity is observed given a high enough electric field. As the excitation density increases, the relative quenching decreases following a logarithmic function with excitation density until it saturates at almost zero relative quenching. At various electric field strengths, the saturation is found to appear at the same excitation density, which disagrees with the popular assumption of field screening resulting from space charges.[272] The assignment of saturation of trap states as the cause of reduced quenching at high excitation density is confirmed by observing the same logarithmic dependence of detrapping of excitons on excitation density. The field induced detrapping of excitons also causes an overshoot of emission intensity at the onset of the electric field.

The electric field shows no effect on emission of multiexcitons (biexciton and triexction) [63,97] and arm excitons [243] that are generated on tetrapods at high excitation density. This null effect is attributed to fast decay rates of multiexcitons and arm excitons since the electrostatic manipulation is not instantaneous.

Field induced quenching of emission is also observed in organic pi-conjugated molecules due to the formation of separated indirect exciton. This quenching is increased in molecules of increased number of chromophores. A monomer consisting of a single chromophore shows zero quenching while a macromolecule of 12 chromophores shows a quenching that is close to that observed in polymers.[28,216,224] This observation indicates that interchromophoric exciton separation is more efficient than the intrachromophoric separation, which also points to the significance of charge-carrier separation between polymer chain in pristine films. In contrast to colloidal NCs, increase of excitation density increases quenching due to increased exciton-exciton annihilation.[213,225]

5.2 Future Work

It is rare to end a scientific work with ultimate conclusions and comprehensive answers to every question. More often, additional questions are raised or a different approach is found to be more suitable to tackle the actual problem. The results shown in this work should be seen as a step toward the final truth. During this work, some experiments are considered to be necessary to provide additional results to construct the full picture. Some of these include:

- The 2 ns time resolution of the ICCD setup for the investigation of field induced quenching prevents the direct study of charge carrier thermalization under the influence of an electric field since the thermalization happens within a few hundred ps.[76,77,99] However, the missing information of how the electric field modifies the exciton transfer from arm to core and the role of trapping during this process is very important for explaining field induced intensity quenching and exciton storage. Transient absorption should be the right choice to study this process considering its high time resolution (a few ten fs) and the delay range from a few ten fs to a few ns.[231] More conveniently, the transient absorption detects not only exciton species but also charge species which provides additional information about whether holes or electrons are localized at trap sites.
- The storage of excitons excited by a single laser pulse did not generate a high enough exciton population to observe multiexcitons in the stored signal. However, the storage of excitons generated from multiple laser pulses might be able to reach this high exciton population. An electronic set up that allows triggering of multiple laser pulses with a single electric field pulse is needed to perform this experiment.

- The saturation of trap states is thought to cause the decrease of quenching in tetrapods. A control experiment to prove this statement can be done on tetrapods with increased number of traps by removal of organic ligands for passivation. Saturation of quenching at relatively high excitation density should be expected in these NCs. In a more controlled way, the doped NCs with intentionally implanted trap sites should be an even more interesting system to investigate for electrostatic exciton storage.[178]
- A dimer consisting of different chromophores with high spectral overlap for FRET should demonstrate compelling results. For example, investigation of this type of dimers in single molecule spectroscopy will further prove the single emitter argument in Chapter 3 if only the low energy chromophore is observed. An open dimer of different chromophores will show correlated depolarization with spectral shift due to FRET.
- Stronger excitation energy delocalization in smaller dimers might be an additional channel for exciton separation and intensity quenching in an electric field. Similar to the case of core/shell nanorods of quasi type-II band alignment,[72,197] the electric field can shift the wavefunction of the delocalized charge carriers and reduce electron-hole overlap in these dimers.

In a broad sense, this work demonstrates the study of dynamics and electrostatic manipulation as effective ways to probe in-depth information in nanostructures. The use of model molecular systems offer a toolbox to study the complex intermolecular interaction in (opto)electronic devices. In colloidal NCs, the usually undesired trap states are given a useful role in electrostatic exciton storage. Even if both material systems have

been studied for over 20 years, this work shows that a lot more can still be learned about their structural and optoelectronic properties.

REFERENCES

1. Alivisatos, A. P., *Science* **1996,** 271, 933-937.

2. Alivisatos, P., *Nat. Biotechnol.* **2004,** 22, 47-52.

3. Peng, X.; Schlamp, M. C.; Kadavanich, A. V. and Alivisatos, A. P., *J. Am. Chem. Soc.* **1997,** 119, 7019-7029.

4. Bartholomew, G. P. and Bazan, G. C., *Acc. Chem. Res.* **2001,** 34, 30-39.

5. Höger, S., *Pure Appl. Chem.* **2010,** 82, 821-830.

6. Zhang, J.; Tang, Y.; Lee, K. and Min, O., *Science* **2010,** 327, 1634-1638.

7. Brus, L. E., *J. Chem. Phys.* **1983,** 79, 5566-5571.

8. Smith, A. M. and Nie, S., *Acc. Chem. Res.* **2010,** 43, 190-200.

9. Wang, J. F.; Gudiksen, M. S.; Duan, X. F.; Cui, Y. and Lieber, C. M., *Science* **2001,** 293, 1455-1457.

10. Hohng, S. and Ha, T., *J. Am. Chem. Soc.* **2004,** 126, 1324-1325.

11. Califano, M.; Franceschetti, A. and Zunger, A., *Nano Lett.* **2005,** 5, 2360-2364.

12. Borys, N. J.; Walter, M. J.; Huang, J.; Talapin, D. V. and Lupton, J. M., *Science* **2010,** 330, 1371-1374.

13. Efros, A. L. and Rosen, M., *Phys. Rev. Lett.* **1997,** 78, 1110-1113.

14. Empedocles, S. A. and Bawendi, M. G., *Science* **1997,** 278, 2114-2117.

15. Rothenberg, E.; Kazes, M.; Shaviv, E. and Banin, U., *Nano Lett.* **2005,** 5, 1581-1586.

16. Kraus, R. M.; Lagoudakis, P. G.; Rogach, A. L.; Talapin, D. V.; Weller, H.; Lupton, J. M. and Feldmann, J., *Phys. Rev. Lett.* **2007,** 98, 017401.

17. Hollingsworth, J. A. and Klimov, V. I., "Soft" Chemical Synthesis and Manipulation of Semiconductor Nanocrystals. In *Nanocrystal Quantum Dots*, 2 ed.; Klimov, V. I., Ed. CRC Press: New York, 2010; pp 1-62.

18. Klimov, V. I.; Mikhailovsky, A. A.; Xu, S.; Malko, A.; Hollingsworth, J. A.; Leatherdale, C. A.; Eisler, H.-J. and Bawendi, M. G., *Science* **2000,** 290, 314-317.

19. Norris, D. J.; Efros, A. L. and Erwin, S. C., *Science* **2008,** 319, 1776-1779.

20. Talapin, D. V.; Lee, J. S.; Kovalenko, M. V. and Shevchenko, E. V., *Chem. Rev.* **2010,** 110, 389-458.

21. Lundstrom, T.; Schoenfeld, W.; Lee, H. and Petroff, P. M., *Science* **1999,** 286, 2312-2314.

22. Winbow, A. G.; Hammack, A. T.; Butov, L. V. and Gossard, A. C., *Nano Lett.* **2007,** 7, 1349-1351.

23. Samsungsm IAMOLED. http://www.samsungsmd.com/eng/skill/EN-skill-1-1.jsp

24. Heeger, A. J. http://www.ia.ucsb.edu/pa/display.aspx?pkey=1634

25. Samuel, I. D. W., *Nature* **2004,** 429, 709-11.

26. Nguyen, T. D.; Hukic-Markosian, G.; Wang, F. J.; Wojcik, L.; Li, X. G.; Ehrenfreund, E. and Vardeny, Z. V., *Nat. Mater.* **2010,** 9, 345-352.

27. Horowitz, G., *Adv. Mater.* **1998,** 10, 365-377.

28. Schindler, F.; Lupton, J. M.; Müller, J.; Feldmann, J. and Scherf, U., *Nat. Mater.* **2006,** 5, 141-146.

29. Spano, F. C., *Annu. Rev. Phys. Chem.* **2006,** 57, 217-243.

30. Park, L. Y.; Munro, A. M. and Ginger, D. S., *J. Am. Chem. Soc.* **2008,** 130, 15916-15926.

31. Liu, Z.; Kumbhar, A.; Xu, D.; Zhang, J.; Sun, Z. and Fang, J., *Angew. Chem., Int. Ed.* **2008,** 47, 3540-3542.

32. Nirmal, M.; Dabbousi, B. O.; Bawendi, M. G.; Macklin, J. J.; Trautman, J. K.; Harris, T. D. and Brus, L. E., *Nature* **1996,** 383, 802-804.

33. Chen, Y.; Vela, J.; Htoon, H.; Casson, J. L.; Werder, D. J.; Bussian, D. A.; Klimov, V. I. and Hollingsworth, J. A., *J. Am. Chem. Soc.* **2008,** 130, 5026-5027.

34. Wang, X.; Ren, X.; Kahen, K.; Hahn, M. A.; Rajeswaran, M.; Maccagnano-Zacher, S.; Silcox, J.; Cragg, G. E.; Efros, A. L. and Krauss, T. D., *Nature* **2009,** 459, 686-689.

35. Kittel, C., *Introduction to Solid State Physics*. 8 ed.; Jone Wiley & Sons, Inc: New York, 2005.

36. Clement, N.; Patriarche, G.; Smaali, K.; Vaurette, F.; Nishiguchi, K.; Troadec, D.; Fujiwara, A. and Vuillaume, D., *Small* **2011,** 7, 2607-2613.

37. Cai, J. M.; Ruffieux, P.; Jaafar, R.; Bieri, M.; Braun, T.; Blankenburg, S.; Muoth, M.; Seitsonen, A. P.; Saleh, M.; Feng, X. L.; Mullen, K. and Fasel, R., *Nature* **2010,** 466, 470-473.

38. Marzin, J. Y.; Gérard, J. M.; Izraël, A.; Barrier, D. and Bastard, G., *Phys. Rev. Lett.* **1994,** 73, 716-719.

39. Springholz, G.; Holy, V.; Pinczolits, M. and Bauer, G., *Science* **1998,** 282, 734-737.

40. Tseng, A. A.; Notargiacomo, A. and Chen, T. P., *J. Vac. Sci. Technol. B* **2005,** 23, 877-894.

41. Lu, W. and Lieber, C. M., *Nat. Mater.* **2007,** 6, 841-850.

42. Ledentsov, N. N.; Bimberg, D. and Alferov, Z. I., *J. Lightwave Technol.* **2008,** 26, 1540-1555.

43. Ediger, M.; Bester, G.; Gerardot, B. D.; Badolato, A.; Petroff, P. M.; Karrai, K.; Zunger, A. and Warburton, R. J., *Phys. Rev. Lett.* **2007,** 98, 036808.

44. Bayer, M.; Hawrylak, P.; Hinzer, K.; Fafard, S.; Korkusinski, M.; Wasilewski, Z. R.; Stern, O. and Forchel, A., *Science* **2001,** 291, 451-453.

45. Berezovsky, J.; Mikkelsen, M. H.; Stoltz, N. G.; Coldren, L. A. and Awschalom, D. D., *Science* **2008,** 320, 349-352.

46. Gerardot, B. D.; Brunner, D.; Dalgarno, P. A.; Öhberg, P.; Seidl, S.; Kroner, M.; Karrai, K.; Stoltz, N. G.; Petroff, P. M. and Warburton, R. J., *Nature* **2008,** 451, 441-444.

47. Mikhrin, S. S.; Kovsh, A. R.; Krestnikov, I. L.; Kozhukhov, A. V.; Livshits, D. A.; Ledentsov, N. N.; Shernyakov, Y. M.; Novikov, II; Maximov, M. V.; Ustinov, V. M. and Alferov, Z. I., *Semicond. Sci. Technol.* **2005,** 20, 340-342.

48. Murray, C. B.; Norris, D. J. and Bawendi, M. G., *J. Am. Chem. Soc.* **1993,** 115, 8706-8715.

49. Talapin, D. V.; Nelson, J. H.; Shevchenko, E. V.; Aloni, S.; Sadtler, B. and Alivisatos, A. P., *Nano Lett.* **2007,** 7, 2951-2959.

50. Battaglia, D.; Blackman, B. and Peng, X. G., *J. Am. Chem. Soc.* **2005,** 127, 10889-10897.

51. Chan, W. C. W. and Nie, S. M., *Science* **1998,** 281, 2016-2018.

52. Mattoussi, H.; Mauro, J. M.; Goldman, E. R.; Anderson, G. P.; Sundar, V. C.; Mikulec, F. V. and Bawendi, M. G., *J. Am. Chem. Soc.* **2000,** 122, 12142-12150.

53. Yin, Y. and Alivisatos, A. P., *Nature* **2005,** 437, 664-670.

54. Burda, C.; Chen, X. B.; Narayanan, R. and El-Sayed, M. A., *Chem. Rev.* **2005,** 105, 1025-1102.

55. Hines, M. A. and Guyot-Sionnest, P., *J. Phys. Chem.* **1996,** 100, 468-471.

56. Zezza, F.; Comparelli, R.; Striccoli, M.; Curri, M. L.; Tommasi, R.; Agostiano, A. and Della Monica, M., *Synth. Met.* **2003,** 139, 597-600.

57. Ito, Y.; Matsuda, K. and Kanemitsu, Y., *Phys. Stat. Solidi (c)* **2009,** 6, 221-223.

58. Seeger, K., *Semiconductor Physics*. 2 ed.; Springer: Bellin, 1982.

59. Donega, C. D.; Bode, M. and Meijerink, A., *Phys. Rev. B* **2006,** 74, 085320.

60. Nirmal, M.; Murray, C. B. and Bawendi, M. G., *Phys. Rev. B* **1994,** 50, 2293-2300.

61. Norris, D. J., Electronic Structure in Semiconductor Nanocrystals. In *Nanocrystal Quantum Dots*, 2 ed.; Klimov, V. I., Ed. CRC Press: New York, 2010.

62. Efros, A. L. and Efros, A. L., *Sov. Phys. Semicond.* **1982,** 16, 772-775.

63. Klimov, V. I., Multiexciton Phenomena in Semiconductor Nanocrystals. In *Nanocrystal Quantum Dots*, 2 ed.; Klimov, V. I., Ed. CRC Press: New York, 2010.

64. Labeau, O.; Tamarat, P. and Lounis, B., *Phys. Rev. Lett.* **2003,** 90, 257404.

65. Norris, D. J.; Efros, A. L.; Rosen, M. and Bawendi, M. G., *Phys. Rev. B* **1996,** 53, 16347-16354.

66. Babentsov, V. and Sizov, F., *Opto-Electro. Rev* **2008,** 16, 208-225.

67. Meulenberg, R. W.; Lee, J. R. I.; Wolcott, A.; Zhang, J. Z.; Terminello, L. J. and van Buuren, T., *ACS Nano* **2009,** 3, 325-330.

68. Amloy, S.; Yu, K. H.; Karlsson, K. F.; Farivar, R.; Andersson, T. G. and Holtz, P. O., *Appl. Phys. Lett.* **2011,** 99, 251903.

69. Achermann, M., *Phys. Rev. B* **2003,** 1, 2837-2843.

70. Efros, A. L., Auger processes in nanosize semiconductor crystals. In *Semiconductor nanocrystals: from basic principles to applications*, Efros, A. L.; Lockwood, D. J.; Tsybeskov, L., Eds. Kluwer academic/Plenum New York, 2003; pp 52-72.

71. Klimov, V. I.; Ivanov, S. A.; Nanda, J.; Achermann, M.; Bezel, I.; McGuire, J. A. and Piryatinski, A., *Nature* **2007,** 447, 441-446.

72. Pandey, A. and Guyot-Sionnest, P., *J. Chem. Phys.* **2007,** 127, 104710.

73. Scholes, G. D., *Adv. Funct. Mater.* **2008,** 18, 1157-1172.

74. Mauser, C.; Limmer, T.; Da Como, E.; Becker, K.; Rogach, A. L.; Feldmann, J. and Talapin, D. V., *Phys. Rev. B* **2008,** 77, 153303.

75. Müller, J.; Lupton, J. M.; Rogach, A. L.; Feldmann, J.; Talapin, D. V. and Weller, H., *Phys. Rev. B* **2005,** 72, 205339.

76. Lupo, M. G.; Sala, D. F.; Carbone, L.; Zavelani-Rossi, M.; Fiore, A.; Lüer, L.; Polli, D.; Cingolani, R.; Manna, L. and Lanzani, G., *Nano Lett.* **2008,** 8, 4582-4587.

77. Mauser, C.; Da Como, E.; Baldauf, J.; Rogach, A. L.; Huang, J.; Talapin, D. V. and Feldmann, J., *Phys. Rev. B* **2010,** 82, 081306.

78. Sapra, S.; Mayilo, S.; Klar, T. A.; Rogach, A. L. and Feldmann, J., *Adv. Mater.* **2007,** 19, 569-572.

79. Efros, A. L. and Rosen, M., *Anuu. Rev. Mater. Sci.* **2000,** 30, 475-521.

80. Klimov, V. I.; McBranch, D. W.; Leatherdale, C. A. and Bawendi, M. G., *Phys. Rev. B* **1999,** 60, 13740-13749.

81. Saba, M.; Minniberger, S.; Quochi, F.; Roither, J.; Marceddu, M.; Gocalinska, A.; Kovalenko, M. V.; Talapin, D. V.; Heiss, W.; Mura, A. and Bongiovanni, G., *Adv. Mater.* **2009,** 21, 4942-4946.

82. Dabbousi, B. O.; Rodriguez-Viejo, J.; Mikulec, F. V.; Heine, J. R.; Mattoussi, H.; Ober, R.; Jensen, K. F. and Bawendi, M. G., *J. Phys. Chem. B* **1997,** 101, 9463-9475.

83. Nirmal, M.; Norris, D. J.; Kuno, M.; Bawendi, M. G.; Efros, A. L. and Rosen, M., *Phys. Rev. Lett.* **1995,** 75, 3728-3731.

84. Tisdale, W. A.; Williams, K. J.; Timp, B. A.; Norris, D. J.; Aydil, E. S. and Zhu, X. Y., *Science* **2010,** 328, 1543-1547.

85. Guyot-Sionnest, P.; Shim, M.; Matranga, C. and Hines, M., *Phys. Rev. B* **1999,** 60, 2181-2184.

86. Hu, J. T.; Li, L. S.; Yang, W. D.; Manna, L.; Wang, L. W. and Alivisatos, A. P., *Science* **2001,** 292, 2060-2063.

87. Shan, C. X.; Liu, Z. and Hark, S. K., *Phys. Rev. B* **2006,** 74, 153402.

88. Jones, M.; Lo, S. S. and Scholes, G. D., *Proc. Natl. Acad. Sci. U. S. A.* **2009,** 106, 3011-3016.

89. Kuno, M.; Lee, J. K.; Dabbousi, B. O.; Mikulec, F. V. and Bawendi, M. G., *J. Chem. Phys.* **1997,** 106, 9869-9882.

90. Zhao, J.; Nair, G.; Fisher, B. R. and Bawendi, M. G., *Phys. Rev. Lett.* **2010,** 104, 157403.

91. Galland, C.; Ghosh, Y.; Steinbrück, A.; Sykora, M.; Hollingsworth, J. A.; Klimov, V. I. and Htoon, H., *Nature* **2011,** 479, 203-207.

92. Hu, Y. Z.; Lindberg, M. and Koch, S. W., *Phys. Rev. B* **1990,** 42, 1713-1723.

93. Hu, Y. Z.; Koch, S. W.; Lindberg, M.; Peyghambarian, N.; Pollock, E. L. and Abraham, F. F., *Phys. Rev. Lett.* **1990,** 64, 1805-1807.

94. Oron, D.; Kazes, M. and Banin, U., *Phys. Rev. B* **2007,** 75, 035330.

95. Oron, D.; Kazes, M.; Shweky, I. and Banin, U., *Phys. Rev. B* **2006,** 74, 115333.

96. Woggon, U., Spectroscopy of Biexcitons and Trions in II–VI Quantum Dots. In *Optics of Semiconductors and their Nanostructures*, Kalt, H.; Hetterich, M., Eds. Springer: New York, 2004; pp 107-129.

97. Sitt, A.; Sala, D. F.; Menagen, G. and Banin, U., *Nano Lett.* **2009,** 9, 3470-3476.

98. Shumway, J.; Franceschetti, A. and Zunger, A., *Phys. Rev. B* **2001,** 63, 155316.

99. Zavelani-Rossi, M.; Lupo, M. G.; Tassone, F.; Manna, L. and Lanzani, G., *Nano Lett.* **2010,** 10, 3142-3150.

100. Schaller, R. D. and Klimov, V. I., *Phys. Rev. Lett.* **2004,** 92, 186601.

101. Htoon, H.; Hollingsworth, J. A.; Dickerson, R. and Klimov, V. I., *Phys. Rev. Lett.* **2003,** 91, 227401.

102. Kazes, M.; Lewis, D. Y.; Ebenstein, Y.; Mokari, T. and Banin, U., *Adv. Mater.* **2002,** 14, 317-321.

103. McGuire, J. A.; Joo, J.; Pietryga, J. M.; Schaller, R. D. and Klimov, V. I., *Acc. Chem. Res.* **2008,** 41, 1810-1819.

104. Nair, G.; Geyer, S. M.; Chang, L. Y. and Bawendi, M. G., *Phys. Rev. B* **2008,** 78, 125325.

105. Pope, M. and Swenberg, C. E., *Electronic Processes in Organic Crystals*. Oxford Unversity press: New York, 1982.

106. Chiang, C. K.; Druy, M. A.; Gau, S. C.; Heeger, A. J.; Louis, E. J.; Macdiarmid, A. G.; Park, Y. W. and Shirakawa, H., *J. Am. Chem. Soc.* **1978,** 100, 1013-1015.

107. Bredas, J. L.; Cornil, J.; Beljonne, D.; dos Santos, D. and Shuai, Z. G., *Acc. Chem. Res.* **1999,** 32, 267-276.

108. Yang, J. S. and Swager, T. M., *J. Am. Chem. Soc.* **1998,** 120, 11864-11873.

109. Schwartz, B. J., *Annu. Rev. Phys. Chem.* **2003,** 54, 141-172.

110. Haskins-Glusac, K.; Pinto, M. R.; Tan, C. Y. and Schanze, K. S., *J. Am. Chem. Soc.* **2004,** 126, 14964-14971.

111. Rauscher, U.; Bässler, H.; Bradley, D. D. C. and Hennecke, M., *Phys. Rev. B* **1990,** 42, 9830-9836.

112. Chandross, M.; Mazumdar, S.; Jeglinski, S.; Wei, X.; Vardeny, Z. V.; Kwock, E. W. and Miller, T. M., *Phys. Rev. B* **1994,** 50, 14702-14705.

113. Kohler, A.; dos Santos, D. A.; Beljonne, D.; Shuai, Z.; Bredas, J. L.; Holmes, A. B.; Kraus, A.; Mullen, K. and Friend, R. H., *Nature* **1998,** 392, 903-906.

114. Schindler, F.; Lupton, J. M.; Feldmann, J. and Scherf, U., *Proc. Natl. Acad. Sci. U. S. A.* **2004,** 101, 14695-14700.

115. Hildner, R.; Lemmer, U.; Scherf, U.; van Heel, M. and Koehler, J., *Adv. Mater.* **2007,** 19, 1978-1982.

116. Schindler, F.; Jacob, J.; Grimsdale, A. C.; Scherf, U.; Müllen, K.; Lupton, J. M. and Feldmann, J., *Angew. Chem., Int. Ed.* **2005,** 44, 1520-1525.

117. Tretiak, S.; Saxena, A.; Martin, R. L. and Bishop, A. R., *Phys. Rev. Lett.* **2002,** 89, 097402.

118. Walter, M. J. Light-Harvesting in Single Conjugated Polymer Chains and Semiconductor Nanocrystals. University of Utah, Salt Lake City, 2009.

119. Mukamel, S.; Tretiak, S.; Wagersreiter, T. and Chernyak, V., *Science* **1997,** 277, 781-787.

120. Schweitzer, B. and Bassler, H., *Synth. Met.* **2000,** 109, 1-6.

121. Walter, M. J. and Lupton, J. M., *Phys. Rev. Lett.* **2009,** 103, 167401.

122. Hernando, J.; van der Schaaf, M.; van Dijk, E. M. H. P.; Sauer, M.; García-Parajó, M. F. and van Hulst, N. F., *J. Phys. Chem. A* **2003,** 107, 43-52.

123. Lippitz, M.; Hübner, C. G.; Christ, T.; Eichner, H.; Bordat, P.; Herrmann, A.; Müllen, K. and Basché, T., *Phys. Rev. Lett.* **2004,** 92, 103001.

124. Hallermann, M.; Kriegel, I.; Da Como, E.; Berger, J. M.; von Hauff, E. and Feldmann, J., *Adv. Funct. Mater.* **2009,** 19, 3662-3668.

125. Ma, D. G.; Lupton, J. M.; Samuel, I. D. W.; Lo, S. C. and Burn, P. L., *Appl. Phys. Lett.* **2002,** 81, 2285-2287.

126. McCamey, D. R.; Seipel, H. A.; Paik, S. Y.; Walter, M. J.; Borys, N. J.; Lupton, J. M. and Boehme, C., *Nat. Mater.* **2008,** 7, 723-728.

127. Kasha, M., *Disc. Farady Soc.* **1950,** 9, 14-19.

128. Chaudhuri, D.; Wettach, H.; van Schooten, K. J.; Liu, S.; Sigmund, E.; Hoger, S. and Lupton, J. M., *Angew. Chem., Int. Ed.* **2010,** 49, 7714-7717.

129. Lupton, J. M.; Pogantsch, A.; Piok, T.; List, E. J. W.; Patil, S. and Scherf, U., *Phys. Rev. Lett.* **2002,** 89, 167401.

130. Reufer, M.; Walter, M. J.; Lagoudakis, P. G.; Hummel, A. B.; Kolb, J. S.; Roskos, H. G.; Scherf, U. and Lupton, J. M., *Nat. Mater.* **2005,** 4, 340-346.

131. Kohler, A. and Beljonne, D., *Adv. Funct. Mater.* **2004,** 14, 11-18.

132. Becker, K.; Lupton, J. M.; Feldmann, J.; Nehls, B. S.; Galbrecht, F.; Gao, D. Q. and Scherf, U., *Adv. Funct. Mater.* **2006,** 16, 364-370.

133. Hoogenboom, J. P.; van Dijk, E.; Hernando, J.; van Hulst, N. F. and Garcia-Parajo, M. F., *Phys. Rev. Lett.* **2005,** 95, 097401.

134. Joachim, C.; Gimzewski, J. K. and Aviram, A., *Nature* **2000,** 408, 541-548.

135. Nitzan, A. and Ratner, M. A., *Science* **2003,** 300, 1384-1389.

136. Cornil, J.; Beljonne, D.; Calbert, J.-P. and Brédas, J. L., *Adv. Mater.* **2001,** 13, 1053-1067.

137. Kersting, R.; Lemmer, U.; Mahrt, R. F.; Leo, K.; Kurz, H.; Bässler, H. and Göbel , E. O., *Phys. Rev. Lett.* **1993,** 70, 3820-3823.

138. Jenekhe, S. A. and Osaheni, J. A., *Science* **1994,** 265, 765-768.

139. Tretiak, S.; Zhang, W. M.; Chernyak, V. and Mukamel, S., *Proc. Natl. Acad. Sci. U. S. A.* **1999,** 96, 13003-13008.

140. Hildner, R.; Lemmer, U.; Scherf, U. and Kohler, J., *Chem. Phys. Lett.* **2006,** 429, 103-108.

141. Becker, K. and Lupton, J. M., *J. Am. Chem. Soc.* **2006,** 128, 6468-6479.

142. Maus, M.; De, R.; Lor, M.; Weil, T.; Mitra, S.; Wiesler, U. M.; Herrmann, A.; Hofkens, J.; Vosch, T.; Mullen, K. and De Schryver, F. C., *J. Am. Chem. Soc.* **2001,** 123, 7668-7676.

143. Möessinger, D.; Chaudhuri, D.; Kudernac, T.; Lei, S.; De Feyter, S.; Lupton, J. M. and Höger, S., *J. Am. Chem. Soc.* **2010,** 132, 1410-1423.

144. Walter, M. J.; Borys, N. J.; van Schooten, K. J. and Lupton, J. M., *Nano Lett.* **2008,** 8, 3330-3335.

145. Huser, T.; Yan, M. and Rothberg, L. J., *Proc. Natl. Acad. Sci. U. S. A.* **2000,** 97, 11187-11191.

146. Goodson, T. G., *Acc. Chem. Res.* **2005,** 38, 99-107.

147. Samuel, I. D. W.; Rumbles, G. and Collison, C. J., *Phys. Rev. B* **1995,** 52, 573-576.

148. Gierschner, J.; Ehni, M.; Egelhaaf, H.-J.; Medina, B. M.; Beljonne, D.; Benmansour, H. and Bazan, G. C., *J. Chem. Phys.* **2005,** 123, 144914.

149. Bredas, J. L.; Beljonne, D.; Coropceanu, V. and Cornil, J., *Chem. Rev.* **2004,** 104, 4971-5003.

150. Kasha, M., *Radiat. Res.* **1963,** 20, 55-70.

151. Beljonne, D.; Pourtois, G.; Silva, C.; Hennebicq, E.; Herz, L. M.; Friend, R. H.; Scholes, G. D.; Setayesh, S.; Müllen, K. and Brédas, J. L., *Proc. Natl. Acad. Sci. U. S. A.* **2002,** 99, 10982-10987.

152. Scholes, G. D., *Annu. Rev. Phys. Chem.* **2003,** 54, 57-87.

153. Varnavski, O. P.; Ostrowski, J. C.; Sukhomlinova, L.; Twieg, R. J.; Bazan, G. C. and Goodson, T. I., *J. Am. Chem. Soc.* **2002,** 124, 1736-1743.

154. Bazan, G. C.; Oldham, W. J. J.; Lachicotte, R. J.; Tretiak, S.; Chernyak, V. and Mukamel, S., *J. Am. Chem. Soc.* **1998,** 120, 9188-9204.

155. Ranasinghe, M. I.; Wang, Y. and Goodson, T., *J. Am. Chem. Soc.* **2003,** 125, 5258-5259.

156. Kuroda, D. G.; Singh, C. P.; Peng, Z. H. and Kleiman, V. D., *Science* **2009,** 326, 263-267.

157. Oelkrug, D.; Tompert, A.; Gierschner, J.; Egelhaaf, H.-J.; Hanack, M.; Hohloch, M. and Steinhuber, E., *J. Phys. Chem. B* **1998,** 102, 1902-1907.

158. Lupton, J. M.; Samuel, I. D. W.; Burn, P. L. and Mukamel, S., *J. Chem. Phys.* **2002,** 116, 455-459.

159. Yang, J. S.; Yoo, H.; Aratani, N.; Osuka, A. and Kim, D., *Angew. Chem., Int. Ed.* **2009,** 48, 4323-4327.

160. Hernando, J.; Hoogenboom, J. P.; van Dijk, E. M. H. P.; García-López, J. J.; Crego-Calama, M.; Reinhoudt, D. N.; van Hulst, N. F. and García-Parajó, M. F., *Phys. Rev. Lett.* **2004,** 93, 236404.

161. Moran, A. M.; Maddox, J. B.; Hong, J. W.; Kim, J.; Nome, R. A.; Bazan, G. C.; Mukamel, S. and Scherer, N. F., *Journal of Chemical Physics* **2006,** 124, 15.

162. Varnavski, O. and Goodson, T., *Chem. Phys. Lett.* **2000,** 320, 688-696.

163. Dexter, D. L., *J. Chem. Phys.* **1953,** 21, 836-850.

164. Nesterov, E. E.; Zhu, Z. G. and Swager, T. M., *J. Am. Chem. Soc.* **2005,** 127, 10083-10088.

165. Rose, A.; Lugmair, C. G. and Swager, T. M., *J. Am. Chem. Soc.* **2001,** 123, 11298-11299.

166. Metivier, R.; Nolde, F.; Mullen, K. and Basche, T., *Phys. Rev. Lett.* **2007,** 98, 047802.

167. Pettersson, K.; Wiberg, J.; Ljungdahl, T.; Martensson, J. and Albinsson, B., *J. Phys. Chem. A* **2006,** 110, 319-326.

168. Nguyen, T.-Q.; Doan, V. and Schwartz, B. J., *J. Chem. Phys.* **1999,** 110, 4068-4078.

169. Wang, S. J.; Bazan, G. C.; Tretiak, S. and Mukamel, S., *J. Am. Chem. Soc.* **2000,** 122, 1289-1297.

170. Birks, J. B., *Rep. Prog. Phys.* **1975,** 38, 903-974.

171. Sims, M.; Bradley, D. D. C.; Ariu, M.; Koeberg, M.; Asimakis, A.; Grell, M. and Lidzey, D. G., *Adv. Funct. Mater.* **2004,** 14, 765-781.

172. Schlegel, G.; Bohnenberger, J.; Potapova, I. and Mews, A., *Phys. Rev. Lett.* **2002,** 88, 137401.

173. Dukes, A. D., III; Samson, P. C.; Keene, J. D.; Davis, L. M.; Wikswo, J. P. and Rosenthal, S. J., *J. Phys. Chem. A* **2011,** 115, 4076-4081.

174. Avidan, A. and Oron, D., *Nano Lett.* **2008,** 8, 2384-2387.

175. Gomez, D. E.; Califano, M. and Mulvaney, P., *Phys. Chem. Chem. Phys.* **2006,** 8, 4989-5011.

176. Fu, H. and Zunger, A., *Phys. Rev. B* **1997,** 56, 1496-1508.

177. Fonoberov, V. A.; Alim, K. A.; Balandin, A. A.; Xiu, F. X. and Liu, J. L., *Phys. Rev. B* **2006,** 73, 165317.

178. Beaulac, R.; Archer, P. I.; van Rijssel, J.; Meijerink, A. and Gamelin, D. R., *Nano Lett.* **2008,** 8, 2949-2953.

179. Vlaskin, V. A.; Janssen, N.; van Rijssel, J.; Beaulac, R. m. and Gamelin, D. R., *Nano Lett.* **2010,** 10, 3670-3674.

180. Jones, M.; Kumar, S.; Lo, S. S. and Scholes, G. D., *J. Phys. Chem. C* **2008,** 112, 5423-5431.

181. Srivastava, B. B.; Jana, S. and Pradhan, N., *J. Am. Chem. Soc.* **2010,** 133, 1007-1015.

182. Sher, P. H.; Smith, J. M.; Dalgarno, P. A.; Warburton, R. J.; Chen, X.; Dobson, P. J.; Daniels, S. M.; Pickett, N. L. and O'Brien, P., *Appl. Phys. Lett.* **2008,** 92, 101111.

183. Kraus, R. M.; Lagoudakis, P. G.; Müller, J.; Rogach, A. L.; Lupton, J. M.; Feldmann, J.; Talapin, D. V. and Weller, H., *J. Phys. Chem. B* **2005,** 109, 18214-18217.

184. Kuno, M.; Fromm, D. P.; Gallagher, A.; Nesbitt, D. J.; Micic, O. I. and Nozik, A. J., *Nano Lett.* **2001,** 1, 557-564.

185. Kuno, M.; Fromm, D. P.; Hamann, H. F.; Gallagher, A. and Nesbitt, D. J., *J. Chem. Phys.* **2001,** 115, 1028-1040.

186. Shimizu, K. T.; Neuhauser, R. G.; Leatherdale, C. A.; Empedocles, S. A.; Woo, W. K. and Bawendi, M. G., *Phys. Rev. B* **2001,** 63, 205316.

187. Wang, S.; Querner, C.; Emmons, T.; Drndic, M. and Crouch, C. H., *J. Phys. Chem. B* **2006,** 110, 23221-23227.

188. Frantsuzov, P.; Kuno, M.; Janko, B. and Marcus, R. A., *Nature Physics* **2008,** 4, 519-522.

189. Banin, U.; Bruchez, M.; Alivisatos, A. P.; Ha, T.; Weiss, S. and Chemla, D. S., *J. Chem. Phys.* **1999,** 110, 1195-1201.

190. Stefani, F. D.; Knoll, W.; Kreiter, M.; Zhong, X. and Han, M. Y., *Phys. Rev. B* **2005,** 72, 125304.

191. Chung, I. H. and Bawendi, M. G., *Phys. Rev. B* **2004,** 70, 165304.

192. Tang, J. and Marcus, R. A., *J. Chem. Phys.* **2005,** 123, 204511.

193. Verberk, R.; van Oijen, A. M. and Orrit, M., *Phys. Rev. B* **2002,** 66, 233202.

194. Tang, J. and Marcus, R. A., *Phys. Rev. Lett.* **2005,** 95, 107401.

195. Tang, J. and Marcus, R. A., *J. Chem. Phys.* **2005,** 123, 054704.

196. Neuhauser, R. G.; Shimizu, K. T.; Woo, W. K.; Empedocles, S. A. and Bawendi, M. G., *Phys. Rev. Lett.* **2000,** 85, 3301-3304.

197. Müller, J.; Lupton, J. M.; Lagoudakis, P. G.; Schindler, F.; Koeppe, R.; Rogach, A. L.; Feldmann, J.; Talapin, D. V. and Weller, H., *Nano Lett.* **2005,** 5, 2044-2049.

198. Schindler, F. and Lupton, J. M., *Nano Lett.* **2010,** 10, 2683-2689.

199. Barkai, E.; Jung, Y. J. and Silbey, R., *Annu. Rev. Phys. Chem.* **2004,** 55, 457-507.

200. Hubner, C. G.; Zumofen, G.; Renn, A.; Herrmann, A.; Mullen, K. and Basche, T., *Phys. Rev. Lett.* **2003,** 91, 093903.

201. Yip, W. T.; Hu, D. H.; Yu, J.; Vanden Bout, D. A. and Barbara, P. F., *J. Phys. Chem. A* **1998,** 102, 7564-7575.

202. Zondervan, R.; Kulzer, F.; Orlinskii, S. B. and Orrit, M., *J. Phys. Chem. A* **2003,** 107, 6770-6776.

203. Haase, M.; Hubner, C. G.; Reuther, E.; Herrmann, A.; Mullen, K. and Basche, T., *J. Phys. Chem. B* **2004,** 108, 10445-10450.

204. Kulzer, F.; Bordat, P.; Basche, T. and Christ, T., *Angew. Chem., Int. Ed.* **2001,** 40, 4192-4195.

205. Cotlet, M.; Gronheid, R.; Habuchi, S.; Stefan, A.; Barbafina, A.; Mullen, K.; Hofkens, J. and De Schryver, F. C., *J. Am. Chem. Soc.* **2003,** 125, 13609-13617.

206. Liu, S.; Schmitz, D.; Jester, S. S.; Borys, N. J.; Höger, S. and Lupton, J. M., *J. Phys. Chem. B* **2012** (In press).

207. Rocke, C.; Zimmermann, S.; Wixforth, A.; Kotthaus, J. P.; Böhm, G. and Weimann, G., *Phys. Rev. Lett.* **1997,** 78, 4099-4102.

208. Gill, K. S.; Moskovitz, N.; Wang, L. C.; Sherwin, M. S.; Badolato, A.; Gerardot, B. and Petroff, P., *Appl. Phys. Lett.* **2005,** 87, 162101.

209. High, A. A.; Novitskaya, E. E.; Butov, L. V.; Hanson, M. and Gossard, A. C., *Science* **2008,** 321, 229-231.

210. Young, R. J.; Dewhurst, S. J.; Stevenson, R. M.; Atkinson, P.; Bennett, A. J.; Ward, M. B.; Cooper, K.; Ritchie, D. A. and Shields, A. J., *New J. Phys.* **2007,** 9, 52883-1.

211. Pfeffer, N.; Neher, D.; Remmers, M.; Poga, C.; Hopmeier, M. and Mahrt, R., *Chem. Phys.* **1998,** 227, 167-178.

212. Choi, C. L.; Li, H.; Olson, A. C. K.; Jain, P. K.; Sivasankar, S. and Alivisatos, A. P., *Nano Lett.* **2011,** 11, 2358-2362.

213. Gulbinas, V.; Zaushitsyn, Y.; Sundstrom, V.; Hertel, D.; Bassler, H. and Yartsev, A., *Phys. Rev. Lett.* **2002,** 89, 107401.

214. Mehata, M. S.; Majumder, M.; Mallik, B. and Ohta, N., *J. Phys. Chem. C* **2010,** 114, 15594-15601.

215. Park, S. J.; Link, S.; Miller, W. L.; Gesquiere, A. and Barbara, P. F., *Chem. Phys.* **2007,** 341, 169-174.

216. Hertel, D.; Soh, E. V.; Bassler, H. and Rothberg, L. J., *Chem. Phys. Lett.* **2002,** 361, 99-105.

217. Döhler, G. H.; Künzel, H.; Olego, D.; Ploog, K.; Ruden, P.; Stolz, H. J. and Abstreiter, G., *Phys. Rev. Lett.* **1981,** 47, 864-867.

218. Zimmermann, S.; Wixforth, A.; Kotthaus, J. P.; Wegscheider, W. and Bichler, M., *Science* **1999,** 283, 1292-1295.

219. Miranda, P. B.; Moses, D. and Heeger, A. J., *Phys. Rev. B* **2001,** 64, 081201.

220. Moses, D.; Dogariu, A. and Heeger, A. J., *Phys. Rev. B* **2000,** 61, 9373-9379.

221. Graupner, W.; Cerullo, G.; Lanzani, G.; Nisoli, M.; List, E. J. W.; Leising, G. and De Silvestri, S., *Phys. Rev. Lett.* **1998,** 81, 3259-3262.

222. Gulbinas, V.; Hertel, D.; Yartsev, A. and Sundstrom, V., *Phys. Rev. B* **2007,** 76, 235203.

223. Moscatelli, A.; Livingston, K.; So, W. Y.; Lee, S. J.; Scherf, U.; Wildeman, J. and Peteanu, L. A., *J. Phys. Chem. B* **2010,** 114, 14430-14439.

224. Arkhipov, V. I.; Emelianova, E. V.; Barth, S. and Bassler, H., *Phys. Rev. B* **2000,** 61, 8207-8214.

225. Haugeneder, A.; Neges, M.; Kallinger, C.; Spirkl, W.; Lemmer, U.; Feldmann, J.; Amann, M. C. and Scherf, U., *Appl. Phys. Lett.* **1999,** 85, 1124-1130.

226. Klimov, V. I.; McBranch, D. W.; Barashkov, N. and Ferraris, J., *Phys. Rev. B* **1998,** 58, 7654-7662.

227. Smith, T. M.; Hazelton, N.; Peteanu, L. A. and Wildeman, J., *J. Phys. Chem. B* **2006,** 110, 7732-7742.

228. Becker, K.; Fritzsche, M.; Höger, S. and Lupton, J. M., *J. Phys. Chem. B* **2008,** 112, 4849-4853.

229. Holzwarth, A. R. and Kenneth, S., *Methods Enzymol.* **1995,** Volume 246, 334-362.

230. Weiss, S., *Science* **1999,** 283, 1676-1683.

231. Berera, R.; van Grondelle, R. and Kennis, J. T. M., *Photosynth. Res.* **2009,** 101, 105-118.

232. de Boeij, W. P.; Pshenichnikov, M. S. and Wiersma, D. A., *Annu. Rev. Phys. Chem.* **1998,** 49, 99-123.

233. Goodson, T., *Annu. Rev. Phys. Chem.* **2005,** 56, 581-603.

234. Hofkens, J.; Cotlet, M.; Vosch, T.; Tinnefeld, P.; Weston, K. D.; Ego, C.; Grimsdale, A.; Müllen, K.; Beljonne, D.; Brédas, J. L.; Jordens, S.; Schweitzer, G.; Sauer, M. and De Schryver, F., *Proc. Natl. Acad. Sci. U. S. A.* **2003,** 100, 13146-13151.

235. Hofmann, C.; Ketelaars, M.; Matsushita, M.; Michel, H.; Aartsma, T. J. and Köhler, J., *Phys. Rev. Lett.* **2003,** 90, 013004.

236. Morello, G.; Della Sala, F.; Carbone, L.; Manna, L.; Maruccio, G.; Cingolani, R. and De Giorgi, M., *Phys. Rev. B* **2008,** 78, 195313.

237. Berberan-Santos, M. N. and Valeur, B., *J. Chem. Phys.* **1991,** 95, 8048-8055.

238. Borys, N. J. Optical Structure-Property Relations in Metal and Semiconductor Nanoparticles. University of Utah, Salt Lake City, 2011.

239. Da Como, E.; Borys, N. J.; Strohriegl, P.; Walter, M. J. and Lupton, J. M., *J. Am. Chem. Soc.* **2011,** 133, 3690-3692.

240. Empedocles, S. A.; Neuhauser, R. and Bawendi, M. G., *Nature* **1999,** 399, 126-130.

241. Vogel, S. S.; Thaler, C.; Blank, P. S. and Koushik, S. V., Time-Resolved Fluorescence Anisotropy. In *FLIM Microscopy in Biology and Medicine*, Periasamy, A.; Clegg, R. M., Eds. Chapman & Hall/CRC: New York, 2009.

242. Lammi, R. K. and Barbara, P. F., *Photochem. Photobiol. Sci.* **2005,** 4, 95-99.

243. Lutich, A. A.; Mauser, C.; Da Como, E.; Huang, J.; Vaneski, A.; Talapin, D. V.; Rogach, A. L. and Feldmann, J., *Nano Lett.* **2010,** 10, 4646-4650.

244. Steiner, D.; Dorfs, D.; Banin, U.; Della Sala, F.; Manna, L. and Millo, O., *Nano Lett.* **2008,** 8, 2954-2958.

245. Anastasio, T. A., *J. Appl. Phys.* **1967,** 38, 2606-2610.

246. Becker, K.; Lagoudakis, P. G.; Gaefke, G.; Höger, S. and Lupton, J. M., *Angew. Chem., Int. Ed.* **2007,** 46, 3450-3455.

247. Lupton, J. M.; Samuel, I. D. W.; Beavington, R.; Burn, P. L. and Bässler, H., *Adv. Mater.* **2001,** 13, 258-261.

248. Lupton, J. M., *Adv. Mater.* **2010,** 22, 1689-1721.

249. Sundström, V.; Pullerits, T. and van Grondelle, R., *J. Phys. Chem. B* **1999,** 103, 2327-2346.

250. Jester, S. S.; Schmitz, D.; Eberhagen, F. and Höger, S., *Chem. Commun.* **2011,** 47, 8838-8840.

251. Kersting, R.; Lemmer, U.; Deussen, M.; Bakker, H. J.; Mahrt, R. F.; Kurz, H.; Arkhipov, V. I.; Bässler, H. and Göbel, E. O., *Phys. Rev. Lett.* **1994,** 73, 1440-1443.

252. Arkhipov, V. I.; Bässler, H.; Deussen, M.; Göbel, E. O.; Kersting, R.; Kurz, H.; Lemmer, U. and Mahrt, R. F., *Phys. Rev. B* **1995,** 52, 4932-4940.

253. Karmakar, R. and Samanta, A., *Chem. Phys. Lett.* **2003,** 376, 638-645.

254. Schaller, R. D.; Lee, L. F.; Johnson, J. C.; Haber, L. H.; Saykally, R. J.; Vieceli, J.; Benjamin, I.; Nguyen, T.-Q. and Schwartz, B. J., *J. Phys. Chem. B* **2002,** 106, 9496-9506.

255. Moran, A. M.; Maddox, J. B.; Hong, J. W.; Kim, J.; Nome, R. A.; Bazan, G. C.; Mukamel, S. and Scherer, N. F., *J. Chem. Phys.* **2006,** 124, 194904.

256. McNeill, J. D.; O'Connor, D. B.; Adams, D. M.; Barbara, P. F. and Kammer, S. B., *J. Phys. Chem. B* **2001,** 105, 76-82.

257. Tikhoplav, R. K. and Hess, B. C., *Synth. Met.* **1999,** 101, 236-237.

258. Shim, M. and Guyot-Sionnest, P., *J. Chem. Phys.* **1999,** 111, 6955-6964.

259. Krauss, T. D. and Brus, L. E., *Phys. Rev. Lett.* **1999,** 83, 4840-4843.

260. Krishnan, R.; Hahn, M. A.; Yu, Z. H.; Silcox, J.; Fauchet, P. M. and Krauss, T. D., *Phys. Rev. Lett.* **2004,** 92, 216803.

261. Jdira, L.; Overgaag, K.; Gerritsen, J.; Vanmaekelbergh, D.; Liljeroth, P. and Speller, S., *Nano Lett.* **2008,** 8, 4014-4019.

262. Antelman, J.; Ebenstein, Y.; Dertinger, T.; Michalet, X. and Weiss, S., *J. Phys. Chem. C* **2009,** 113, 11541-11545.

263. Gerhard, A. and Bassler, H., *J. Chem. Phys.* **2002,** 117, 7350-7356.

264. Krenner, H. J.; Pryor, C. E.; He, J. and Petroff, P. M., *Nano Lett.* **2008,** 8, 1750-1755.

265. Fisher, B.; Caruge, J. M.; Zehnder, D. and Bawendi, M., *Phys. Rev. Lett.* **2005,** 94, 087403.

266. Klimov, V. I., *Annu. Rev. Phys. Chem.* **2007,** 58, 635-673.

267. Fairfield, J. A.; Dadosh, T. and Drndic, M., *Appl. Phys. Lett.* **2010,** 97, 143112.

268. Finley, J. J.; Skalitz, M.; Arzberger, M.; Zrenner, A.; Böhm, G. and Abstreiter, G., *Appl. Phys. Lett.* **1998,** 73, 2618-2620.

269. Reimer, M. E.; van Kouwen, M. P.; Hidma, A. W.; van Weert, M. H. M.; Bakkers, E. P. A. M.; Kouwenhoven, L. P. and Zwiller, V., *Nano Lett.* **2011,** 11, 645-650.

270. QD.Laser QD laser. http://qdlaser.com/?page_id=20

271. Chen, X.; Yeganeh, S.; Qin, L.; Li, S.; Xue, C.; Braunschweig, A. B.; Schatz, G. C.; Ratner, M. A. and Mirkin, C. A., *Nano Lett.* **2009,** 9, 3974-3979.

272. Luttjohann, S.; Meier, C.; Lorke, A.; Reuter, D. and Wieck, A. D., *Appl. Phys. Lett.* **2005,** 87, 163117.